



Les résidus carbonés de feux dans les sédiments: Implications méthodologiques, climatiques et anthropiques

Florian Thevenon

► To cite this version:

Florian Thevenon. Les résidus carbonés de feux dans les sédiments: Implications méthodologiques, climatiques et anthropiques. Minéralogie. Université de droit, d'économie et des sciences - Aix-Marseille III, 2003. Français. NNT: . tel-00008908

HAL Id: tel-00008908

<https://theses.hal.science/tel-00008908>

Submitted on 30 Mar 2005

HAL is a multi-disciplinary open access archive for the deposit and dissemination of scientific research documents, whether they are published or not. The documents may come from teaching and research institutions in France or abroad, or from public or private research centers.

L'archive ouverte pluridisciplinaire **HAL**, est destinée au dépôt et à la diffusion de documents scientifiques de niveau recherche, publiés ou non, émanant des établissements d'enseignement et de recherche français ou étrangers, des laboratoires publics ou privés.

UNIVERSITE DE DROIT, D'ECONOMIE ET DES SCIENCES D'AIX-MARSEILLE III
ECOLE DOCTORALE : SCIENCES DE L'ENVIRONNEMENT

03 AIX 30016

THESE

Pour obtenir le grade de

DOCTEUR DE L'UNIVERSITE D'AIX-MARSEILLE III

Discipline : Géosciences de l'Environnement

Présentée et soutenue publiquement par

Florian THEVENON

le 4 Juillet 2003

**Les résidus carbonés de feux dans les sédiments
lacustres et océaniques intertropicaux :
Implications méthodologiques, climatiques et anthropiques.**

JURY

Edouard BARD	Professeur (Aix-Marseille 3)	Président
Luc BEAUFORT	Directeur de Recherche (CNRS)	Examinateur
Hélène CACHER	Maître de Conférence (Paris 7)	Rapporteur
Christopher CARCAILLET	Directeur d'Etudes (EPHE)	Rapporteur
Amos MAJULE	Professeur (Dar es Salaam)	Examinateur
David WILLIAMSON	Chargé de Recherche (CNRS)	Directeur de thèse

RESUME

Bien que les émissions de gaz à effet de serre et d'aérosols carbonés par les feux tropicaux, étroitement liées aux conditions de sécheresse et à l'action anthropique, aient un impact significatif sur le cycle du carbone et sur le climat global, la dynamique passée de ces émissions reste encore peu documentée. Cette étude a pour but de caractériser les produits de combustion carbonés piégés dans les sédiments lacustres et marins, afin d'établir des enregistrements fiables de la variabilité des feux tropicaux.

L'analyse du comportement de standards carbonés sur des matrices synthétiques et naturelles à l'aide de différentes techniques d'extraction a permis de discriminer, selon un degré croissant de résistance à l'oxydation : le charbon, le carbone réfractaire, et le Black Carbon (BC). Bien que l'analyse de mélanges expérimentaux présente des pertes de masse d'environ 20% dans le cas du graphite mélangé à des poudres synthétiques, la méthode d'extraction et de mesure du BC s'avère reproductible et fiable pour reconstituer les changements de concentration enregistrés dans la plupart des sédiments.

L'analyse du carbone élémentaire résistant aux traitements chimiques et/ou thermique, combinée au comptage automatisé des microcharbons, a ensuite été appliquée à une séquence pélagique du Pacifique Ouest (WPWP) couvrant les derniers 360 ka, et à un enregistrement lacustre Tanzanien couvrant les derniers 4 ka.

L'enregistrement marin (carotte MD972140) montre que les émissions de BC sont fortement contraintes par les variations d'insolation en région intertropicale et équatoriale (cycles de précession et semi-précession). Elles sont également associées à la variabilité (pluri)millénaire du climat de l'hémisphère nord et de la mousson d'hiver est-asiatique, et suggèrent un couplage entre le gradient zonal des précipitations dans le Pacifique Equatorial et le climat des hautes latitudes. De plus, les aérosols carbonés enregistrent clairement l'action de l'homme sur le régime des feux dans la région Indo-Pacifique, avec une forte augmentation des apports de BC et de microcharbons entre 53-43 ka et 12-10 kyr.

Au lac Masoko (carotte MM8), l'abondance et la nature des assemblages de particules de charbon reflètent en partie les apports détritiques liés au ruissellement des sols forestiers ou à l'érosion lors de bas niveaux lacustres. De plus, l'augmentation rapide des aérosols carbonés (microcharbons <1µm et BC) entre 1,8 et 1,6 ka BP suggère une intensification des incendies régionaux, contemporaine de l'expansion de la métallurgie et de l'agriculture dans le Rift Est Africain.

L'identification et la quantification du carbone réfractaire piégé dans le réservoir sédimentaire montre ainsi que la dynamique des feux a été fortement contrainte par la variabilité du cycle hydrologique saisonnier et pluriannuel, et par l'action anthropique. Depuis plusieurs dizaines de milliers d'années, cette dernière est probablement déterminante vis-à-vis des quantités de carbone réfractaire émises dans l'environnement.

Mots clés : Feux de végétation, sédiment, charbon, Black Carbon, impact climatique et anthropique, mousson, Afrique de l'Est, Australie/Papouasie Nouvelle Guinée.

ABSTRACT

Biomass burning in the tropics release about 25% of annual anthropogenic CO₂ emissions, and large amounts of aerosol particles that play an important role in atmospheric chemistry and climate. The sedimentary carbonaceous particles emitted by plant organic matter combustion represent proxies of past fire activity.

The analysis of refractory carbonaceous species behavior with different analytical methods has allowed to characterize with an increasing oxidation level : charcoal, refractory carbon and Black Carbon (BC). Despite that the analysis of the graphite concentration introduced in synthetic powders presents ca. 20% mass loss, the BC extractive methods indicate a satisfactory reproducibility and reliability to reconstruct sedimentary changes in biomass burning.

Elemental analysis of carbon resistant to thermal and/or chemical extraction, combined with automatic-image analysis of charcoal, was applied to a marine record from the Western Pacific Warm Pool (WPWP) spanning the last 360 kyr and to a Tanzanian lacustrine record spanning the last 4 kyr.

In the oceanic record, carbonaceous aerosols (charcoal and BC) display orbital precession plus its harmonics related frequencies, suggesting that fire activity closely responded to the variations in seasonal radiation forcing at the equator, but also that changes in high-latitudes forcing (Dansgaard-Oeschger periodicities) on the winter monsoon contribute to ENSO-like conditions. In addition, carbonaceous aerosol clearly registered human-induced fire-regime alteration in the Indo/Pacific area, with great increases in fire-activity between 53-43 and 12-10 kyr.

Charcoal abundance and distribution in lake Masoko reveal that runoff and erosion on woodland soils are the dominant processes for charred particle transportation. However, the carbonaceous aerosol fraction (charcoal<1µm and BC) clearly illustrate fire activity. Its abrupt increase between 1,8 and 1,6 cal. kyr B.P. in lake Masoko testifies regional emissions from forest fires prior the local fire extend. This latter event is contemporaneous with an abrupt deforestation and coincides with the extend of Late Iron Age and agricultural activities in the East African Rift.

These results demonstrate that carbonaceous residues analysis in sediments provides informations on past-climatic changes, human impact on the environment, and global carbon budget.

Key words: Biomass burning, sediment, charcoal, Black Carbon, monsoon, climatic and anthropic impact, East Africa, Australia/Papua New Guinea

Remerciements

Je voudrais exprimer tous mes remerciement aux personnes qui ont contribué de près ou de loin au bon déroulement de ce travail.

Tout d'abord, j'aimerais remercier *Edouard Bard* et *David Williamson* d'avoir encadré cette thèse. Je les remercie de leur confiance, de leur soutien, et de leur disponibilité à mon égard. Ils m'ont permis de mener à bien ce travail, en me faisant profiter de leur rigueur scientifique et de leurs compétences dans plusieurs domaines, ainsi qu'en reprenant avec beaucoup de patience les parties rédigées sous la forme d'articles.

Je suis très reconnaissant à *Helène Cachier* et *Cristopher Carcaillet* de m'avoir fait l'honneur d'être les rapporteurs de cette thèse, ainsi qu'à *Luc beaufort*, et *Amos Majule*, pour leur participation au jury.

Je remercie particulièrement *Helène Cachier* de m'avoir montrer son protocole d'extraction des aérosols carbonés actuels, au CNRS de Gif sur Yvette. Ses travaux m'ont permis de comprendre une partie de ce domaine, et elle a répondu à mes nombreuses questions.

Je tiens aussi à témoigner ma gratitude à *Luc Beaufort*, pour m'avoir initié aux comptages de charbon automatisé, mais aussi pour de nombreuses discussions, en particulier pour tout ce qui touche aux analyses spectrales. Avec *Noëlle Buchet*, ils m'ont ouvert les portes du laboratoire des bio-indicateurs. Je remercie aussi *Thibault de Garidel* de m'avoir permis d'utiliser des données non publiées.

Un grand merci à l'équipe de géochimie organique. *Franke Rostek* et *Corine Sonzoni* m'ont accueilli chaleureusement du DEA à la thèse. Les portes de leur bureau et de leur laboratoire m'étaient toujours ouvertes, et elles m'ont aidé à résoudre de nombreux problèmes techniques et méthodologiques. Merci à mon voisin de bureau, *Yann Ternois*, pour m'avoir encouragé au moment où j'en avais besoin, et aidé à comprendre la géochimie organique. Merci également à *Sonia Schulte* puis à

Laurence Vidale, pour leurs discussions scientifiques, mais aussi pour la sympathique cohabitation et leurs encouragements.

Un grand merci aussi à l'équipe de palynologie, *Raymonde Bonnefille, Annie Vincens, Doris Barboni*, et le précieux *Guillaume Buchet*. Ils m'ont permis de travailler dans leur laboratoire, et leur communication de données, ainsi que de nombreuses discussions scientifiques, m'ont permis d'enrichir l'interprétation des résultats.

Je remercie aussi les membres de l'équipe de magnétisme, *Pierre Rochette, Didier Vandamme, Pierre-Etienne Mathe* et *Fabienne Vadeboin*, pour avoir fait partie de cette équipe, et souvent participé aux amicaux cafés du chalet.

Merci beaucoup à *Maurice Taieb*, pour m'avoir soutenu et souvent encouragé. Son avis et ses conseils ont été précieux.

Merci à *Michel Decobert, Jean-Jacques Motte*, et *Christine Vambesien*, pour leurs multiples aides à la création de poster, cartes et dessins, mais aussi pour leur agréable compagnie.

Merci encore aux sympathiques *Philippe Dussouilliez* et *Dagnashew Legesse*, qui m'ont généreusement aidé lors de défis informatiques.

En quatre ans, au comptoir de la bibliothèque, en mission en Afrique ou entre Aix et Marseille, j'ai eu la chance de découvrir des personnes très attachantes avec lesquelles j'ai passé de formidables moments. Merci à tous les collègues (*Ouassila, Yanick, Anne, Fabien, Christophe, Régis, Eva, Claire, Moktar, Julien, Martine, Sarah, Jérôme, Laurent*).

Je n'oublie pas *Brigitte Crubézy, Joël Guiot, Françoise Gasse, Françoise Chalié, Christine Pailles, Jean-Paul Ambrosi, Jean-Dominique Meunier, Anne Alexandre, Stéphane Moustier, Daniel Borschneck, Martine Tiercelin, Annie-Claude Agnesse, Nicole Page, Marie-Magdeleine Nehlil*, et tous les autres. Pas plus que je n'oublierai cette magnifique région, entre les calanques et la Sainte Victoire, et mes nombreuses ballades autour du CEREGE.

Enfin, je remercie mes parents pour tout.

Mille merci à Stéphanie et Léonore.

TABLE DES MATIERES

RESUME.....	I
ABSTRACT.....	II
REMERCIEMENTS.....	III
TABLE DES MATIERES.....	V
LISTE DES ABREVIATIONS.....	IX
Introduction.....	1
1. Dynamique et impact des feux de biomasse.....	3
1.1 Feu et climat.....	3
1.2 Les enregistrements des feux passés.....	4
1.3 L'observation et la modélisation des feux actuels.....	4
1.4 Caractéristiques des feux.....	6
1.5 Quantité de biomasse brûlée et feux tropicaux.....	9
1.6 Les émissions gazeuses.....	11
1.7 Les émissions solides.....	13
1.8 Impact radiatif des aérosols carbonés.....	14
1.9 Importance des feux dans le cycle du carbone.....	16
1.10 Climat tropical et dynamique des feux.....	19
1.10.1 Les feux en Afrique.....	19
1.10.2 Les feux du SE Asiatique.....	21
1.11 Conclusion.....	22
2. Méthodologie.....	23
2.1 Les méthodes optiques.....	23
2.2 Les méthodes thermiques.....	24
2.3 Les méthodes chimiques.....	27
2.4 Définition des principaux résidus carbonés issus de la combustion.....	29

2.5 Les réservoirs et le temps de résidence du carbone réfractaire.....	30
2.6 Méthode optique.....	31
2.6.1 Préparation des lames.....	31
2.6.2 Acquisition et traitement des images.....	32
2.7 Analyse du carbone élémentaire.....	33
2.7.1 Appareillage: l'analyseur élémentaire de carbone.....	34
2.7.2 Analyse du carbone total, du carbone organique, et calcul de la teneur en carbonate de calcium.....	35
2.7.3 Méthode thermique.....	35
2.7.4 Méthode chimique.....	35
2.8 Conclusion.....	37
 3. Testing the Thermally Refractory Carbon (TRC) and Black Carbon (BC) extraction methods for reconstructing past biomass fires from the sedimentary record.....	 39
3.1 Introduction.....	39
3.2 General background.....	40
3.3 Experimental section.....	41
3.3.1 Total Carbon (TC) and Organic Carbon (OC) determinations.....	41
3.3.2 Thermally Refractory Carbon (TRC) extraction.....	42
3.3.3 Black Carbon (BC) extraction.....	42
3.3.4 Synthetic matrices and natural sediments.....	43
3.3.5 Determination of elemental carbon abundance.....	44
3.4 Results.....	44
3.4.1 Detection limit of the elemental analyzer.....	44
3.4.2 Characteristics of the carbonaceous standards.....	45
3.4.3 Reproducibility of carbon determinations.....	47
3.4.4 Testing the extraction of Thermally Refractory Carbon.....	48
3.4.5 Testing the extraction of Black Carbon.....	51
3.5 Discussion.....	54
3.5.1 Reliability of the TRC extraction.....	54
3.5.2 Reliability of the BC extraction.....	55
3.6 Conclusion.....	58

4. A 360 kyr record of carbonaceous biomass burning proxies from core MD972140, West Equatorial Pacific: Sedimentary, climate and human implications.....	61
4.1 Introduction.....	61
4.2 Regional setting.....	62
4.3 Lithology, stratigraphy and sampling.....	64
4.4. Methods.....	65
4.4.1 Organic Carbon (Corg) and carbonate calcium (CaCO_3) analyses.....	65
4.4.2 Oxidant Resistant Elemental Carbon (OREC) and Black Carbon (BC) analyses.....	70
4.4.3 Microscopic charcoal counting.....	71
4.5 Results.....	72
4.5.1 Organic and mineral carbon records.....	72
4.5.2 Oxidant carbonaceous particle records.....	75
4.5.3 Frequency domain comparisons.....	77
4.6 Discussion.....	81
4.7 Conclusion.....	84
5. A Late Holocene charcoal record from Lake Masoko, SW Tanzania: Climatic and anthropologic implications.....	87
5.1 Introduction.....	87
5.2 The study site.....	89
5.3 Sediment stratigraphy.....	91
5.4. Methods.....	91
5.5 Results.....	94
5.6 Discussion.....	97
5.7 Conclusion.....	100

6. Conclusion générale et prospectives.....	101
6.1 Méthodologie.....	101
6.2 Les charbons, la suie, et le BC dans les sédiments.....	102
6.3 La dynamique des feux ; implications climatiques et anthropiques.....	103
6.4 Perspectives de recherche.....	105
LISTE DES FIGURES.....	107
LISTE DES TABLEAUX.....	111
BIBLIOGRAPHIE.....	113

ANNEXE

A 22 kyr BP sedimentological record of Lake Rukwa (8°S, S-W Tanzania): environmental, chronostratigraphic and climatic implications *

Florian Thevenon, David Williamson, Maurice Taieb. Palaeogeography, Palaeoclimatology, Palaeoecology 187 (2002).

LISTE DES ABREVIATIONS

~ ou *ca.* : environ

AP : Arboreal Pollen

BC : Black Carbon

CaCO₃ : Carbonate de calcium

cal. yr BP : calibrated year Before Present

CHAR : Charcoal Accumulation Rate

Corg ou OC : Carbone organique

DOC : Dissolved Organic Carbon (carbone organique dissous)

Gt : 10¹⁵ grammes, équivalent à 1 milliard de tonnes

ha : hectare

ENSO : El Niño/Southern Oscillation

IOC : zone de confluence interocéanique

ITCZ : zone de convergence intertropicale (InterTropical Convergence Zone)

ka ou kyr : milliers d'années

LGM : Last Glacial Maximum

MAR : Mass Accumulation Rate

MCG : Modèle de circulation générale

ms : matière sèche

Mt : Millions de tonnes, équivalent à 1 Terra Gramme

NAP : Non Arboreal Pollen

OREC : Oxidant Resistant Elemental Carbon, carbone résistant au traitement au bichromate

Tg : Terragramme, 1Tg=10¹²g de CO₂

TOC ou Corg : Total Organic Carbon

TOM : Total Organic Matter

TRC : Thermally Refractory Carbon, carbone résistant au traitement thermique

WPWP : Western Pacific Warm Pool

Introduction

La dynamique des feux de biomasse et des produits de combustion au cours des derniers cycles climatiques et de l'Holocène est encore largement méconnue. Pourtant, les gaz et particules émis par les feux actuels (à plus de 90% d'origine humaine) modifient le fonctionnement de l'atmosphère à l'échelle globale, et il devient urgent de mieux connaître leur impact climatique (IPCC, 2001). En effet, les feux libèrent le tiers du dioxyde de carbone d'origine anthropique, et certainement autant d'aérosols carbonés que la totalité des combustions industrielles (Andreae, 1991; Cachier-Rivault, 1996). Mais la nature, l'origine, et la quantité d'aérosols carbonés anthropiques, qui en terme de forçage direct semblent être les seconds responsables du réchauffement climatique global après le CO₂, sont encore relativement méconnus (Jacobson, 2001; Penner et al., 2001).

Afin d'appréhender l'activité passée des feux et leur impact sur l'environnement, cette étude propose de reconstituer leur changement de dynamique, liée aux variations climatiques naturelles, mais aussi aux activités humaines. La réponse est apportée par l'étude des sédiments tropicaux, là où sont localisés la majorité des feux (Hao et al., 1990). En effet, les sédiments contiennent des particules carbonées issues de la combustion de végétaux et transportées dans les systèmes aquatiques et les sols, puis incorporées dans les sédiments. La relative résistance à la biodégradation de ces particules en fait de bons marqueurs de paléo-feux (Goldberg, 1985). Toutefois, les données existantes présentent une part d'incertitude qui résulte de: i) la faible résolution chronologique et géographique de ces enregistrements ii) les aspects équivoques des divers protocoles analytiques employés iii) l'absence de prise en compte de l'origine et du temps de résidence du carbone analysé. Tant sur le continent que dans l'océan, la faible quantité de données, ainsi que la variabilité des mesures effectuées, excluent une compréhension intégrée du problème des apports de charbons et de leur relation avec les cycles d'érosion/dépôt ainsi qu'avec la variabilité du climat.

Après un rappel des connaissances sur les feux actuels et sur l'importance de leurs émissions (chapitre 1), ce travail propose une approche tant méthodologique que stratigraphique pour reconstituer la contribution des feux et de l'érosion des sols aux apports de matériel détritique organique en domaine tropical lacustre et marin, au cours des derniers cycles glaciaires et de l'Holocène. Il s'agit de coupler les méthodes actuelles de comptage optique des charbons et

d'analyse chimique du carbone élémentaire résistant à l'oxydation (chapitre 2). Les méthodes d'extraction chimiques sont calibrées sur des standards afin de simuler le comportement de composés carbonés naturels (chapitre 3). L'étude d'enregistrements sédimentaires tropicaux est ensuite entreprise. Elle concerne un site pélagique au large de la Papouasie Nouvelle Guinée (carotte MD972140, 2°N, 141°E ; chapitre 4) et un lac de cratère dans le Sud Ouest de la Tanzanie (carotte MM8, 9°S, 33°E ; chapitre 5).

Enfin, un bilan des résultats de cette étude est effectuée (chapitre 6) et des perspectives de recherches sont proposées.

1. Dynamique et impact des feux de biomasse

1.1 Feu et climat

Les feux exercent un rôle important dans l'évolution biologique et atmosphérique depuis que les plantes terrestres produisent de grandes quantités de matière organique, soit environ 350 à 400 millions d'années (Ma) (Cope and Chaloner, 1980). Par exemple, les fortes concentrations en charbon et suie mesurées dans certains sédiments datant de la limite du Crétacé et de l'ère tertiaire (65 Ma) témoignent de vastes incendies qui ont injecté d'énormes quantités de particules et de fumées dans l'atmosphère, ayant pu contribuer au refroidissement du climat de la Terre et aux grandes extinctions biologiques (Wolbach et al., 1985; Wolbach et al., 1988).

Actuellement, les feux anthropiques contribuent significativement au changement climatique, puisqu'ils représentent la seconde source de gaz à effet de serre après la combustion d'énergie fossile industrielle (Andreae, 1991). Les effets immédiats des feux concernent d'une part la chimie de l'atmosphère avec les émissions de gaz à effets de serre et d'aérosols carbonés (Penner et al., 1992), et d'autre part la dynamique des écosystèmes tropicaux. En effet, outre la dénitrification des sols, les feux modifient l'hydrologie des régions qu'ils affectent i) directement, avec l'émission de carbone particulaire dans la troposphère qui forme des *nuclei* potentiels pour la condensation des nuages (Cachier and Ducret, 1991; Ducret and Cachier, 1992) ii) indirectement, la déforestation diminuant l'évapo-transpiration, la pluviosité et le ruissellement.

Plus de 90% des feux actuels sont provoqués par les activités humaines (les éclairs, les éruptions volcaniques et les phénomènes d'auto-combustion étant les uniques causes naturelles de feux). Mais le développement de grands incendies reste néanmoins tributaire des conditions climatiques et écologiques (Pyne, 2001). Par ailleurs, l'actuel changement climatique global modifie la structure et la composition des forêts, mais aussi le comportement des feux (Fosberg et al., 1990). Plus le climat se réchauffe, plus le risque d'incendies augmente, et plus l'émission de gaz à effet de serre augmente.

1.2 Les enregistrements des feux passés

La variabilité des feux au cours des derniers cycles climatiques reste encore largement méconnue. A l'échelle du Pléistocène, les enregistrements de suie des sédiments de l'Atlantique subéquatorial suggèrent le développement des feux de savane au début (Bird and Cali, 1998) ou pendant (Verardo and Ruddiman, 1996) les périodes glaciaires, et ce depuis 400 ka. Pour les autres régions, les données sont presque inexistantes, excepté pour la région Indo-Pacifique qui révèle d'importants feux de végétation entre 65 et 35 ka (Kershaw et al., 2002) en relation probable avec l'arrivée de l'homme moderne dans la région (Roberts et al., 1994; Turney et al., 2001).

Les enregistrements continentaux (lacs et tourbières) des feux de biomasse en région intertropicale sont également rares malgré leur intérêt complémentaire évident: proximité des sources, temps de résidence du carbone inférieur à celui du domaine océanique, meilleure résolution chronologique, et possibilité d'identifier les phénomènes locaux et régionaux par l'étude de plusieurs sites. Les résultats actuels indiquent une association générale entre les changements de concentration de charbon et les spores de graminées, ainsi qu'une augmentation de la fréquence des feux pendant les périodes favorisant le développement de la savane (Burney, 1987; Mworia-Maitima, 1997; Hope and Pask, 1998). Pour la période Holocène, une synthèse d'enregistrements continentaux de charbons (Europe, Amérique du nord et Centrale, région Amazonienne) (Carcaillet et al., 2002) montre que la dynamique des feux a été associée aux principales tendances hydrologiques et climatiques régionales. Globalement, la déforestation par le feu s'est accrue au cours de l'Holocène, en association avec l'activité anthropique (Bird and Cali, 1998).

1.3 L'observation et la modélisation des feux actuels

La télédétection spatiale, grâce à des capteurs sensibles aux spectres visible et infrarouge, permet de détecter les anomalies de température, les feux, et les nuages de fumée. Le calcul de la superficie de végétation brûlée permet ensuite d'évaluer les émissions liées aux incendies. Des bases de données mondiales sur les feux actifs sont disponibles sur le web (http://firemaps.geog.umd.edu/GlobalFires_HTML/viewer.htm/) sous forme de mise en cartes

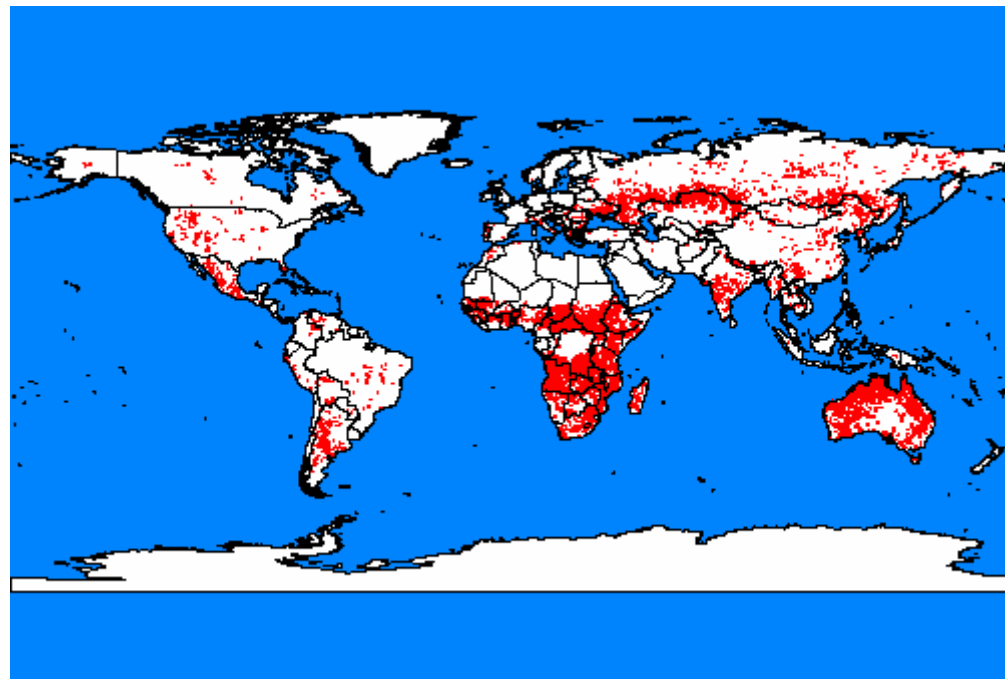


Figure 1-1 : Détection des feux actifs pour l'année 2000
[\(http://www.grid.unep.ch/activities/earlywarning/preview/ims/gba/\).](http://www.grid.unep.ch/activities/earlywarning/preview/ims/gba/)

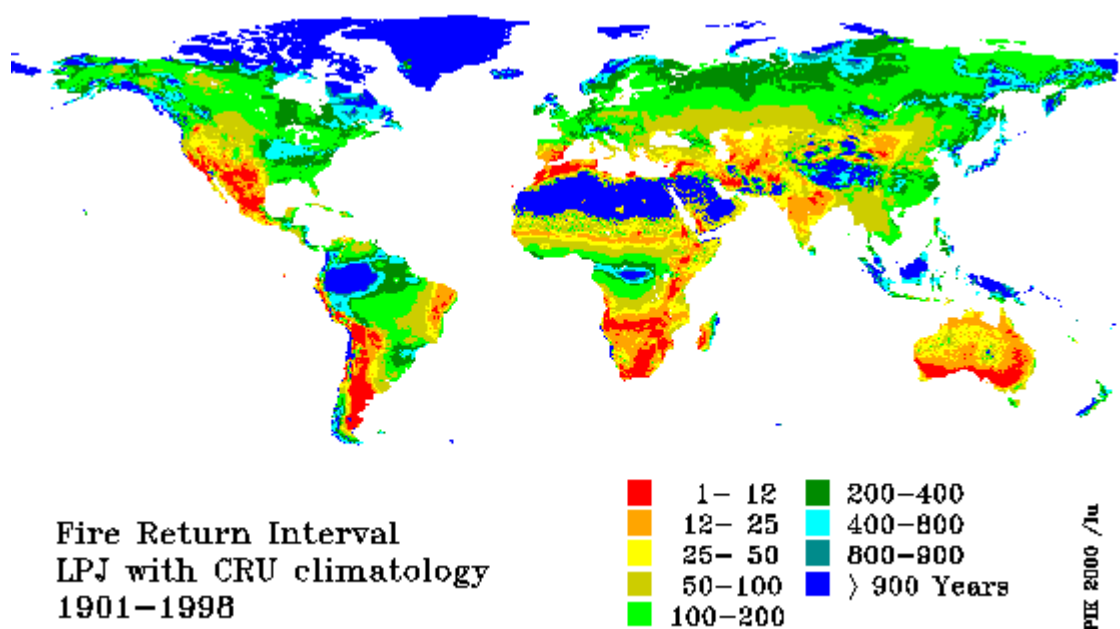


Figure 1-2 : Historique de la fréquence des feux simulée par le modèle LPJ-DGVM pour la période 1901-98 (<http://www.pik-potsdam.de>).

avec une résolution de 1 km (figure 1-1). Il apparaît clairement que les régions d'Afrique, du SE Asiatique, d'Amérique Centrale et d'Australie, situées dans la Zone de Convergence InterTropicale (ITCZ), ont été les plus touchées par les incendies durant l'année 2000.

L'étude des feux actuels et passés montre que l'extension des feux et l'augmentation de leur fréquence dépendent du prolongement des périodes sèches, mais aussi de l'accumulation de biomasse végétale (Heinselman, 1973; Carcaillet and Richard, 2000). Grâce aux modèles de circulation générale (MCG), il est possible de prendre en compte les processus climatiques et l'état du combustible. Ces modèles considèrent généralement que l'estimation de la teneur en eau de la litière est le principal agent de contrôle du développement des feux. La longueur de la saison sèche pendant laquelle le combustible présente une humidité inférieure à un seuil critique est utilisée pour calculer la surface brûlée annuelle (Thonicke et al., 2001) (figure 1-2). Cette aire est rapportée à la surface observée pour obtenir une moyenne de retour des feux, ou fréquence de feux, qui peut être comparée avec les observations actuelles. Pour le vingtième siècle, les modèles sont en bon accord avec la plupart des régions brûlées au cours de l'année 2000 (figures 1-1 et 1-2). Pour le futur, si les MCG prévoient des vagues de sécheresse accrues dans certaines forêts tropicales, la fréquence de grands incendies incontrôlés et dévastateurs comme ceux du SE Asiatique pourrait augmenter (Goldamer and Seibert, 1990).

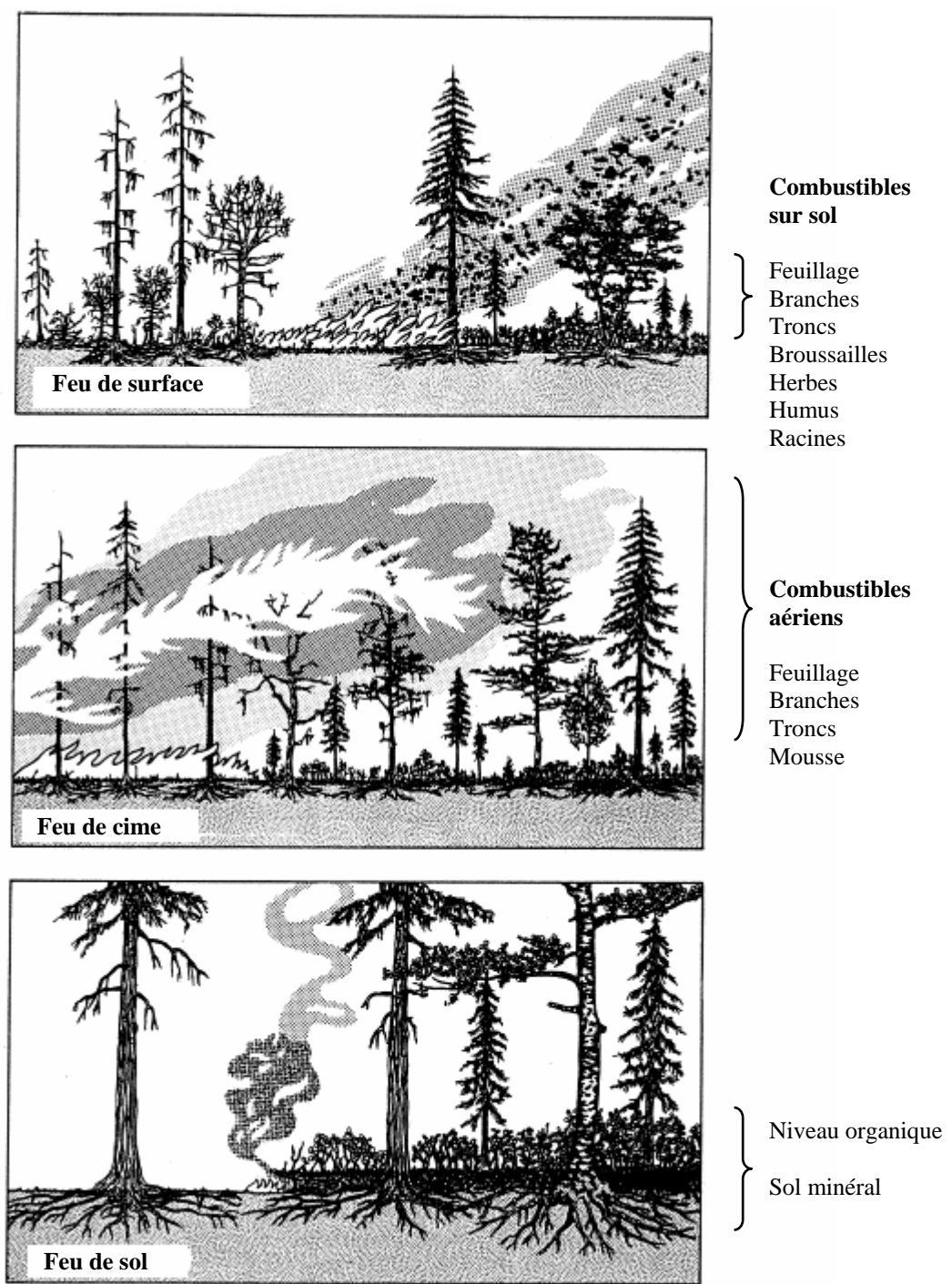
1.4 Caractéristiques des feux

Les feux sont une des composantes essentielles de l'agriculture et de l'économie moderne et passée (déforestation, pratiques agricoles, besoins industriels et domestiques) (Coutinho, 1990; Koonce and Gonzales-Caban, 1990). Dans de nombreuses régions, les pratiques agricoles et forestières durables, ainsi que le pastoralisme, dépendent du recours aux feux (Pielou, 1952). Certains écosystèmes sont adaptés à l'occurrence régulière d'incendies qui jouent un rôle régénérant sur l'ensemble de la chaîne écologique (Chidumayo et al., 1996). Cela concerne par exemple les savanes tropicales en Afrique et Amérique du sud (Coutinho, 1990), les forêts de conifères boréales et Asiatiques (Goldamer and Penafiel, 1990), et de nombreux écosystèmes australiens (Gill et al., 1990). En revanche, dans d'autres écosystèmes, comme les forêts tropicales humides en Amazonie et en Asie, les incendies ont des effets destructeurs. Ils surviennent dans des conditions météorologiques extrêmes et ont de graves effets sur

l'économie, la santé et la sécurité de l'homme, de façon comparable aux risques naturels majeurs (IPCC 2001).

La pyrolyse (destruction par le feu) se produit lorsqu'un certain seuil de température interne est atteint (variable selon la teneur en carbone du combustible par rapport à sa teneur en eau). Par la suite, si le feu s'entretient tout seul et que les vapeurs produites sont suffisamment oxygénées, une flamme naît. En fonction des caractéristiques du combustible et du feu, trois types d'incendies peuvent être distingués (Scott, 1989) (figure 1-3).

Figure 1-3 : Types d'incendies naturels et sources de combustible (Scott, 1989).



- Le feu de surface ou feu courant rampe au-dessus du sol sur la litière des forêts formée d'éléments secs légers et combustibles. Le feu de surface dégage beaucoup de flammes et de chaleur, rayonnant d'une broussaille à l'autre et pouvant prendre de l'altitude s'il rencontre des buissons et des arbustes. Il décolle alors de la surface et devient un feu de cime.

- Le feu de cime porté par le vent est le plus rapide et le plus intense des feux. Des flammes d'une vingtaine de mètres de hauteur, liées au vent qui renouvelle l'oxygène peuvent atteindre 1600°C. Dans une forêt claire, seule l'énergie du feu de surface qui l'a engendré permet le passage de cimes en cimes. Il s'appelle alors feu de cime dépendant. En revanche, là où la couronne des arbres ombrage plus des trois quarts du sol, le feu de cime devient autonome et feu de cime roulant.

- Le feu de sol s'alimente à quelques centimètres de profondeur sous terre, et consume l'humus du sol couche par couche, depuis la surface. Le feu de sol descend vers les couches profondes, où l'oxygène est raréfié. Sans flamme ni fumée, il peut couver en attendant un souffle de vent pour repartir. Il stérilise le sol en détruisant les racines et toute forme de vie animale microscopique.

Les incendies intenses créent de puissants courants de convection qui entraînent des petits végétaux en flammes à des altitudes supérieures à 5 kilomètres (km), pouvant ensuite être emportés par le vent jusqu'à 10 ou 20 km (Strazzulla, 1991). La vitesse de progression des grands incendies permet de différencier : i) Les tempêtes de feu, qui sont un embrasement généralisé, engendré par la fusion d'un grand nombre de petits foyers. ii) Les conflagrations, qui présentent un front mobile concentré sur une zone relativement étroite, mais qui peut avancer sur des distances considérables. Lors d'un grand incendie, la chaleur émise fait monter la fumée en colonnes puis en volutes de convection. Une fumée invisible résulte d'un feu intense, où l'air est très sec et le vent puissant, les gaz séchant au fur et à mesure qu'ils s'élèvent dans la colonne de chaleur. Si les hydrocarbures restent en concentration suffisante pour diffracter la lumière, ils donnent une couleur bleutée à la fumée. Si le vent et le feu ne sont pas assez puissants et que l'oxygène manque, la combustion est incomplète et la fumée de couleur blanche. L'eau se condense en gouttelettes qui se concentrent et ne diffractent plus la lumière mais opacifient l'air. Plus la fumée contient de grosses particules, plus sa couleur s'assombrit.

1.5 Quantité de biomasse brûlée et feux tropicaux

Les estimations globales de biomasse brûlée et de leurs émissions ont été calculées il y a une dizaine d'années par plusieurs auteurs (Seiler and Crutzen, 1980; Hao et al., 1990; Andreae, 1991). Les résultats sont exprimés en terra grammes (Tg) de matière sèche (ms) ou de carbone (C) par an, Tg C/an, soit 10^{12} grammes (g) de C, ou million de tonnes (Mt) de C.

La masse brûlée (**M**) est calculée en fonction de la surface brûlée (**A**), de la quantité de matière organique par unité d'aire (**B**), de la partie de la biomasse terrestre par rapport à la biomasse totale (**a**), et de la capacité à brûler des espèces concernées (**b**) :

$$\mathbf{M} \text{ (grammes de matière sèche par an, g ms/an)} = \mathbf{A} \text{ (m}^2\text{/an)} \times \mathbf{B} \text{ (gdm/an)} \times \mathbf{a} \times \mathbf{b}$$

En considérant que la biomasse continentale contient 45% de carbone, la masse de carbone émise (principalement sous forme de CO₂) est ensuite estimée (Seiler and Crutzen, 1980).

Ces estimations montrent un lien étroit entre les activités humaines et la combustion de biomasse végétale. En effet, plus des trois-quarts de la population vit dans les tropiques, et les pays en voie de développement sont particulièrement sujets aux feux (tableaux 1-1 et 1-2). Dans ces régions, les feux de végétation, mais aussi les feux domestiques qui utilisent le bois comme combustible sont très importants (cuisine, chauffage, métallurgie, fabrication de poteries, etc.). Afin de limiter les coûts de transport vers les villes, le bois est généralement remplacé par le charbon, moins encombrant et de plus forte capacité calorifique. La proportion de carbone introduite (sous la forme de bois) par rapport à celle produite (sous la forme de charbon) qui varie entre 2.0 et 1.2, est prise ici comme étant égale à 1.4. La quantité de charbon brûlée est donc multipliée par 1.4 pour tenir compte des pertes dues à l'étape de transformation. Les pays tropicaux ajoutent donc 28 Tg C/an (du tableau 1-1 : 20 Tg ms/an pour les tropiques) par la production et la combustion de charbon aux émissions totales tropicales de 3410 Tg C/an (tableau 1-2) comprenant les feux de forêts et de savane, l'utilisation de bois comme combustible, et l'incinération des déchets agricoles. La grande disparité de la collecte et de l'utilisation de bois domestique place les estimations entre 1050 et 1430 Tg ms/an pour le bois combustible (tableau 1-1). Bien que la pollution atmosphérique engendrée par les pratiques agricoles dans les régions tropicales soit très importante, son estimation reste également difficile. En supposant que la quantité de déchets agricoles équivaut à celle de céréales produites (FAO, 1986), la quantité globale de déchets agricoles brûlés équivaut à 2020 Tg ms/an (tableau 1-1), dont 67% provient des régions tropicales.

Tableau 1-1 : La consommation de bois combustible, charbon, et déchets agricoles dans les régions tropicales et extra-tropicales (Andreae 1991).

Région	Population (1985, mill.) ^a	Tg ms/an			
		Bois combustible ^b	Bois combustible ^c	Charbon ^b	Déchets agricoles ^d
Tropiques :					
Amérique	430	150	170	7.5	200
Afrique	550	240	240	9.3	160
Asie	2820	490	850	3.3	990
Océanie	25	6	8	0	17
Total tropiques	3830	890	1260	20	1360
Etats-Unis et Canada	260	80	80	0.5	250
Europe de l'Ouest	380	40	40	0.2	170
URSS et Europe de l'Est	390	50	50	0.2	230
Total mondial	4840	1050	1430	21	2020

a. (FAO, 1986)

b. (FAO, 1989)

c. (Andreae, 1991)

d. Basé sur la production de céréales

Tableau 1-2 : Les feux de biomasse en régions tropicales (Andreae 1991).

Région	Tg ms/an				Total région	
	Forêt ^a	Savane ^a	Bois combustible ^b	Déchets agricoles ^b	Tg ms/an	Tg C/an
Amérique	590	770	170	200	1730	780
Afrique	390	2430	240	160	3210	1450
Asie	280	70	850	990	2190	980
Océanie	—	420	8	17	450	200
Total tropiques	1260	3690	1260	1360	7580	3410

a. (Hao et al., 1990)

b. Du tableau 1-1

Selon (Hao et al., 1990), les feux de savanes émettent trois fois plus de carbone dans l'atmosphère que les feux de forêts. En Afrique (tableau 1-2) les feux de savane représentent quasiment 90% des émissions de feux de forêts et de savanes et presque un tiers des émissions globales des feux. La déforestation des forêts tropicales par le feu rejette 570 Tg C/an, contre 130 Tg C/an pour les forêts tempérées et boréales (tableau 1-3). L'élimination des déchets agricoles par le feux émet 910 Tg C/an. L'utilisation de bois pour la cuisine et le chauffage

produit 640 Tg C/an. Les émissions totales des feux tropicaux (3440 Tg C/an) représentent donc 87% des émissions totales imputables aux feux de biomasse (3940 Tg C/an, tableau 1-3).

Tableau 1-3 : Estimations globales de la quantité annuelle de biomasse brûlée et du carbone émis dans l'atmosphère (Andreae 1991).

Source	Biomasse brûlée (Tg ms/an)			
	Seiler and Crutzen ^a	Hao et al. ^b	Andreae ^c	Carbone émis (Tg C/an) ^d
Savanes	1190	3690	3690	1660
Déchets agricoles	1900	660	2020	910
Forêt tropicale	2420	1260	1260	570
Bois combustible	1050	620	1430	640
Forêt tempérée et boréale	280	—	280	130
Charbon	—	—	21	30
Total mondial	6840	6230	8700	3940

a. (Seiler and Crutzen, 1980)

b. (Hao et al., 1990)

c. Forêt tropicale et savane de Hao et al. (1990); Forêt tempérée et boréale de Seiler and Crutzen (1980); bois combustible, charbon, et déchet agricole de la tableau 1-1

d. Basé sur une teneur en carbone de 45% dans la matière sèche. Dans le cas des charbons, le taux de combustion (basé sur les statistiques de production de la FAO) a été multiplié par 1.4 pour tenir compte des pertes de la fabrication

1.6 Les émissions gazeuses

Dioxyde de carbone (CO₂)

Les estimations des émissions atmosphériques liées aux feux actuels dépendent à la fois du volume de biomasse brûlée, mais aussi de la variabilité de la combustion de la matière organique (représentée ici par CH₂O) selon la réaction :



Cette réaction équivaut à celle de la respiration photosynthétique (photosynthèse de droite à gauche, et respiration de gauche à droite), puisque les feux renvoient à l'atmosphère le CO₂ prélevé par les plantes pendant leur période de croissance. L'efficacité de combustion, généralement comprise entre 85 et 95% (Ward et al., 1996), est ici fixée à 90% (i.e. 90% du C émis est sous forme de CO₂). Ainsi, la combustion périodique des savanes influe peu sur l'effet de serre lié au CO₂, parce que le CO₂ émis par le feu est généralement réincorporé dans l'année dans le même écosystème. A l'échelle annuelle, les 1660 Tg C/an émises par les savanes (tableau 1-3) sont donc à retrancher du bilan brut de CO₂ (3500 Tg C/an, tableau 1-4). En revanche, la

contribution de la déforestation des forêt tropicales est très importante, puisque le CO₂ émis par la combustion de l'important stock de biomasse forestière n'est pas réabsorbé par la végétation herbacée ou la culture de céréales. Les émissions nettes de carbone émis sous forme de CO₂ par les feux de biomasse atteignent ainsi 1800 Tg C/an, soit 26 % des émissions globales de CO₂ par combustion, contre 5200 Tg C/an imputables aux rejets industriels (tableau 1-4).

Tableau 1-4 : Contribution des feux de biomasse aux émissions atmosphériques globales (incluant les feux de biomasse, Andreae 1991).

Composés émis	Feux de biomasse (Tg élément/an)	Toutes sources (Tg élément/an)	Feux de biomasse (%)
CO ₂ brut (combustion)	3500	8700 ^a	40
CO ₂ net (déforestation)	1800	7000 ^b	26
Monoxyde de carbone (CO)	350	1100	32
Méthane	38	380	10
Oxyde nitrique	8.5	40	21
Ammoniac	5.3	44	12
Gaz sulfuriques	2.8	150	2
Chlorure de méthyle	0.51	2.3	22
Ozone	420	1100	38
Matière particulaire totale	104	1530	7
Carbone organique particulaire	69	180	39
Carbone élémentaire ou Black Carbon ^{c,d}	6-28	19-52	~50

a. Feux de biomasse et combustible fossile

b. Déforestation et combustible fossile

c. (Crutzen and Andreae, 1990)

d. (Penner et al., 1993)

Autres gaz

Les autres gaz à effet de serre émis par les feux, le monoxyde de carbone (CO), le méthane (CH₄), les composés azotés comme les oxydes d'azote (NO et NO₂) restent en totalité dans l'atmosphère. Ce mélange de gaz conduit à la formation photochimique d'ozone troposphérique par les mêmes processus qui conduisent à l'augmentation des concentrations d'ozone dans les régions urbaines en été. Comme les feux de végétation ont lieu régulièrement (en particulier dans les tropiques) et affectent de grandes étendues, ils constituent une source importante de l'ozone troposphérique (38% du bilan global, tableau 1-4). Les émissions de chlorure de méthyle (22% de source pyrogénique) détruisent l'ozone stratosphérique (tout comme le bromure de méthyle, encore quarante fois plus actif).

Suite aux feux, les émissions d'oxyde nitrique et de nitrates des sols augmentent. Elles

peuvent même surpasser la production instantanée de ces gaz par le feu lui-même (8.5 Tg N/an). Ces composés participent de façon complexe à la formation d'ammoniac, et les feux contribuent à 12% des rejets totaux supposés d'ammoniac (44 Tg N/an), la principale source étant la dégradation des sols.

Les feux représentent moins de 3% des émissions de sulfures anthropiques, et 1.3% dans le bilan atmosphérique des sulfures. La présence d'acide nitrique et surtout d'acides organiques naturels et biogéniques (en particulier les acides formiques et acétiques émis par les feux) est pour beaucoup dans les pluies acides des tropiques. Alors que dans les régions industrialisées tempérées, l'acide sulfurique prédomine avec l'acide nitrique (Andreae, 1991; Lacaux et al., 1993).

1.7 Les émissions solides

En plus des gaz, les feux émettent dans l'atmosphère un grand nombre de particules. Les fumées émettent actuellement environ 104 Tg/an de matière particulaire, pour la plupart composée de carbone organique (69 Tg/an), et dont environ un quart est sous forme de carbone élémentaire de type Black Carbon (BC) (tableau 1-4). Cependant, il est difficile de quantifier ces composés, puisque les méthodes d'extraction sont peu contraintes (chapitre 2) et que la concentration de BC au sein des particules de fumée varie non seulement en fonction du type de matériel brûlé, mais aussi et surtout en fonction de l'efficacité de la combustion (Ducret and Cachier, 1992).

Des tests expérimentaux de combustion ont été établis afin de calculer le taux de formation de BC par le feu (figure 1-4). La méthode utilisée pour mesurer le BC est celle développée par (Kuhlbusch, 1995) qui consiste à

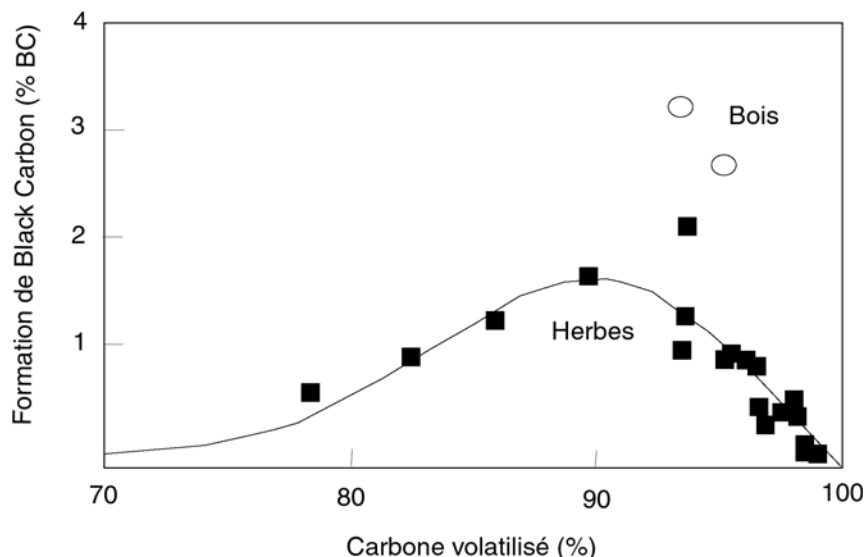


Figure 1-4 : Formation de BC mesurée après combustion expérimentale en fonction de degré de combustion pour les échantillons d'herbes (carrés et ligne noire) et pour deux échantillons de bois décidu.

oxyder la matière organique résiduelle par attaque à l'acide nitrique et traitement thermique. Pour les savanes, le rapport du BC dans le résidu par rapport au carbone émis sous forme de CO₂ est compris entre 0.7 et 2%. La formation de BC par le bois décidu (représentant le bois utilisé comme combustible) est encore plus importante, avec 3.42% et 2.81% (Kuhlbusch et al., 1996). La formation de BC totale annuelle ainsi calculée est comprise entre 50-270 Tg de BC (Kuhlbusch and Crutzen, 1995). En considérant que 90% du BC produit par les feux reste en place, la fraction de BC atmosphérique émis par le feu équivaut à 6-28 Tg C/an (Crutzen and Andreae, 1990). Les savanes produisent à elles seules 10-26 Tg de BC par an (dont 70% pour les savanes africaines), soit 4-52% du BC total produit annuellement par les feux (Kuhlbusch et al., 1996). L'estimation des émissions de BC par les combustions industrielles de matériel fossile, 13-24 Tg BC/an selon (Penner et al., 1993) (tableau 1-4) est elle aussi relativement incertaine. Des études récentes (Penner et al., 2001) proposent une production de 7 Tg de BC/an pour le matériel fossile, tandis que 70 Tg de fumée composée de carbone organique et BC serait émise par les incendies.

1.8 Impact radiatif des aérosols carbonés

Actuellement, les aérosols anthropiques, majoritairement issus de la combustion des matières organiques fossiles et de la biomasse, altèrent significativement le bilan radiatif terrestre. Mais l'ampleur du forçage climatique causé par ces aérosols est très incertaine (figure 1-5, IPCC 2001). L'effet radiatif et absorbant des aérosols carbonés dépend de la quantité de BC et de son degré de mixité au sein des autres aérosols (Jacobson, 2001; Penner et al., 1992). La présence d'aérosols augmente indirectement le nombre de noyaux de condensation des nuages et l'effet radiatif des nuages, et diminue les précipitations (Chameides and Bergin, 2002; Menon et al., 2002). Un forçage radiatif négatif s'exerce sur les régions les plus touchées par les incendies, tandis que les aérosols émis par la combustion de fuel fossile qui contiennent un rapport BC/C_{organique} supérieurs exercent un forçage positif autour des régions industrielles (IPCC, 2001). On estime que le forçage radiatif direct est de -0.4 Wm^{-2} pour les sulfates, de -0.2 Wm^{-2} pour les aérosols provenant de la combustion de biomasse, de -0.1 Wm^{-2} pour les aérosols carbonés organiques provenant de la combustion des combustibles fossiles et de $+0.2 \text{ Wm}^{-2}$ pour les aérosols carbonés de type suie provenant de la combustion des combustibles fossiles (figure 1-5).

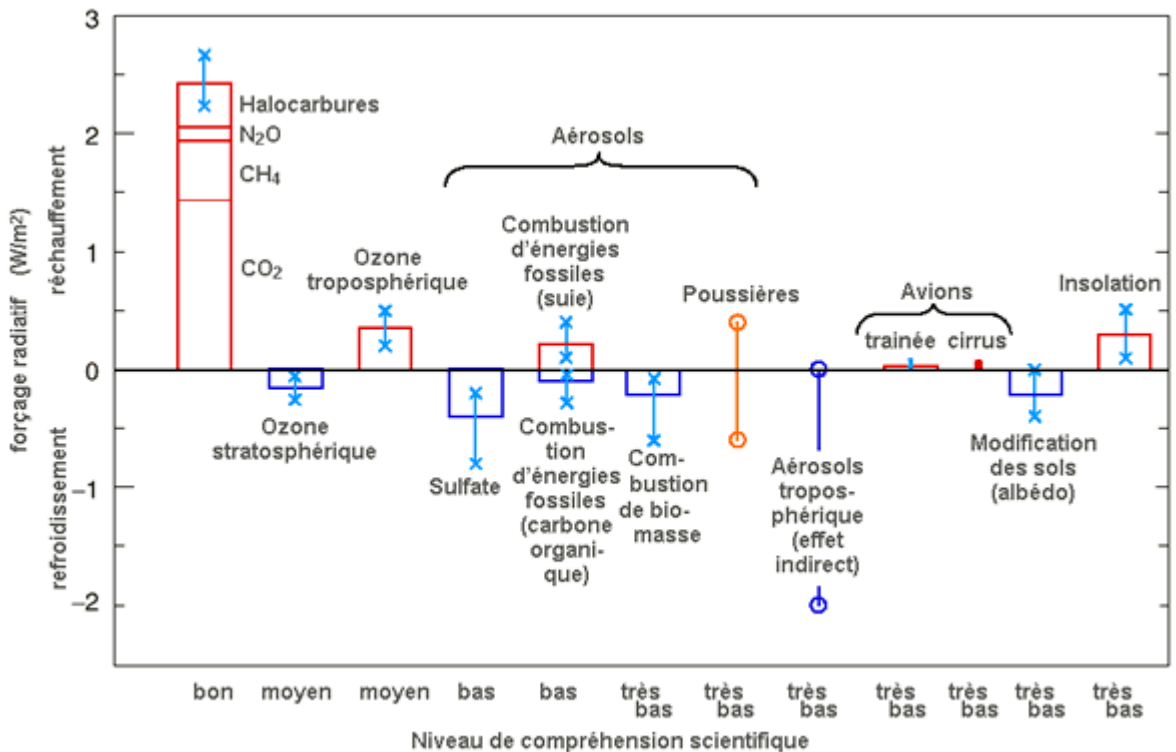


Figure 1-5 : Forçage radiatif moyen global du système climatique en l'an 2000 par rapport à 1750 (IPCC 2001).

De récents modèles (Menon et al., 2002) ont montré que la variation de la teneur en BC au sein des aérosols pourrait être, en partie au moins, responsable des perturbations climatiques observées ces dernières années en Asie. La figure 1-6 montre la simulation du changement des précipitations d'été. Dans l'expérience A, les aérosols sont choisis comme représentatifs des aérosols industriels chinois,

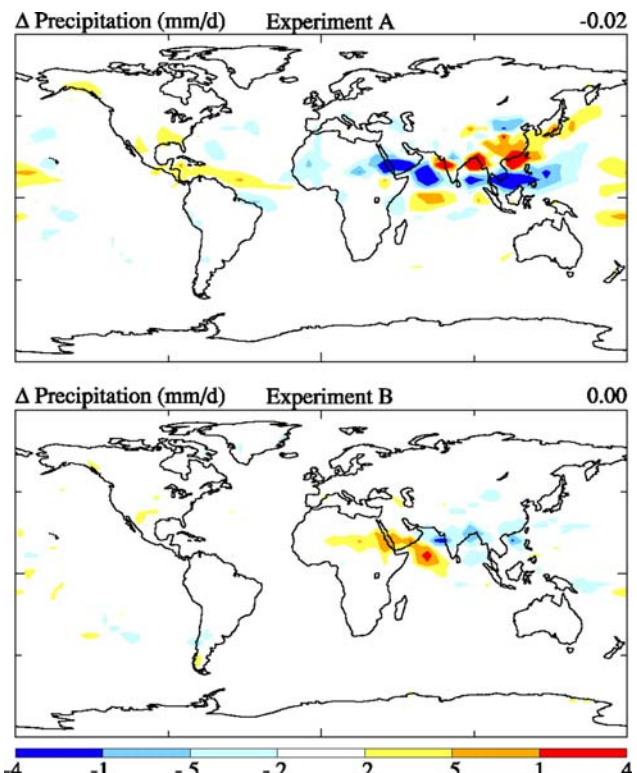


Figure 1-6 : Modélisation de changements des précipitations d'été (mm/jour) dans le cas d'aérosols contenant du BC, Expérience A, et dans le cas d'aérosols blancs, Expérience B.

i.e. riches en BC. Dans l'expérience B, les aérosols ne contiennent pas de BC, ils sont considérés comme « blancs ». Les simulations de précipitations estivales (mm/jour) montrent qu'une proportion relativement faible de BC peut avoir un impact climatique important. Dans l'expérience A, les aérosols contenant du BC augmentent les précipitations sur le Sud de la Chine, en Inde, et en Birmanie. Les changements de précipitations sont moindres avec l'expérience B, et contrairement aux observations, il n'y a pas d'augmentation de précipitations dans le Sud de la Chine. Les aérosols réduisent la surface de radiation solaire, mais ils modifient aussi les transferts de chaleur atmosphériques, et donc le bilan hydrologique régional.

1.9 Importance des feux dans le cycle du carbone

Comme le montrent l'augmentation des rejets de carbone anthropiques totaux (Tg C/an) et l'augmentation du CO₂ atmosphérique mesuré (figure 1-7, tableau 1-4), l'homme modifie considérablement le cycle du carbone. La concentration en CO₂ atmosphérique était de 280 partie par million en volume (ppmv) en 1700, alors qu'elle atteint 370 ppmv actuellement (soit une augmentation de 32%). Cette concentration avait été relativement constante (~275 ±10 ppmv) au cours des 1000 années précédant l'ère industrielle qui se caractérise par une augmentation rapide des teneurs en CO₂ atmosphérique (+1.5 ppmv ou 0.4% par an ces 20 dernières années).

Chaque année, les végétaux terrestres absorbent par photosynthèse 102 Gt C atmosphérique sous forme de CO₂, et relâchent 100 Gt C dans l'atmosphère par respiration et décomposition de la matière organique (1 Gt = 10¹⁵ grammes, soit 1000 Tg) (figure 1-8). La production primaire nette sur les continents est estimée à 50 Gt C/an. Les eaux de surface des océans (couche euphotique) absorbent 92 Gt C/an et rejettent 90 Gt C/an. Le stock atmosphérique de carbone est de 750 Gt C, sous forme de CO₂, principal gaz à effet de serre. Une petite partie des particules qui tombent sur les fonds marins n'est pas dégradée (0,2 Gt C) mais progressivement enfouie dans les sédiments (78 000 000 Gt C), et soustraite du cycle du carbone car incorporée dans les couches géologiques. Le stock d'énergie fossile est compris entre 5 et 10000 Gt C.

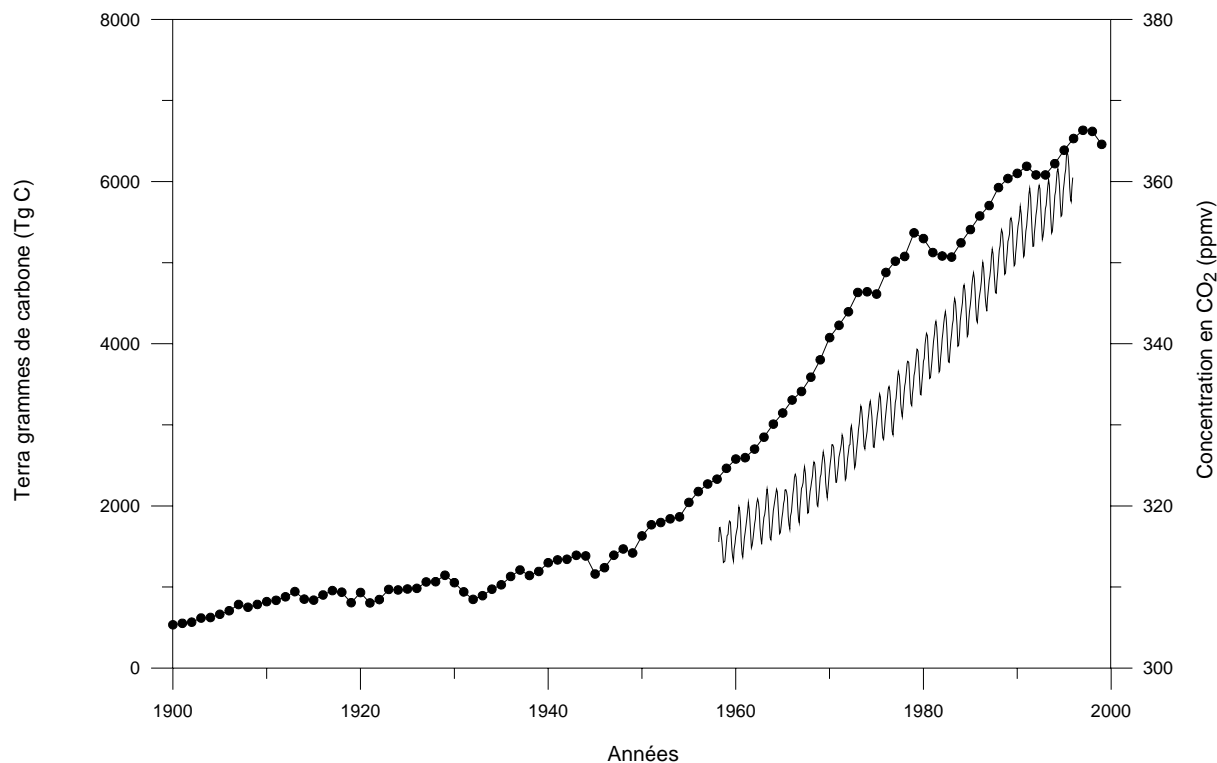


Figure 1-7 : Augmentation des rejets totaux annuels de carbone anthropique en Tg C (points noirs, Marland et al., 2002) et courbe mensuelle de CO₂ atmosphérique mesurée à Mona Loa (Hawaï) entre 1958 et 1995 en ppmv (Keeling and Whorf, 2002).

Les activités humaines injectent chaque année un surplus de 7 Gt C, avec 5 Gt C issues de la combustion d'énergie fossile par les industries et 2 Gt C dues aux feux de biomasse. Le bilan est excédentaire de 3 Gt C/an. Dans le cycle du carbone, les feux jouent un rôle significatif mais complexe. A court terme, leur émission de CO₂ dans l'atmosphère est une source conséquente de gaz à effet de serre, mais l'enfouissement de résidus carbonés solides dans les sols et les sédiments pourrait constituer un puits de carbone au cours des temps géologiques. Le BC formé par les savanes représente ainsi un puits de CO₂ de 10-26 Tg de C/an (Kuhlbusch et al., 1996). Sur les 50-270 Tg de BC produit annuellement par les feux, 40 et 240 Tg C/an restent sur place tandis que 6-28 Tg C/an sont émis sous forme d'aérosols (Crutzen and Andreae, 1990; Kuhlbusch and Crutzen, 1995). Les apports de BC aériens varient en fonction de la distance au continent, et de la zonation latitudinale des vents (Smith et al., 1973; Suman et al., 1997). Selon Suman et al. (1997), environ un tiers du BC émis dans l'atmosphère est transporté vers la

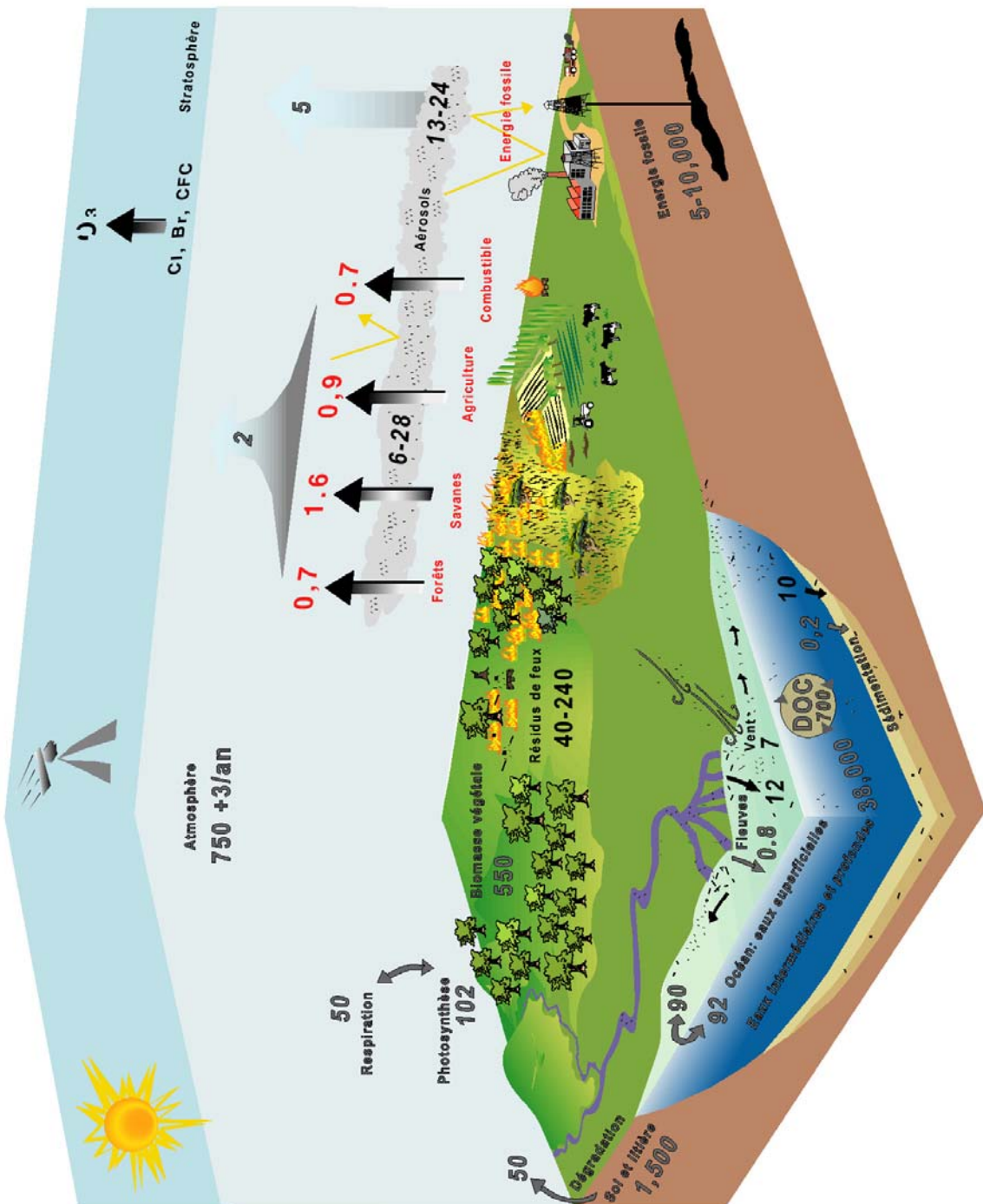


Figure 1-8 : Cycles du carbone (C) et du Black Carbon (BC). Pour le cycle du carbone, chiffres gris, les stocks de C sont en giga tonnes ($1 \text{ Gt} = 10^{15} \text{ g}$) de C et les échanges ou flux de C sont en Gt C/an. Pour les émissions des feux, les chiffres rouges sont en péta grammes de C ($1 \text{ Pg} = 10^{15} \text{ g}$). Pour le cycle du BC, chiffres noirs, les flux sont en terra grammes ($1 \text{ Tg} = 10^{12} \text{ g}$) de C/an.

surface des océans (7 Tg BC/an), et la moitié est déposée dans la partie côtière. Les rivières transportent 12 Tg BC/an vers les océans, et 95% du flux de l'ensemble du BC exporté vers les sédiments océaniques (environ 10 Tg BC/an) se dépose sur les plateaux continentaux (figure 1-8). Le BC piégé en domaine pélagique est ainsi enrichi en particules d'origine atmosphérique (partie 4).

1.10 Climat tropical et dynamique des feux

A l'échelle globale, la circulation atmosphérique générale engendre la succession de périodes décennales à millénaires humides et sèches, respectivement favorables à l'accumulation de combustible et à leur combustion, aujourd'hui largement contrôlée par l'homme (Wilgen et al., 1990). A l'échelle inter-annuelle, les climats de la zone intertropicale sont particulièrement favorables aux feux de biomasse. D'une part, les fortes précipitations et l'ensoleillement importants sont favorables à la croissance végétale et donc à l'accumulation de combustible. D'autre part, les sécheresses saisonnières privilégient les incendies.

1.10.1 Les feux en Afrique

En Afrique, le développement des feux est étroitement contraint par la dynamique du climat régional. La succession des saisons humides et sèches est déterminée par le déplacement de deux fronts séparant l'air chaud et sec continental des masses plus froides et humides océaniques (figure 1-9). La zone de confluence interocéanique (IOC) sépare l'air en provenance de l'Atlantique sud, de celui de l'Océan Indien. La Zone de Convergence InterTropicale (ITCZ) se forme par la convergence des masses d'air océaniques Sahélienne et Equatoriale. A l'échelle annuelle, les positions les plus extrêmes de ces limites sont atteintes en Juillet et en Janvier, qui correspondent respectivement à la saison sèche et à l'extension des feux de savane, dans l'hémisphère sud (Juillet) et dans l'hémisphère nord (Janvier) (Lacaux et al., 1993) (figure 1-10).

La saisonnalité des feux en Afrique illustre clairement l'interaction entre les feux, le climat, et l'homme. Les deux tiers des savanes poussent en Afrique, et l'Afrique est le continent qui brûle le plus (Hao et al., 1990). La distribution géographique des savanes Africaines dans les deux hémisphères montrent que les 2×10^8 ha de forêt sont encastrés dans les 1×10^9 ha de savane

dont environ la moitié brûle chaque année (Delmas et al., 1991). La majorité des feux de savane en Afrique se déroule entre les latitudes 15° nord et 15° sud. Les régions où la saison des pluies et la durée de sécheresse présentent une forte variabilité inter-annuelle sont les zones les plus propices aux incendies.

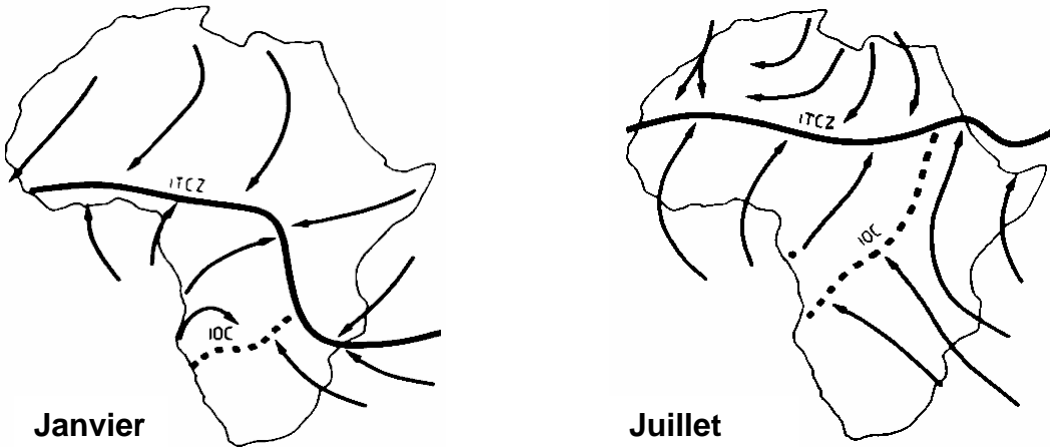


Figure 1-9 : L'extension de l'ITCZ et de l'IOC sur le continent Africain en janvier (à gauche) et en juillet (à droite) (http://ceos.cnes.fr:8100/cdrom-98/ceos1/casestud/burnbio/itcz_map.htm).

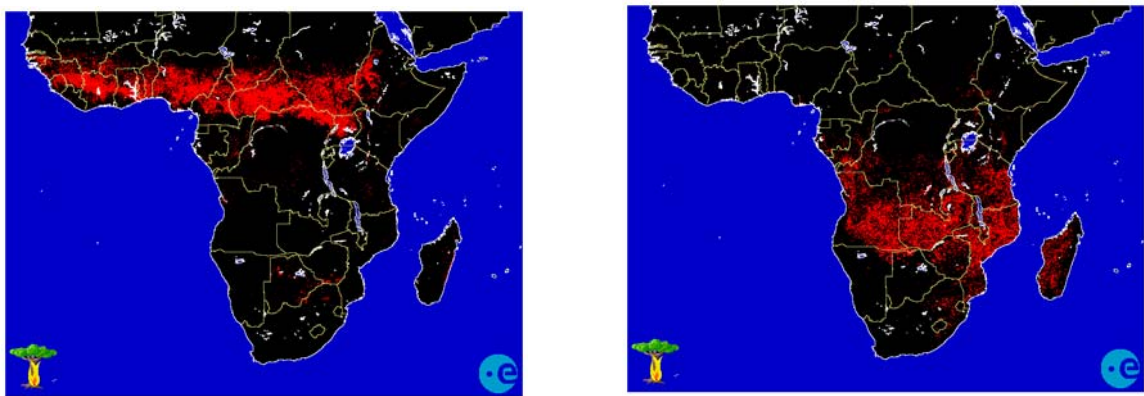


Figure 1-10 : La saisonnalité des feux sur le continent africain, avec les feux en janvier (à gauche) et en juillet (à droite) (<http://shark1.esrin.esa.it/FIRE/AF/AVHRR>.).

1.10.2 Les feux du SE Asiatique

Ces vingt dernières années, de grands incendies ont ravagé de vastes étendues de forêts tropicales humides en Asie du SE, en particulier en 1982/83, 1987/88, 1997/98. Ils étaient associés à d'extrêmes événements El Niño et représentatifs de l'état de sécheresse de la végétation (Goldamer and Seibert, 1990; Siegert et al., 2001). Comme le montre la figure 1-11, lors d'événements de type El Niño, les alizés s'inversent, et les précipitations habituellement abondantes sur le SE Asiatique se déplacent vers l'Est, provoquant une aridité exceptionnelle dans cette région. La végétation tropicale fragilisée par l'exploitation de homme est alors soumise à un fort stress hydrique et le feu se révèle dévastateur. La vulnérabilité de la forêt tropicale au feu augmente avec le passage d'incendies récurrents qui augmentent la mortalité des arbres en période de croissance et facilitent la conversion en zones de savane (Trapnell, 1959; Goldamer, 1999). Lors de grands incendies, l'émission d'aérosols augmente à l'échelle régionale, entraînés par les vents zonaux.

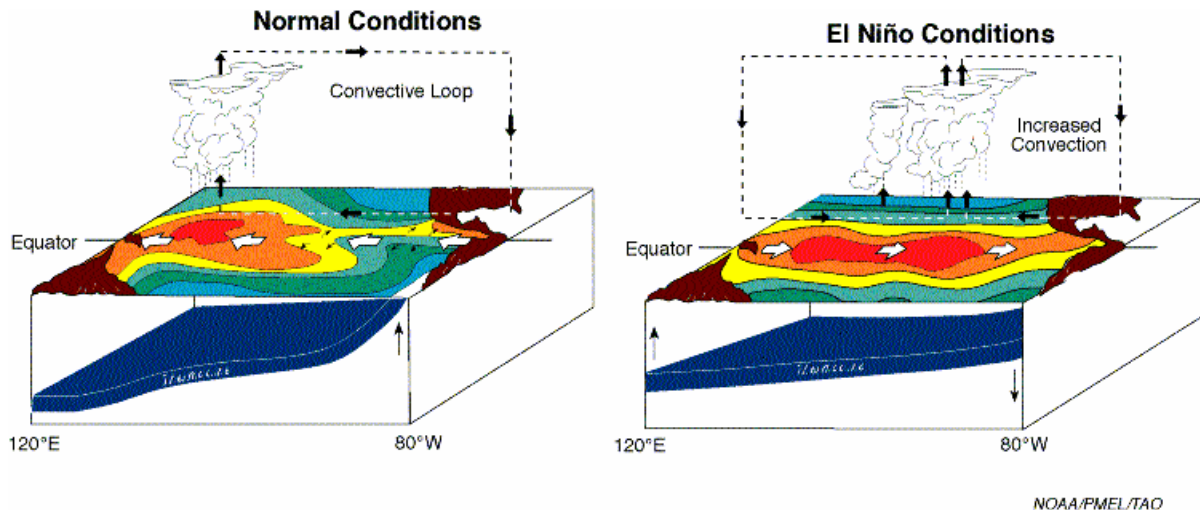


Figure 1-11 : Schéma représentant la circulation de surface et la position de la thermocline dans le Pacifique Ouest en situation normale (à gauche) et lors d'événements El Niño (à droite) (<http://www.pmel.noaa.gov/tao/elnino/nino-home.html>).

1.11 Conclusion

Cette synthèse illustre la complexité du rôle des feux vis à vis du cycle du carbone et du climat global. Elle montre l'importance des feux intertropicaux vis à vis

- 1) du bilan global des émissions atmosphériques de gaz et d'aérosols
- 2) du fonctionnement des écosystèmes actuels
- 3) de l'économie locale et régionale

Bien que la dynamique des feux actuels constitue une des composantes clé des interactions homme/climat, celle-ci est encore mal comprise pour les échelles de temps supérieures à quelques années, principalement en raison des incertitudes méthodologiques et du manque d'enregistrements sédimentaires.

2. Méthodologie

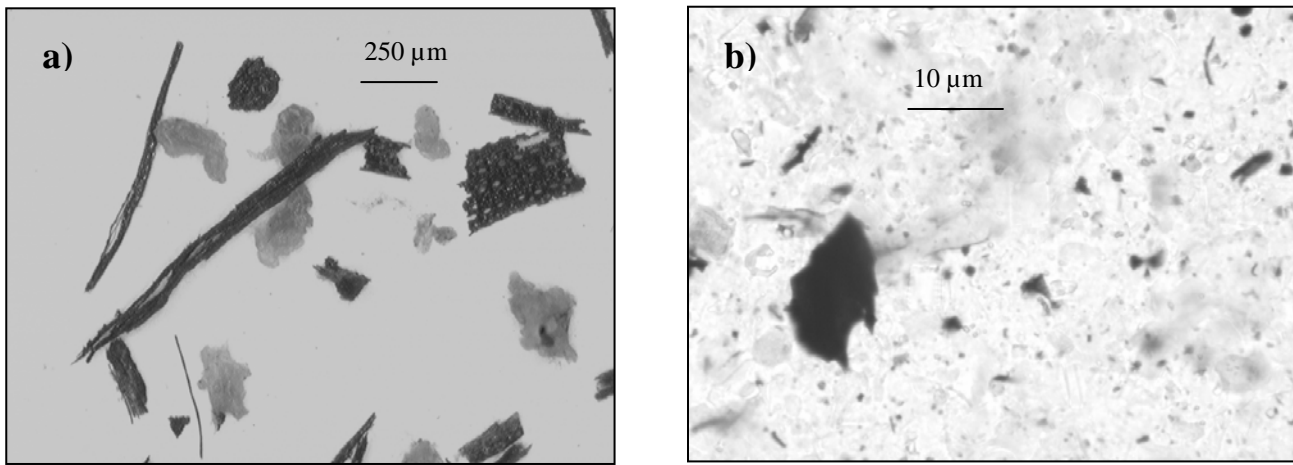
Les particules carbonées constituent actuellement les seuls marqueurs physico-chimiques directs de la dynamique des feux de biomasse. La quantification des charbons et des aérosols carbonés dans les sédiments s'effectue à l'aide de méthodes optiques (Clark, 1984) et chimiques (Wolbach and Anders, 1989).

2.1 Les méthodes optiques

Les méthodes optiques ont été développées en collaboration avec les études palynologiques dans les années 1980 (Clark, 1988a). Elles permettent d'étudier i) la fraction macroscopique (macrocharbons) après tamisage à des seuils variables en fonction des auteurs, et observation au microscope binoculaire (figure 2-1a) ii) la fraction microscopique (microcharbons) par comptage au microscope photonique (figure 2-1b). Si les charbons sont bien conservés, ils peuvent être extraits par flottation à l'aide de liqueurs denses et subir une analyse anthracologique, afin d'identifier l'essence (genre, voire espèce) (Carcaillet and Thimon, 1996) (tableau 2-1).

Pour les enregistrements lacustres, l'analyse d'images sur sections fines (après déshydratation du sédiment à l'acétone puis imprégnation par résine) peut renseigner sur la source, le transport, et la déposition des particules charbonnées (Clark, 1988b; Clark and Hussey, 1996). Afin d'estimer la surface réelle occupée par les charbons, ces analyses doivent néanmoins être complétées par des comptages sur lames, le plus souvent à l'aide de préparations palynologiques (Clark, 1988b; Carcaillet et al., 2001). L'inconvénient majeur des préparations palynologiques est qu'elles ne détruisent pas la matière organique, obligeant un comptage manuel des charbons, et qu'elles modifient les distributions de taille de particules.

Afin de limiter le fractionnement des charbons et de faciliter leur reconnaissance, l'absence de centrifugation et une oxydation préalable de la matière organique sont préconisés (Rhodes, 1998) (figure 2-1). Néanmoins, comme les seuils de détection des comptages manuels de charbons sont généralement supérieurs à 10 micromètres (μm), la fraction des



Figures 2-1 a et b : Images de charbons lacustres après oxydation de la matière organique par attaques à l'acide nitrique et eau oxygénée (Lac Masoko ; Tanzanie) a) macrocharbons au microscope binoculaire (après tamisage à 150 µm) b) microcharbons au microscope photonique.

aérosols n'est pas prise en compte. En effet, les aérosols de combustion entraînés par convection sont composés pour 50 à 80% de carbone particulaire ($\leq 1 \mu\text{m}$). Pour comparer la concentration en aérosols carbonés obtenue par extraction thermique ou chimique, le comptage automatisé des particules de charbons micrométriques est donc indispensable. La méthodes de détection et de comptage automatisé que nous avons développée (partie 2.6) tient compte de ces impératifs.

2.2 Les méthodes thermiques

Les méthodes thermiques (Cachier et al., 1989; Kuhlbusch, 1995) ont été récemment appliquées aux sédiments marins afin d'extraire les aérosols carbonés (Gustafsson et al., 1997; Gustafsson and Gschwend, 1998; Middelburg et al., 1999; Gustafsson et al., 2001) (tableau 2-1). Ces techniques reposent sur des mesures effectuées par des thermogrammes qui montrent qu'entre 340 et 375 °C (sous oxygène) le carbone organique est oxydé en dioxyde de carbone, contrairement aux aérosols carbonés (non volatiles) qui sont formés à des températures supérieures. Sur un thermogramme de sédiment lacustre riche en matière organique (figure 2-2) on constate que les pics de cellulose et de lignine se recouvrent, et qu'il n'existe pas toujours de limite franche entre les pics de lignine et de Black Carbon (BC) (Novakov et al., 1997). Il est aussi important de noter que les argiles perdent leur eau de constitution à des températures

Tableau 2-1 : Principales méthodes d'extraction des résidus traceurs de feux (modifié de Schmidt and Noack, 2000).

Matériel	Méthode				Référence
	Traitement	Oxydation	Détermination	Terminologie	
Techniques optiques					
sols	flottation		identification au microscope	charbon	(Carcaillet and Thinon, 1996)
sédiment lacustre	imprégnation		comptage au microscope	charbon	(Clark, 1988b)
sédiment lacustres	HCL, HF		comptage au microscope	charbon	(Clark, 1984)
sédiment lacustre, sol		H ₂ O ₂	comptage au microscope	charbon	(Rhodes, 1998)
Techniques thermiques					
plantes, aérosols	HCL, filtration	2 h à 340°	1100°C, CO ₂ colorimètre	suie	(Cachier, 1989)
plantes, cendres	NaOH, HCL, HNO ₃	2 h à 340° sous O ₂	chromatographie	black carbon	(Kuhlbusch, 1995)
matrices sédiments	broyage	24 h à 375°C sous O ₂	HCl puis chromatographie	suie	(Gustafsson et al., 1997)
matrices, sédiments		24 h à 375°C	HCl, filtré, combustion, MS	black carbon	(Gustafsson et al., 2001)
sédiments marins	broyage	14 h à 375°C sous O ₂ ± HNO ₃ à chaud	HCl puis chromatographie	suie	(Middelburg et al., 1999)
Techniques chimiques					
matrices, sédiments marins	HCl / HF	H ₂ O ₂ / KOH	infra rouge spectrophotomètre	carbone élémentaire	(Smith et al., 1975)
sédiment marin	HCl / HF	KOH / H ₂ O ₂ T° ambiante 24h	combustion, MS	carbone élémentaire	(Emiliani et al., 1991)
sédiment lacustre, marécage	HCl	HNO ₃ à chaud	combustion et perte de masse	charbon	(Winkler, 1985)
sédiment marin	HCl	HNO ₃ à chaud	chromatographie	charbon	(Verardo, 1997)
sédiment marin, K/T	HCl / HF	Cr ₂ O ₃ O ₇ / H ₂ SO ₄ à 50°C	perte de masse, Cr ³⁺ spectrophotomètre	carbone élémentaire	(Wolbach and Anders, 1989)
sédiments	HCl / HF	Cr ₂ O ₃ O ₇ / H ₂ SO ₄ à 55°C 60h	CO ₂ colorimètre	black carbon	(Lim and Cachier, 1996)
sédiments, plantes, sols	HCl / HF	Cr ₂ O ₃ O ₇ / H ₂ SO ₄ à 60°C 72h + KOH / H ₂ O ₂ à 60°C 8h	HCl puis combustion, MS	carbone élémentaire, OREC	(Bird and Gröcke, 1997)
sédiment lacustre	méthanol		GC-MS	levoglucosan	(Elias et al., 2001)

MS : Spectromètre de Masse

GC-MS : chromatographie gazeuse et spectromètre de masse

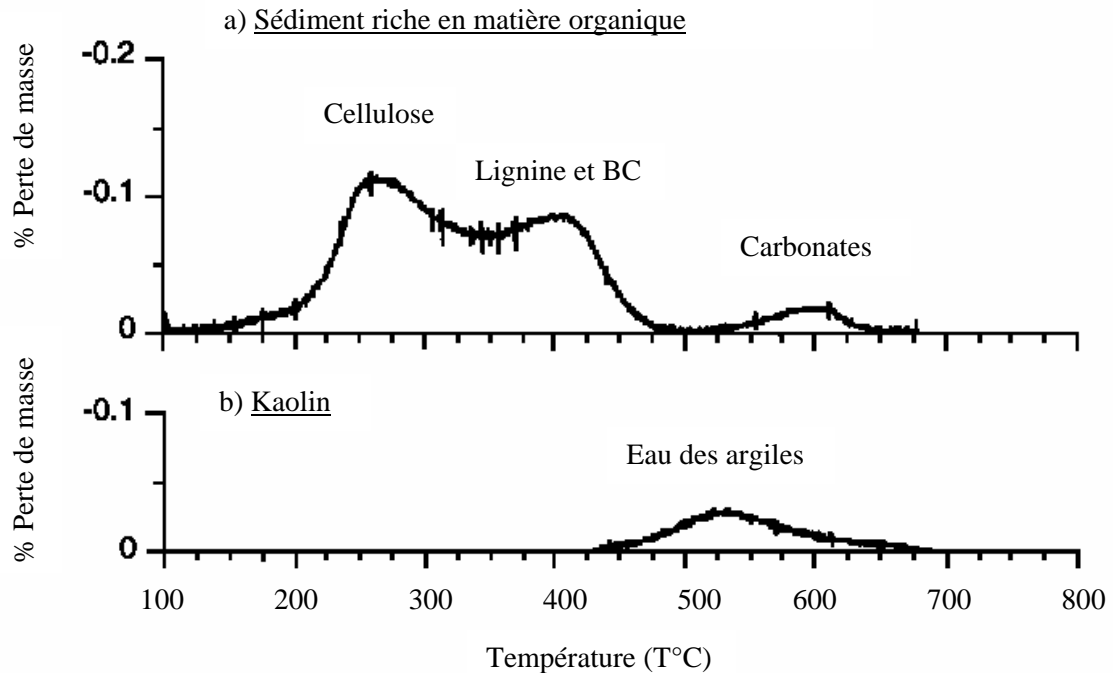


Figure 2-2 : Thermogrammes d'échantillons chauffés de 30 à 800°C sous oxygène a) les pics de cellulose et de lignine se recouvrent, et le pic de lignine peut inclure le BC. b) les pics de carbonates et BC peuvent chevaucher la perte d'eau des argiles (Novakov et al., 1997).

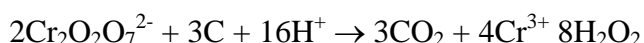
qui peuvent recouvrir les pics de BC et de carbonates ($\sim 600^{\circ}\text{C}$) (figure 2-2).

Comme le montre le tableau 2-1, le carbone résistant au traitement thermique est appelé suie ou BC en fonction des conditions expérimentales et des auteurs. Pourtant, la suie n'est pas composée uniquement de BC, mais de divers composés organiques plus ou moins polymérisés, difficilement séparables par les méthodes thermiques ou optiques (Cachier et al., 1989). C'est pourquoi dans ce travail, nous préférerons utiliser le terme de Carbone Résistant au traitement Thermique (TRC) afin i) de différencier le carbone réfractaire à l'oxydation thermique de celui extrait par oxydation chimique (voir 2.3) ii) qu'il n'y aie pas d'ambiguïté avec le terme BC, composant intrinsèque de la suie, extrait par le couplage des oxydations thermique et chimique.

2.3 Les méthodes chimiques

Les méthodes chimiques commencent généralement par la destruction des phases minérales silicatées et carbonées, par traitements aux acides fluorhydrique et chlorhydrique (HF/HCl). Pour détruire le kérogène (carbone organique insoluble), les substances humiques et toute autre matière organique présente dans les sédiments marins ou lacustres, des oxydants chimiques comme l'eau oxygénée (H_2O_2), l'acide nitrique (HNO_3), ou le bichromate de potassium ($K_2Cr_2O_7/H_2SO_4$), sont ensuite utilisés (tableau 2-1).

- L'eau oxygénée oxyde la matière organique (Smith et al., 1973; Smith et al., 1975; Emiliani et al., 1991). Toutefois, la procédure est longue et peu reproductible car le réactif se transforme en eau au cours de la réaction (Wolbach and Anders, 1989). Le carbone résiduel peut-être mesuré par infrarouge (bande d'absorbance à 1580 cm^{-1}) ou avec un spectromètre de masse après combustion et transformation en CO_2 (carbone élémentaire).
- L'oxydation de la matière organique peut se faire par attaque à l'acide nitrique. Cependant, la pesée avant et après chauffe à $500^\circ C$, qui détermine la concentration de charbon, peut être faussée par la capacité de rétention en eau des argiles (Winkler, 1985; MacDonald et al., 1991) (figure 2-2). De manière similaire, l'attaque *in situ* à l'acide nitrique à chaud utilisée par Verardo (1997) sur une faible quantité de sédiment (~5 mg) semble ne pas oxyder la totalité du carbone organique, et conduire à une surestimation de la concentration en charbon (Bird and Cali, 1998).
- La méthode d'oxydation de la matière organique par le bichromate de potassium est la technique la plus utilisée. En effet, le carbone organique, le kérogène et le carbone élémentaire sont oxydés par le bichromate de potassium selon l'équation :



Le carbone résiduel peut être pesé (perte de masse), transformé en CO_2 et analysé par chromatographie ou par colorimétrie, ou encore mesuré au spectrophotomètre par dosage du Cr^{3+} produit. Il est nommé Carbone Élémentaire Résistant à l'Oxydation (OREC) ou BC selon les auteurs (tableau 2-1).

La cinétique de l'oxydation au bichromate de potassium varie fortement selon les composés (Wolbach and Anders, 1989). Pour un échantillon de la limite Crétacé-Tertiaire, la demi-vie du kérogène réactif est estimée à 7 h, à 59 h pour le kerogène résistant, et à 610 h pour

le carbone élémentaire (figure 2-3). L'échantillon de BC graphitique présente une perte de masse très limitée au début de l'attaque. Lim et Cachier, (1996) ont ainsi démontré qu'un temps d'oxydation d'environ 60 h était nécessaire pour l'attaque du carbone organique avec une perte en OREC négligeable (1-6%).

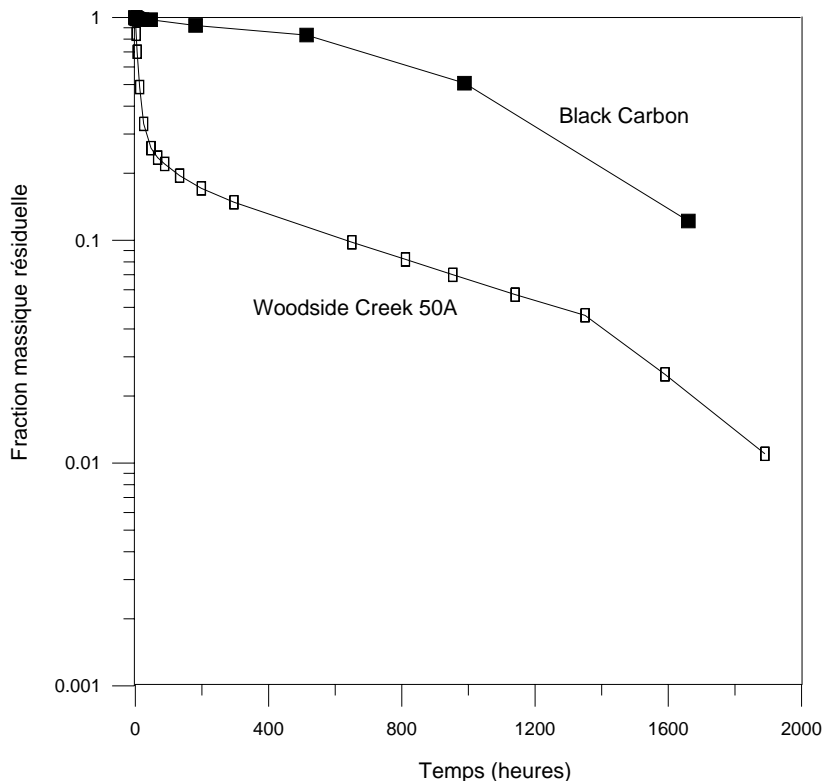


Figure 2-3 : Perte de masse (oxydation au bichromate de potassium) pour un échantillon de la limite Crétacé-Tertiaire, Woodside Creek 50A (carrés blancs) et pour un échantillon de graphite (Black Carbon, carrés noirs, Wolbach and Anders, 1989).

L'abondance en OREC peut donc être utilisée comme marqueur des phénomènes de combustion/pyrolyse. Toutefois, cette méthode préserve une fraction organique réfractaire et n'est pas applicable dans certains environnements sédimentaires (Bird and Gröcke, 1997). Une étape d'oxydation supplémentaire à l'eau oxygénée et/ou thermique permet de se débarrasser des composés carbonés organiques réfractaires qui composent en grande partie la suie, et de quantifier le carbone élémentaire résiduel ou BC (Bird et al., 1999).

- Il existe des méthodes d'extraction par solvant organique qui ne sont pas développées dans ce travail. Ces méthodes permettent d'extraire des composés tels que les Hydrocarbonés Aromatiques Polycycliques (HAP), analysés par chromatographie gazeuse/spectromètre de masse (GC-MS) ou chromatographie liquide à haute performance (HPLC). Les HAP d'origine pyrolytique sont conservés dans les sédiments jusqu'à plusieurs millions d'années et les nouvelles techniques isotopiques permettraient de séparer les HAP provenant de la combustion d'énergie fossile de ceux issus des feux de biomasse (Zep and Macko, 1997). Par ailleurs, l'analyse en GC-MS a récemment mis en évidence un nouvel indicateur moléculaire, le lévoglucosan (1,6-anhydro- β -D-glucopyranose) utilisé comme marqueur de combustion dans les aérosols puis dans les sédiments (Simoneit et al., 1999; Elias et al., 2001). Ce composé provient de la transformation de la cellulose à des températures supérieures à 300°C.

2.4 Définition des principaux résidus carbonés issus de la combustion

Devant la nécessité de s'entendre sur la terminologie des résidus carbonés issus des feux, un effort d'homogénéisation été entrepris par la communauté scientifique, mais certaines définitions demeurent relativement ambiguës. En fonction du degré de combustion et/ou de la méthode d'analyse, on distingue les résidus carbonés suivants (Jones et al., 1997):

- Charbon ou fusain : Le charbon est un dérivé de plante noirci, obtenu par combustion incomplète du bois ou d'autre matière organique, le plus souvent par chauffage en présence limitée d'oxygène. La composition chimique et la structure originelles sont altérées, mais des traces de structures anatomiques sont encore visibles et permettent éventuellement d'identifier l'essence (analyse anthracologique).
- Microcharbons : Petites particules de charbons dont la taille est comprise entre 1 μ m à plusieurs millimètres (mm), produites par le feu *in situ* et transportées par la fumée. Les microcharbons sont caractérisés à l'aide de microscope photonique par leur opacité à la lumière.
- Carbone suie ou aérosols carbonés : Particules carbonées noires formées par condensation gazeuse et émises avec la fumée. Leur taille est généralement inférieure voir égale au μ m. Tout comme les fragments de charbons, les particules de suie sont enrichies en acides humiques aromatiques. L'extraction de la suie est possible après oxydation (thermique ou chimique) de la matière organique labile. En revanche, la caractérisation de ses composés

organiques fortement condensés est difficile (Cachier et al., 1989) et la distinction suie-BC n'est pas toujours faite (Chameides and Bergin, 2002).

- Black Carbon (BC): Tout comme la suie, le BC est une substance carbonée noire, issue de la combustion incomplète de charbon, bois ou huile, à haute température. Les particules de BC se forment par condensation gazeuse au sein des nuages ou des combustibles. Elles sont de forme plus ou moins sphérique et de taille inférieure au micromètre. Le BC est défini comme le composant carboné de la suie le plus condensé (Ogren and Charlson, 1983). En réalité, le terme BC est très répandu mais il n'existe toujours pas de définition définitive du BC (Goldberg, 1985), si ce n'est par analogie au graphite, carbone élémentaire arrangé en molécules cycliques. La définition du BC est fixée en fonction des techniques d'extraction ou de mesure.

Lorsque la combustion est lente et faible, la formation de charbon est favorisée. En revanche, dans le cas d'une combustion flamboyante à haute température, l'émission d'aérosols carbonés peut-être multipliée par 10 (Lobert and Warnatz, 1993).

2.5 Les réservoirs et le temps de résidence du carbone réfractaire

Bien que les particules carbonées résistantes à l'oxydation, ou carbone réfractaire, puissent avoir comme origine les feux de biomasse, leur concentration variable dans les sédiments n'est pas de façon univoque causée par les feux (Bird and Gröcke, 1997). En effet, des substances humiques dissoutes et des débris de plantes dérivés de la matière organique terrigène (lignine) sont largement incorporés dans les systèmes aquatiques par les rivières (Emerson and Hedges, 1988). L'érosion de terrains sédimentaires exporte aussi du carbone organique réfractaire fossile vers le plus grand réservoir de carbone marin : le Carbone Organique Dissous (DOC). Le mode de fonctionnement du DOC est mal connu, mais il semble qu'environ 10% du DOC est d'origine terrestre dans le Pacifique Equatorial (Meyers-Schulte and Hedges, 1986). Le taux de formation de DOC réfractaire dépend de l'activité microbienne. Les bactéries transforment la structure moléculaire des particules organiques et les rend résistantes à l'oxydation (Ogawa et al., 2001). Ainsi, les changements de carbone réfractaire dans les sédiments peuvent être influencés par la dynamique d'érosion et les processus de dépôt. Une partie du DOC est recyclée au sein même de l'océan et stockée dans ce réservoir intermédiaire avant sa sédimentation. Il en est de même pour les particules de BC qui apparaissent plus vieilles

de quelques milliers d'années que leur encaissant, et qui ont apparemment transité par le DOC ou les sols (Williams and Druffel, 1987; Masiello and Druffel, 1998).

Pour identifier la contribution relative des feux de biomasse dans les apports de matériel détritique organique (au cours des derniers cycles glaciaires et de l'Holocène) nous focalisons notre étude sur un site océanique pélagique (carotte MD97-2140, Warm Pool) et un lac de cratère (carotte MM8, Lac Masoko, Tanzanie), dans lequel les apports terrigènes de matière organique sont établis indépendamment (Merdaci, 1998).

2.6 Méthode optique

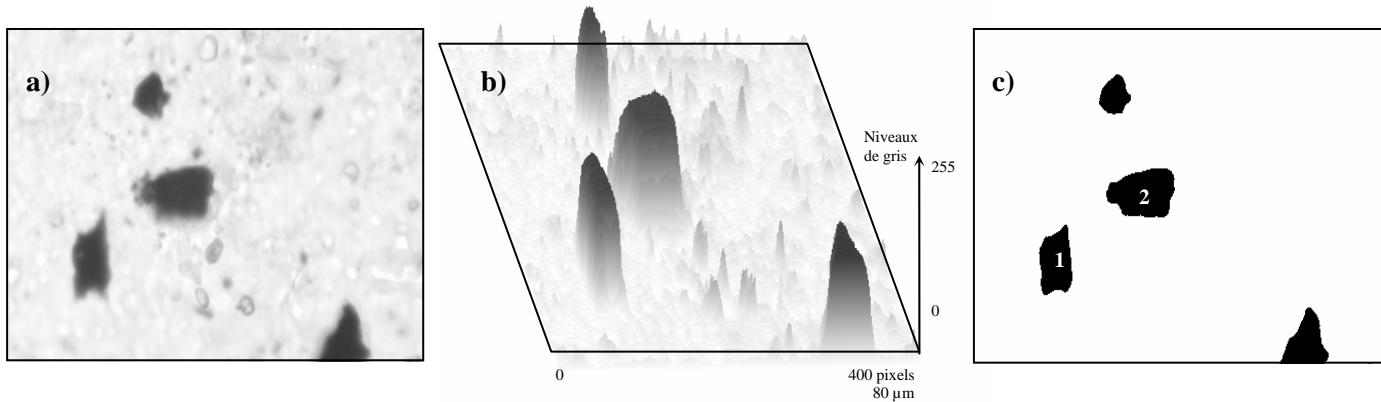
Les méthodes optiques concernent le comptage des grains de charbons, et/ou la mesure de leur surface et leur taille. Le tamisage du sédiment sépare les charbons les plus grossiers (macrocharbons) des charbons les plus petits (microcharbons). L'observation au microscope binoculaire et/ou photonique couplée à l'acquisition d'images permet ensuite de compter un grand nombre de particules avec une résolution de l'ordre du micromètre (μm) et d'obtenir des paramètres quantifiés comparables d'un site à l'autre. La distribution des tailles renseigne sur le mode de transport des charbons, le transport des particules les plus petites étant favorisé par la voie aérienne (Clark and Royall, 1995).

2.6.1 Préparation des lames

Afin d'éviter le fractionnement des charbons par centrifugation, l'ensemble des attaques s'effectue dans le même Becher, sans rinçage. Une première attaque à l'HCl 3M (décarbonatation) est pratiquée sur 50 à 500 mg de sédiment jusqu'à arrêt des bulles de dégazage. Les ajouts successifs de 20 à 30 ml d'acide nitrique (NO_3) et d'eau oxygénée (H_2O_2) purs détruisent la pyrite et la matière organique qui sont opaques et pourraient être confondues avec des charbons (Winkler, 1985). Après l'arrêt des bulles de dégazage, la solution est ramenée à un volume connu par adjonction d'eau. En fonction de la densité de la solution, une partie plus ou moins grande est filtrée par une pompe à vide à travers une membrane de filtration en nitrocellulose. Une partie du filtre est enfin coupée et montée entre lame et lamelles sur baume du Canada.

2.6.2 Acquisition et traitement des images

Les lames sont observées au microscope optique sur 100 à 150 champs (1.7 à 2.6 mm²). Une image en noir et blanc (composée de 255 niveaux de gris) par champ est saisie par le programme automatique de reconnaissance optique *SYRACO* (SYstème de Reconnaissance Automatique de Cocolites ; Dolfus and Beaufort, 1999). Le programme *Scion Image* (<http://www.scioncorp.com>) permet ensuite de traiter ces images en programmant une macro en langage Pascal. Les images sont ouvertes automatiquement les unes après les autres et les particules noires de charbon sont isolées par seuillage de l'image à un niveau de gris fixé (figures 2-4).

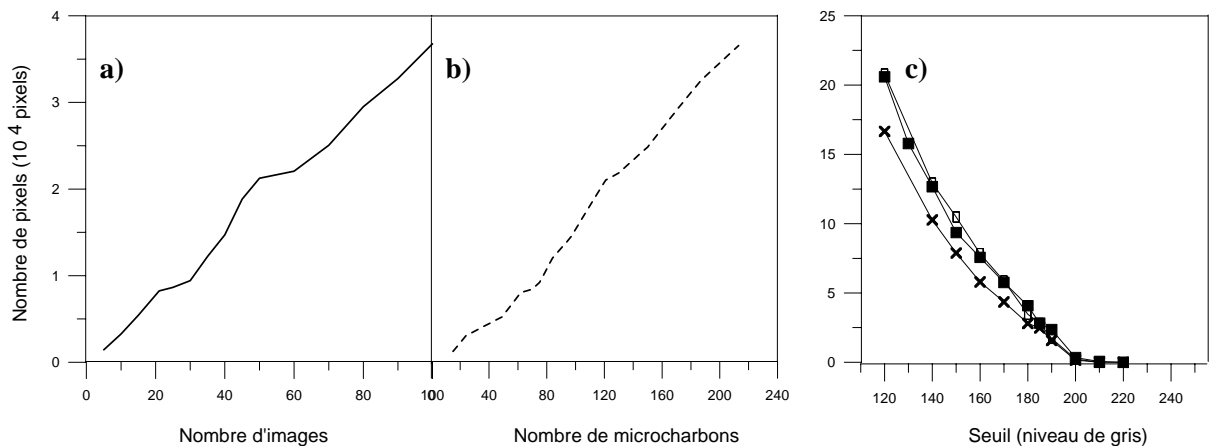


Figures 2-4 : Comptage automatique des charbons par analyse d'image : Les images composées de 255 niveaux de gris sont ouvertes (a et b) puis seuillées à un niveau de gris défini (c). Les particules sont indexées et les paramètres choisis sont mesurés. Ici, les particules inférieures à 50 µm² et celles qui touchent le bord ont été ignorées.

Pour une analyse morphologique, les particules retenues sont caractérisées en fonction des options choisies : calcul de l'aire, du périmètre, des axes principaux. La taille et la surface des particules (en pixels) sont ensuite mises à l'échelle à l'aide d'un micromètre et rapportées à l'ensemble du filtre et de la masse de sédiment analysée (µm, mm²/g). Des tailles limites de particules peuvent être choisies afin de discriminer plusieurs classes de distribution.

La surface totale de charbon augmente proportionnellement avec le nombre d'images analysées (figure 2-4a). Elle est considérée comme fiable à partir de 75 images. Dans ce travail,

l'acquisition de 100 à 150 images par échantillon a été choisie comme étant représentative de l'échantillon. Le nombre de particules de charbons est proportionnel à leur surface totale (figures 2-4b). Comme le montre les figures 2-4 et 2-5c, le choix de la valeur de seuil est primordial. Des tests sur des sédiments naturels ont permis de fixer un seuil autour de 190 niveaux de gris. Toutefois, la valeur de seuil n'a pas été calibrée avec des charbons expérimentaux et elle peut varier sensiblement en fonction de la chimie du sédiment et de l'opacité de la préparation. Cette méthode qui peut être utilisée de façon quantitative est surtout performante d'un point de vue qualitatif.



Figures 2-5 : Nombre de pixels en fonction du nombre images analysées (a) et du nombre de microcharbons (b) pour le même échantillon lacustre. Nombre de pixels de 3 échantillons lacustres pour une valeur de seuil variable (c).

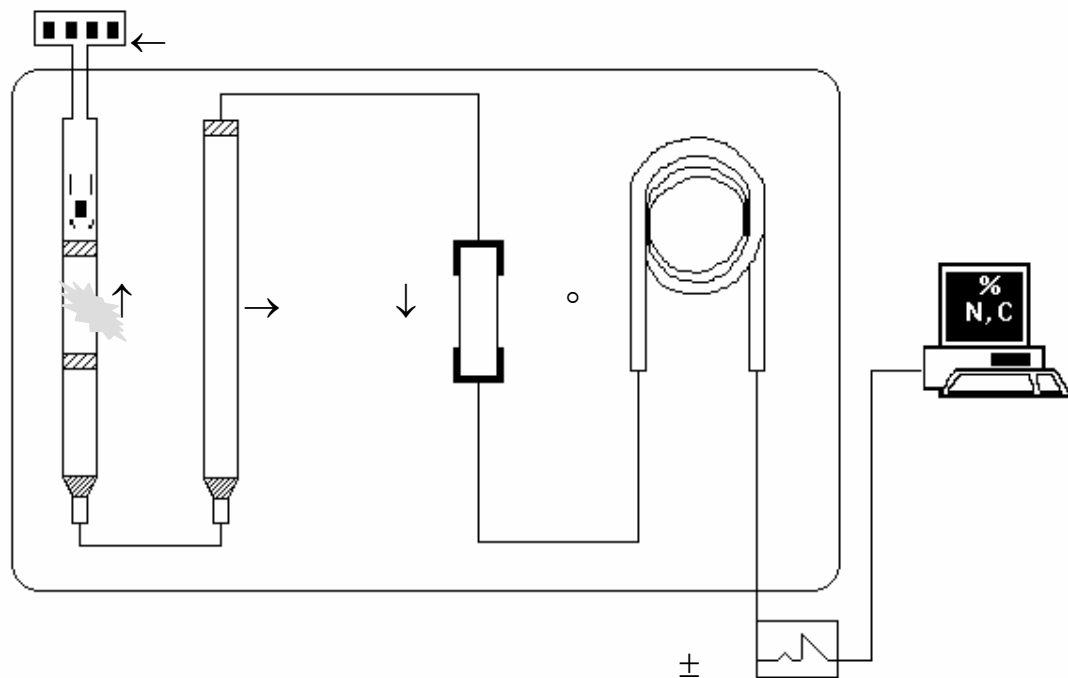
2.7 Analyse du carbone élémentaire

L'analyse du carbone élémentaire (converti en CO₂) se fait par chromatographie. L'extraction du carbone résistant aux traitements oxydants dans les sédiments nécessite l'élimination préalable de toutes les autres formes de carbone organique (végétal, animal, terrestre et aquatique) et inorganique (carbonates).

2.7.1 Appareillage: l'analyseur élémentaire de carbone

Le CN (*Fisons Na 1500*) est un chromatographe en phase gazeuse qui permet de mesurer la teneur en carbone (C) et en azote (N) sur de très petites quantités d'échantillons solides (5 à 15 mg). Le principe de fonctionnement est représenté sur la figure 2-6 : L'échantillon à analyser est placé dans une capsule, elle-même disposée dans un passeur automatique (1). L'échantillon tombe dans la chambre à combustion (2) maintenue à 1020°C sous une atmosphère enrichie en oxygène et brûle violemment (combustion par flash). Les produits de combustion oxydés sont entraînés par de l'hélium à travers une colonne de réduction (3) contenant du cuivre métallique porté à 650°C. L'excès d'oxygène est piégé, et les oxydes d'azote réduits en azote élémentaire (N) passent avec CO₂ et H₂O par un piège à eau contenant du perchlorate de magnésium (4). La colonne de chromatographie (5) fournit un signal en millivolts, proportionnel à la concentration des composants (N₂ et CO₂), grâce à un détecteur de conductivité thermique (6). Le signal est traité par le logiciel *Eager 200*, et les pourcentages de C et N sont calculés en fonction de la masse de sédiment traitée, après soustraction du blanc qui dépend du type de capsule utilisée.

Figure 2-6 : Schéma de l'analyseur élémentaire CN (*Fisons 1500*).



2.7.2 Analyse du carbone total (Ctotal), du carbone organique (Corg), et calcul de la teneur en carbonate de calcium (CaCO₃)

Les échantillons sont lyophilisés puis broyés finement. La mesure du Ctotal se fait sur 5-10 mg de sédiment brut introduit dans une capsule en étain (Sn, 3x5 mm) placée dans le passeur automatique. La teneur en Corg est mesurée sur 5-20 mg de sédiment brut après décarbonatation à l'acide chlorhydrique (HCl) dans des capsules en argent (Ag, 3x5 mm). Ces valeurs permettent de calculer la teneur en CaCO₃ en appliquant l'équation suivante (Verardo et al., 1990):

$$(\% \text{ Ctotal} - \% \text{ Corg}) * M_{\text{CaCO}_3}/M_C = \% \text{ CaCO}_3$$

avec $M_{\text{CaCO}_3}/M_C = 8.3$

2.7.3 Méthode thermique

L'oxydation de la matière organique se fait par traitement thermique. Le sédiment sec et broyé est placé dans un creuset en porcelaine et chauffé à 375°C. Le Carbone Résistant au traitement Thermique (TRC) est ensuite mesuré après décarbonatation dans des capsules en argent (Ag 3x5 mm) sur environ 5-20 mg de sédiment.

2.7.4 Méthode chimique

Les protocoles d'exactions chimiques que nous utilisons (figure 2-7) sont basés sur une synthèse des méthodes existantes (Cachier et al., 1989; Wolbach and Anders, 1989; Gustafsson et al., 1997; Bird and Gröcke, 1997; Bird et al., 1999). Afin d'augmenter l'efficacité des attaques, un rinçage à l'eau permutee est effectué entre chaque attaque :

- A) 0.2-0.5 g de sédiment sec et broyé est placé dans des tubes de centrifugeuse en polypropylène. Contrairement aux méthodes décrites précédemment, la quantité de sédiment traitée n'est pas limitée par la petite taille du contenant. Afin de réduire les pertes expérimentales, l'ensemble de la procédure se déroule dans les mêmes tubes. Pour les sédiments riches en CaCO₃ une première attaque à l'HCl 3M évite toute projection de sédiment par une décarbonatation trop brutale.

- B) 20 cm³ du mélange acide fluorhydrique/chlorhydrique, HF (10M)/HCl (1M) sont introduits dans les tubes disposés sur un agitateur à 400 tours/minute pendant 24h, afin d'augmenter l'efficacité de l'attaque des silicates.
- C) 20 cm³ d'HCl 10M sont versés dans les tubes, maintenus agités pendant 24h afin de dissoudre la totalité des carbonates.
- D) 20 cm³ d'acide sulfochromique (0.1M K₂Cr₂O₇/2M H₂SO₄) sont introduits dans les tubes, placés dans un bain marie à une température de 55°C pendant 65h, afin de détruire le carbone organique labile.

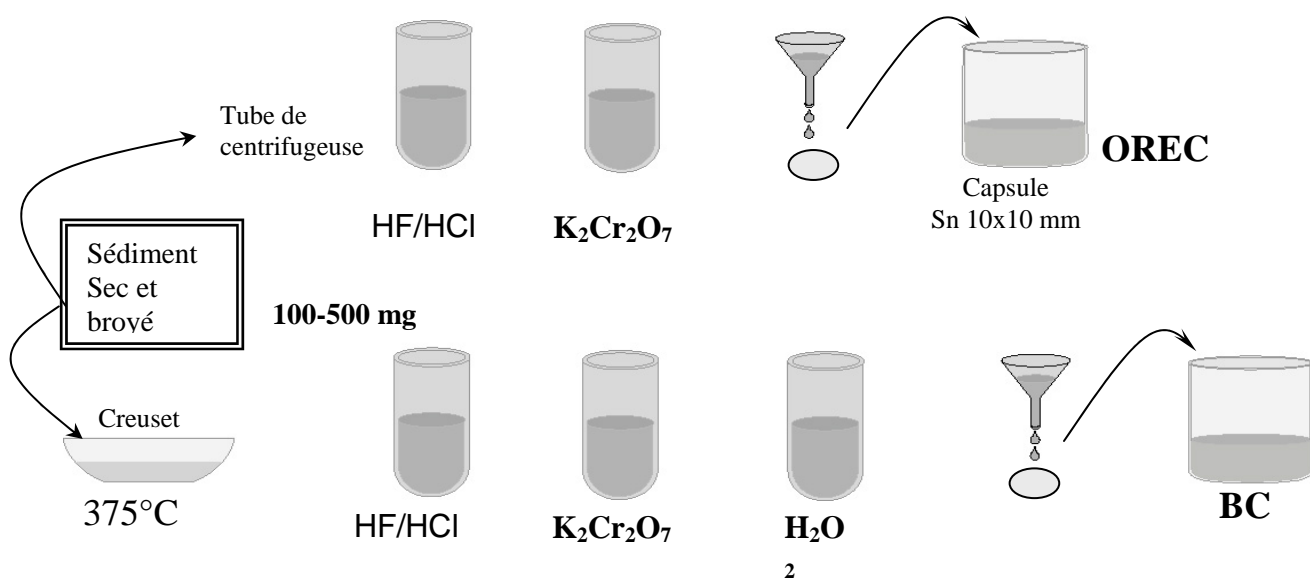


Figure 2-7 : Protocoles d'extraction chimique de OREC et de BC.

Le résidu de ces attaques est récupéré sur des filtres en silice, à l'aide d'une pompe à vide. Les filtres en silice sont auparavant chauffés à 500°C pendant 6 heures afin d'éliminer toute pollution. La teneur en C mesurée sur ces filtres, grâce à des capsules en étain (Sn, 10x10 mm)

introduites dans le CN, correspond au Carbone Élémentaire Résistant à l’Oxydation (OREC ; figure 2-7).

Afin d’extraire la fraction Black Carbon (BC) (figure 2-7) le sédiment pesé est placé dans un creuset en porcelaine et chauffé à 375°C. Après l’attaque chimique décrite précédemment et avant la filtration, 20 cm³ d’eau oxygénée pure (H₂O₂) sont introduits dans les tubes pendant 24 heures.

2.8 Conclusion

Afin de rendre les comparaisons entre les différentes études possibles, la nomenclature des produits pyrogéniques a été récemment affinée. En fonction des techniques employées et des conditions expérimentales, plusieurs types de résidus de combustion de matière organique végétale peuvent être distingués : charbons, suie et BC. Leur fraction atmosphérique est souvent désignée par le terme générique « suie », ou « aérosols carbonés ». La combinaison de méthodes chimiques et optiques, prenant en compte la plus grande partie du spectre des particules issues de processus de combustion, s’impose à la compréhension des enregistrements de paleo-feux. Afin d’appliquer les méthodes d’extraction de TRC et de BC aux sédiments, des tests sur des matrices synthétiques sont présentés dans la partie suivante.

3. Testing the Thermally Refractory Carbon (TRC) and Black Carbon (BC) extraction methods for reconstructing past biomass fires from sedimentary records

3.1 Introduction

The determination of combustion-derived products in sedimentary archives is a key issue to reconstruct major changes in biomass burning and aerosol fallout through time, and to further improve the quantification and the understanding of global carbon budgets. For instance, due to their resistance to biochemical degradation in soils and sediments, the residues of vegetation fires represent a significant sink of terrestrial carbon (Kuhlbusch and Crutzen, 1995; Suman *et al.*, 1997). In addition, the carbonaceous aerosols modify the Earth's climate by warming the atmosphere while decreasing solar radiation reaching the surface (Penner *et al.*, 1992). It has been recently pointed out that the magnitude of the direct radiative forcing from Black Carbon (BC) itself exceeds that due to methane, suggesting that BC may be the second most important component of global warming after the CO₂ in terms of direct forcing (Jacobson, 2001). BC also affects the large-scale circulation and the hydrologic cycle with significant effects on regional climate (Menon *et al.*, 2002).

However, the composition and sources of BC and their changing fluxes with time are still uncertain, a complication arising from the uncertainty inherent in BC measurements in the environment (Chameides and Bergin, 2002). To date, there is no standard protocol and terminology for determining BC, and interlaboratory analyses of carbonaceous aerosol samples largely differ due to methodological differences (Countess, 1990; Schmidt and Noack, 2000). In this context, this study aims to improve the quantification of carbonaceous aerosols as produced by biomass burning in sedimentary records.

Ambiguous terms are applied to the dark carbon-rich aerosols originating from the combustion processes (Chameides and Bergin, 2002). It is generally assumed that soot is equivalent to BC, but also that soot is not primarily composed of pure BC, encompassing a wide range of highly condensed organic compounds (Cachier *et al.*, 1989; Gustafsson and Gschwend, 1998). In this study, we defined 1) soot as the Thermally Refractory Carbon (TRC) which survives the thermal treatment and 2) BC as the carbon which results from the combination of thermal and chemical procedures as described below.

3.2 General background

The production of charcoal, soot and BC particles by burning of organic materials is referred as charring. However, the nomenclature of charred particulate material is defined by physical and chemical properties, which do not univocally refer to combustion processes (Jones *et al.*, 1997). Charcoals are optically counted by smear slides analysis (Clark and Hussey, 1996). Elemental carbon is determined by measuring the CO₂ (elemental analysis) after thermal and/or chemical oxidation of the organic components (Bird and Gröcke, 1997). Any clear discrimination between combustion-derived products and natural refractory organic compounds can be difficult to obtain (Cachier *et al.*, 1989; Novakov *et al.*, 1997). In addition, there is a lack of accepted standard materials corresponding to the complex form of natural BC, and interlaboratory comparisons still yield variable results (Middelburg *et al.*, 1999; Schmidt and Noack, 2000).

Several methods are used to extract fire-originating carbonaceous particles. The complete removal of inorganic and organic forms of carbon is especially required for analyzing complex environmental matrices such as sediments (Bradbury, 1997). The response of the charred carbon to the oxidative treatment mostly depends on the degree to which the precursor plant material has been carbonized (Bird and Gröcke, 1997). In this study, the thermal and chemical inertness of the fire-altered material are respectively used to discriminate respectively TRC and BC from other organic compounds.

Thermal treatments

Thermal treatments have been performed to remove organic matter for extracting atmospheric fire-originating carbonaceous material such as soot, which remains non-volatile at 340-375°C (Cachier *et al.*, 1989). In the same way, the carbon remaining after thermal oxidation and HCl acidification is used for determining soot in sediments (Gustafsson *et al.*, 1997).

Chemical methods

Several chemical methods have been applied to remove natural organic components. Organic Carbon (OC) removal using peroxide (H₂O₂) or hot nitric acid digestion remains

uncertain, as the first reagent fluctuates in concentration, while the second does not efficiently remove OC (Smith *et al.*, 1973; Winkler, 1985; Verardo and Ruddiman, 1996; Bird and Cali, 1998). In the chemical procedure of Wolbach and Anders (1989), organic matter is removed during a prolonged oxidation in a sulfo-dichromate solution ($K_2Cr_2O_7/H_2SO_4$). This technique enables to extract soot as Oxidant Resistant Elemental Carbon (OREC), despite relatively small and quantifiable losses (e.g. 1-6% OREC for a reaction time of 60h; Lim and Cachier, 1996). Further experiments have demonstrated that OREC measurements can be reproducible in carbonized organic matter samples and some marine sediments, providing a reliable proxy for combustion/pyrolysis processes (Bird and Gröcke, 1997). Subsequently to the dichromate oxidation, peroxide oxidation and/or thermal combustion can be used to remove any organic contaminants, while the resulting BC is eventually left for elemental analysis (Bird *et al.*, 1999; Bird and Cali, 1998). However, the loss of BC associated with extraction needs to be known to assess the BC content in sedimentary records (Gustafsson *et al.*, 2001).

3.3 Experimental section

Based on the techniques described above, we tested on synthetic samples i) a thermal treatment (TRC extraction) and ii) a combination of thermal and chemical procedures (BC extraction). An overall reaction scheme is presented in figure 3-1.

3.3.1 Total Carbon (TC) and Organic Carbon (OC) determinations

TC was measured on *ca.* 5-10 mg of bulk standard within small tin caps (Sn caps 3 x 5 mm), using an automatic CN-elemental analyzer. OC was determined on *ca.* 5-20 mg of matrices after partitioning the inorganic and organic carbon phases by *in situ* HCl acidification (HCl 2M) within silver caps (Ag caps 3 x 5 mm).

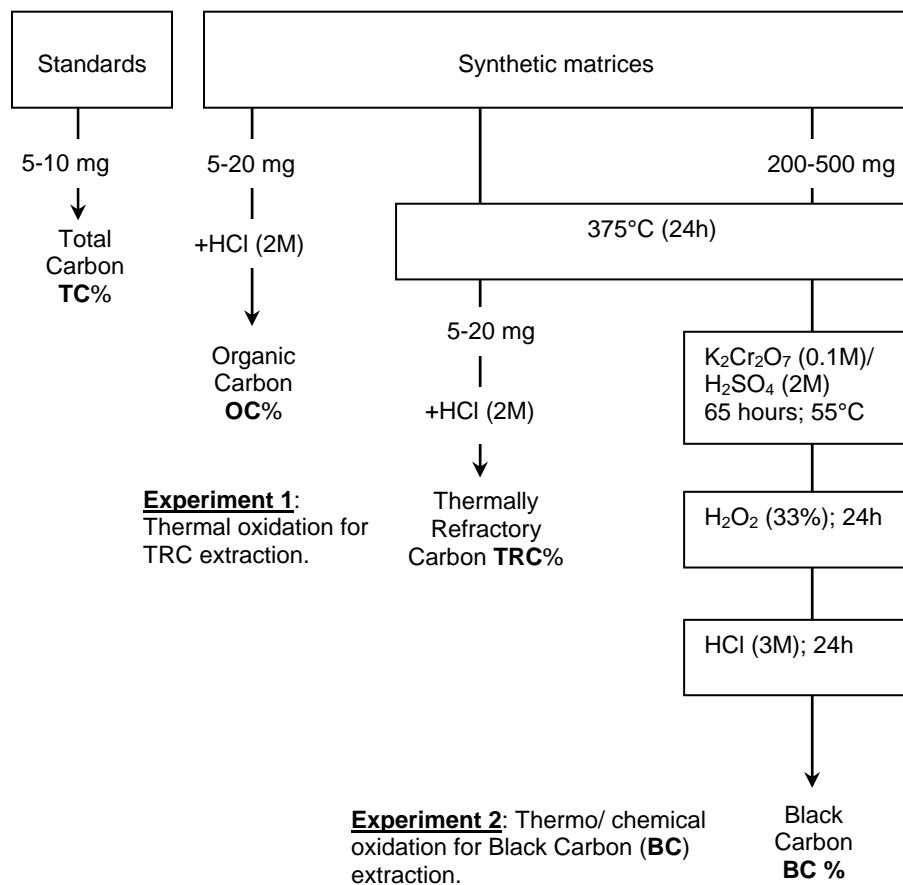


Figure 3.1 : The sequence reaction scheme of the various elemental-carbon analyses: Total Carbon (TC), Organic Carbon (OC), Thermally Refractory Carbon (TRC; first experiment), and Black Carbon (BC; second experiment).

3.3.2 Thermally Refractory Carbon (TRC) extraction

In the first experiment, TRC extraction, the prepared matrices were placed into a porcelain crucible, and heated in a muffle furnace at 375 °C during 24 h. TRC content was then determined by CN-elemental analysis on *ca.* 5-20 mg of thermally altered matrices, after HCl acidification (HCl 2M) in Ag caps to remove carbonate.

3.3.3 Black Carbon (BC) extraction

The method described in this paper was adapted from the earlier works of Wolbach and Anders (1989), Bird and Gröcke (1997), and Gustafsson *et al.* (2001). Our procedure has been

satisfactory compared with the optical quantification of microscopic charcoal in oceanic and lacustrine sediments (chapter 4 and 5).

Approximately 200-500 mg of samples were weighted, placed into a porcelain crucible and heated in a muffle furnace at 375 °C during 24 h. The cooled residues were then transferred into polyethylene test tubes. Natural samples were first treated with 10 M HF/1M HCl and 10 M HCl in order to remove carbonates, part of silicates, and any carbonaceous material which can be trapped between the silicate sheets. The dissolution of silica was not conducted on synthetic samples, because in the absence of clay, such treatment would favor graphite losses during the rinsing as performed between each steps of the procedure. The chemical treatment on synthetic matrices therefore began with the dichromate oxidation (figure 3-1). OC was attacked by a 20 cm³ sulfo-dichromate solution (0.1 M K₂Cr₂O₇/2 M H₂SO₄) during 65h into a water bath maintained at 55°C, in order to maximize the removal of OC while extracting OREC (Wolbach and Anders, 1989). A peroxide oxidation step (33% H₂O₂, 24h; Bird and Gröcke, 1997) was subsequently carried out to remove any remaining thermal/acidic-resistant organic compounds. The carbonate fraction was then dissolved with 15 cm³ 3 M HCl. The residue of the rinsing solution was finally filtered with a vacuum pump on a pre-cleaned glass-microfiber filter (GF/C Whatman, 1.2µm size-particle retention; 6h at 500°C). The filter was then dried (5 hours at 45°C), folded, placed into large Sn caps (10 x 10 mm), and subjected to CN-elemental analysis.

3.3.4 Synthetic matrices and natural sediments

Due to the complexity of the sedimentary records and to the potential interference of some of their constituents (OC and carbonates), the TRC and the BC extraction methods were applied on experimental matrices of known composition. Two synthetic powders were chosen to approach experimentally the composition of natural sediments: Silica powder (SiO₂, CAS No. 7699-41-4; purity >99.9% refined) and calcium carbonate powder (CaCO₃, CAS No. 471-34-1; purity >99.0 %).

The BC method was then tested on natural sediments. Intertropical lake and marine sediments were chosen for testing the reliability of the method, because most of the current global vegetation fires occurred in the Tropics and Subtropics (Goldamer, 1993). The MM8 lacustrine sediment was taken from a crater-lake in Tanzania (Lake Masoko; 9°S, 33°E). It consists in organic-rich silty mud, with OC ranging between 2 and 10%, biogenic SiO₂ ranging between 10 and 51%, and absence of CaCO₃ (Merdaci, 1998; Williamson *et al.*, 1999). The MD40 marine sediment was collected from 2547 meters water depth in the western tropical

Pacific, several hundred kilometers north off Papua New Guinea (2°N , 141°E). CaCO_3 and OC contents of core MD40 range between 50 and 75% and 0.1 to 0.7% (chapter 4).

3.3.5 Determination of elemental carbon abundance

The elemental carbon contents (TC, OC, TRC and BC) were determined by gas chromatography, using a Fisons NA-1500 elemental analyzer. Encapsulated samples are introduced into a combustion column maintained at 1020°C in enriched atmosphere of oxygen. The material is volatilized by “flash combustion”. The gaseous combustion products are swept through a reduction reactor, dried through a water-absorbing filter, and separated on a chromatographic column. The quantity of carbon is determined by comparing the signal with a carbonaceous standard reference material (acetanilide). Detection of CO_2 made by thermal conductivity and electronic integration of the peak allows to calculate the mass of carbon (M_C) in a sample by least-squares linear regression of area counts of carbon (A_S) and blanks (A_0).

$$M_C = (A_S - A_0)/k$$

Where k is the slope of the standard calibration curve. The weight percent carbon (%C) is calculated as a function of the sample mass (M_S).

$$\%C = 100 \times (A_S - A_0)/(k \times M_S)$$

3.4 Results

3.4.1 Detection limit of the elemental carbon analyzer

Analysis of empty sample cups was performed to estimate the detection limit (table 3-1). The mean blank value and standard deviation (SD) for small tin cups (Sn, 3x5mm) used for TC analysis accounts for $1.55 \mu\text{g C}$ (0.16). The blank value of the acidified silver cups (Ag, 3x5 mm) used for OC and TRC determinations accounts for $2.67 \mu\text{g C}$ (0.43). The combustion of the large Sn cups (10x10 mm) with the glass-filter used for BC analysis yields a blank of $4.21 \mu\text{g C}$ (0.78).

The detection limit (L_D) is defined as the carbon mass that produces a signal greater than three SD of the mean blank (Currie, 1968). The resulting L_D values (table 3-1) mostly depend on the type of cups used and/or glass-filter. The L_D can be used to approximate the determination

limit (L_Q), *i.e.* the signal level above which a quantitative measurement can be performed, as the carbon mass that produces a signal greater than ten SD of the mean blank (table 3-1; Currie, 1968).

Type of analysis	Type of container	n	Blank (A_0) μV Sec	Blank ^a μg C (SD)	L_D 3(SD)	L_Q 10(SD)
TC analysis	Sn cap	15	1269	1.55 (0.16)	0.48	1.6
OC and TRC extraction (experiment 1)						
	Ag cap	15	2188	2.67 (0.43)	1.29	4.3
BC extraction (experiment 2)	Large Sn cap and glass-filter	15	3449	4.21 (0.78)	2.34	7.8

a. $1000 \times (A_0/k)$, with $k = 819756 \mu\text{V Sec mg}^{-1}$

Table 3.1 : The determination limit (L_Q) is approximated by multiplying the standard deviation (SD) of the mean blank value by 10 (Currie, 1968).

3.4.2 Characteristics of the carbonaceous standards

Several commercially available standards were used for testing the applicability of the method to natural components (tables 3-2 and 3-3). The carbonaceous standards were dried in a oven at 100°C and grounded into a fine homogeneous powder using an agate mortar. The Total Carbon (TC) concentration of the standards was measured on pure chemical compounds (tables 3-2 and 3-3). Replicate analyses on different samples of the same material were performed to check the reliability of the method and to calculate the SD. The characteristics of the standards are described below.

Acetanilide (SRM No. 141c; TC = 71.211%) was used as a reference sample of labile OC. Humic acids (Aldrich; TC = 38.20%) was chosen to represent the behavior of resistant natural OC.

Natural charcoal (willow; TC = 82.738%) and lithogenic graphite (Alibert mine, Siberia; TC = 99.251%) were used to estimate the impact of the treatments on contrasted combustion-derived products. As the combustion process is relatively limited for charcoal compared to BC, the charcoal standard rather models the behavior of wood, while the graphite models the behavior of BC. We also used a synthetic graphite powder (CAS No. 7782-42-5; TC = 99.460%)

Carbon content of acetanilide	Carbon content of charcoal
% TC	% TC
71.108	82.597
71.037	82.668
71.354	82.727
70.178	82.959
71.508	mean = 82.738
71.351	n=4; SD = 0.156
71.598	
71.231	
71.354	
71.392	
mean = 71.211	
n=10; SD = 0.399	
Carbon content of humic acid	Carbon content of synthetic graphite
% TC	% TC
38.142	99.703
38.171	99.559
38.284	99.117
mean = 38.199	mean = 99.460
n=3; SD = 0.075	n=3; SD = 0.305
Carbon content of lithogenic graphite	
% TC	
99.411	
99.501	
98.841	
mean = 99.251	
n=3; SD = 0.358	

Table 3-2: Total Carbon content (%TC) measured on the bulk standard, mean, number of replicate analyses (n), standard deviation (SD).

Standard description	%TC	n	SD
Acetanilide (SRM No. 141c)	71.211	10	0.399
Humic acids (Aldrich)	38.199	3	0.075
Charcoal (Willow)	82.738	4	0.156
Synthetic graphite (CAS No. 7782-42-5)	99.460	3	0.305
Lithogenic graphite (Alibert mine, Siberia)	99.251	3	0.358

Table 3-3 : Description of the carbonaceous standards. Mean Total Carbon (%TC), number of replicate analyses (n), standard deviation (SD) (see details in table 3-2).

for comparison with the lithogenic graphite.

Experiments showed that the analyses on bulk charcoal and graphite standards (containing more than 80% of elemental carbon) required very small sample masses of sample (≤ 5 mg). In addition, several empty samples (“by-pass samples”) within the run can be required to recover the complete integration of the CO₂ signal. Otherwise, the quantification of the carbon in the standard can be underestimated, and the chromatogram of the subsequent analysis would be overestimated by the memory effect of the elemental analyzer. Despite such caution, the TC concentration of the synthetic and lithogenic graphite (99.25 and 99.46%) remained inferior to 100%. This may be explained by the sensitivity of the microbalance (10 µg) and the error of mass measurements (± 50 µg), corresponding to $\pm 1\%$ for a 5 mg sample, and $\pm 0.3\%$ for a 15 mg sample.

3.4.3 Reproducibility of carbon determinations

In order to evaluate the reproducibility of the carbon determinations, we prepared five synthetic matrices composed of SiO₂ and CaCO₃, in which we added one carbonaceous standard in known proportion (% weight of initial standard). Because one of the most important parameters in quantitative determination is the homogeneity of the sample to be analyzed, the prepared matrices were well homogenized using an agate mortar and an automatic homogenizer.

The initial concentration of carbon added from carbonaceous standard was compared to that measured (% OC, figure 3-2). The linear relation (Y= 1.03 X – 0.012, r² = 0.94, n=30) indicates that the carbonate phase is completely removed and that the carbonaceous standards are entirely recovered. The variability of OC measurements within the set of standards containing some graphite or charcoal is lower than 0.05%. The lower reproducibility of the samples sets containing some humic acids and acetanilide (<0.2%) likely results from weighting uncertainties.

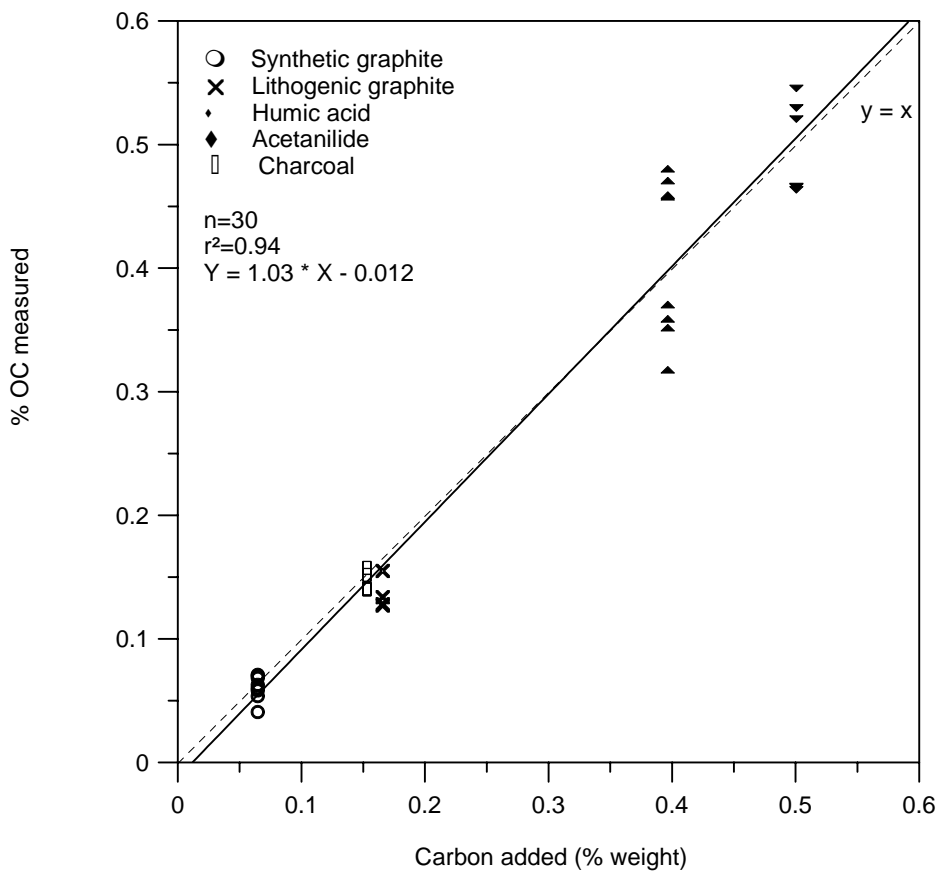


Figure 3-2: The concentration of carbon added from carbonaceous standards (excluding CaCO_3), as a function of the carbon measured after HCl acidification (% OC).

3.4.4 Testing the extraction of Thermally Refractory Carbon

Mass loss experiments on pure BC standards demonstrated that the thermal treatment did not alter significantly synthetic and lithogenic graphite (table 3-4, figure 3-3).

Time (hr)	Graphite synthetic	Graphite lithogenic
0	100	100
7	100.05	100.09
16	99.93	100.03
20	99.87	99.98
37	99.92	100.11
42	99.93	100.25
65	99.83	
94	99.90	

Initial masses were 382.96 and 1067.99 mg

Table 3-4: Mass loss experiments of BC standards (% initial mass) during the thermal treatment.

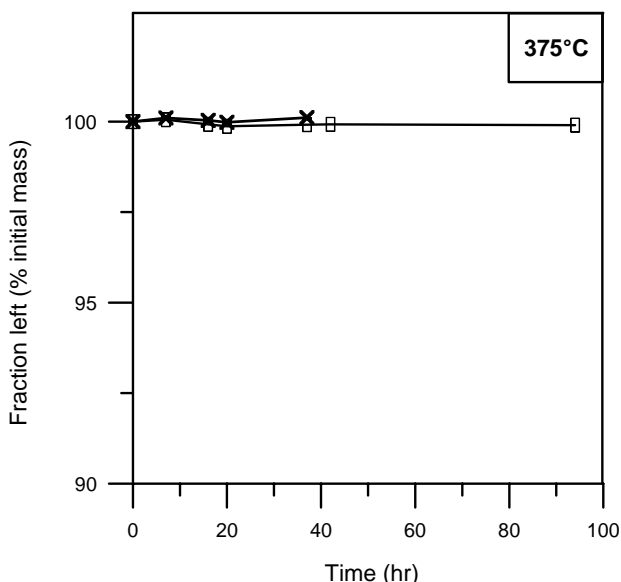


Figure 3-3: The behavior of the BC standards during an extended period of thermal oxidation.

To estimate the loss of carbon (from the carbonaceous standard) associated with the thermal treatment procedure, we measured the carbon content i) prior (% OC) and ii) after the thermal treatment (% TRC). The results of this first experiment are summarized in table 3-5 for each set of samples, and presented in details in table 3-6. Data are expressed as the mean values from at least four replicates, given the standard deviation (SD). The functional term “charred TRC” used hereafter referred to the carbon which survives the thermal treatment (TRC), as a function of the initial OC measured in the matrix (% charred TRC = 100 x TRC/OC; Kuhlbusch, 1995).

Table 3-5 : Summary of the results from the first experiment (see details in table 3-6).

	Initial standard weight ^a %	Carbon added ^b %	OC measured %	SD	n	TRC measured %	SD	n	Charred TRC % 100xTRC/OC
Acetanilide	0.703	0.501	0.498	(0.037)	6	0.046	(0.025)	6	—
Charcoal	0.185	0.153	0.148	(0.009)	4	0.016	(0.018)	4	—
Humic acids	1.038	0.396	0.408	(0.065)	8	0.286	(0.041)	9	70
Synthetic graphite	0.065	0.065	0.061	(0.010)	8	0.044	(0.004)	9	—
Lithogenic graphite	0.167	0.166	0.136	(0.013)	4	0.139	(0.035)	4	100

a. From table 3-6.

b. Carbon added (excluding CaCO₃) = 100 x standard weight x TC_{standard}, with TC_{standard} from table 3-3.

— Insignificant data (see mass of carbon after thermal treatment, table 3-6).

Gte stc 0.065 ; CaCO ₃ 59.99; SiO ₂ 39.94 %									
Total mass of matrice = 4000.60 mg									
					mass (mg)	%C			
Sample	C	OC	TRC	Sample	C	OC			
						TRC			
9.17	0.049	0.530	7.26	0.026	0.359	12.56			
10.53	0.057	0.545	8.13	0.029	0.352	10.10			
10.02	0.046	0.463	8.21	0.028	0.318	7.27			
10.65	0.050	0.466	5.31	0.024	0.459	14.15			
8.72	0.041	0.466	9.19	0.042	0.458	17.93			
6.46	0.034	0.521	11.78	0.055	0.471	10.57			
n=6; mean (SD) 0.498 (0.037)				14.39	0.069	0.480			
8.12	0.002	0.025	7.63	0.028	0.371	20.13			
9.99	0.004	0.037	*12.88	0.083	0.648	n=8; mean (SD) 0.408 (0.065)			
9.59	0.007	0.078	6.87	0.019	0.276	12.18			
7.66	0.005	0.072	6.96	0.015	0.223	14.72			
11.65	0.002	0.017	7.20	0.016	0.221	10.67			
7.11	0.003	0.047	6.36	0.017	0.271	13.06			
n=6; mean (SD) 0.046 (0.025)				17.15	0.031	0.179			
				16.93	0.043	0.251			
				12.33	0.037	0.300			
				11.79	0.036	0.305			
				8.05	0.021	0.264			
				n=9; Mean (SD) 0.286 (0.041)					
*Rejected sample									
Gte litho 0.167 ; CaCO ₃ 74.87; SiO ₂ 24.96 %									
Total mass of matrice = 2003.34 mg									
					mass (mg)	%C			
Sample	C	OC	TRC	Sample	C	OC			
						TRC			

Hc acid 1.038 ; CaCO ₃ 59.97; SiO ₂ 38.98 %							
Total mass of matrice = 2000.77 mg							
					mass (mg)	%C	
Sample	C	OC	TRC	Sample	C	OC	
						TRC	
9.17	0.049	0.530	7.26	0.026	0.359	12.56	
10.53	0.057	0.545	8.13	0.029	0.352	10.10	
10.02	0.046	0.463	8.21	0.028	0.318	7.27	
10.65	0.050	0.466	5.31	0.024	0.459	14.15	
8.72	0.041	0.466	9.19	0.042	0.458	17.93	
6.46	0.034	0.521	11.78	0.055	0.471	10.57	
n=6; mean (SD) 0.498 (0.037)				14.39	0.069	0.480	
8.12	0.002	0.025	7.63	0.028	0.371	20.13	
9.99	0.004	0.037	*12.88	0.083	0.648	n=8; mean (SD) 0.408 (0.065)	
9.59	0.007	0.078	6.87	0.019	0.276	12.18	
7.66	0.005	0.072	6.96	0.015	0.223	14.72	
11.65	0.002	0.017	7.20	0.016	0.221	10.67	
7.11	0.003	0.047	6.36	0.017	0.271	13.06	
n=6; mean (SD) 0.046 (0.025)				17.15	0.031	0.179	
				16.93	0.043	0.251	
				12.33	0.037	0.300	
				11.79	0.036	0.305	
				8.05	0.021	0.264	
				n=9; Mean (SD) 0.286 (0.041)			

Charcoal 0.185 ; CaCO ₃ 74.86; SiO ₂ 24.95 %						
Total mass of matrice = 2003.7 mg						
					mass (mg)	%C
Sample	C	OC	TRC	Sample	C	OC
						TRC
12.62	0.020	0.157	11.44	0.018	0.155	11.52
12.67	0.018	0.141	13.93	0.019	0.134	14.5
11.48	0.017	0.152	15.33	0.019	0.127	16.1
10.65	0.015	0.140	12.00	0.015	0.128	12.68
n=4; mean (SD) 0.148 (0.009)				n=4; mean (SD) 0.136 (0.013)		
15.96	0.001	0.006	11.44	0.018	0.155	11.52
11.84	0.001	0.005	13.93	0.019	0.134	14.5
16.93	0.002	0.012	15.33	0.019	0.127	16.1
10.43	0.004	0.043	12.00	0.015	0.128	12.68
n=4; mean (SD) 0.016 (0.018)				n=4; mean (SD) 0.136 (0.013)		

Table 3-6 : Estimation of the carbon loss associated with the thermal treatment procedure (375°C, 24h). Carbon (C) measurements were performed prior (OC) and after (TRC) the thermal treatment on synthetic mixture of known composition (weight %). Number of replicate analyses (n); mean and standard deviation (SD) in bold characters.

The thermal treatment efficiently removed, acetanilide and charcoal carbon (mass of TRC $\leq L_Q$, tables 3-1 and 3-6), preserving significant percentages of humic acids carbon (*ca.* 70%). The lithogenic graphite was more resistant with 100% of charred TRC. The set of samples containing some synthetic graphite suggests that the masses of carbon in the samples, slightly superior to the L_Q , were not sufficient for the applicability of the carbon determination (tables 3-5 and 3-6). One approach to measure low-carbon concentrations is the enrichment of the sample in carbon, by taking larger sample masses, as performed for the extraction of BC.

3.4.5 Testing the extraction of Black Carbon

Separate lithogenic graphite samples were exposed to the unique sulfo-dichromate procedure (OREC extraction). The rate of oxidation was monitored as a function of the dry loaded filter sample (graphite mass loss) with time (table 3-7, figure 3-4). The results were corrected given an initial weight loss of 6%, due to our filtration technique.

The behavior of the lithogenic graphite during an extended period of oxidation in the acid dichromate solution is consistent with the rate of oxidation given by Wolbach and Anders (1989) for a commercial BC standard (*ca.* 2% at 65h).

Time (hr)	Graphite lithogenic	Time (hr)	Black Carbon
0	100	0	100
24	99.19	1.5	99.4
48	98.84	4	98.8
65	97.88	6	98.6
92	97.71	11.2	98.1
161	95.89	20	97.8
		46	97.7
		181	92.0

Table 3-7: Dichromate oxidation of the lithogenic graphite used in this study compared to the BC standard used by Wolbach and Anders (1989).

To ensure that handling losses were negligible, we performed a rinsing test on

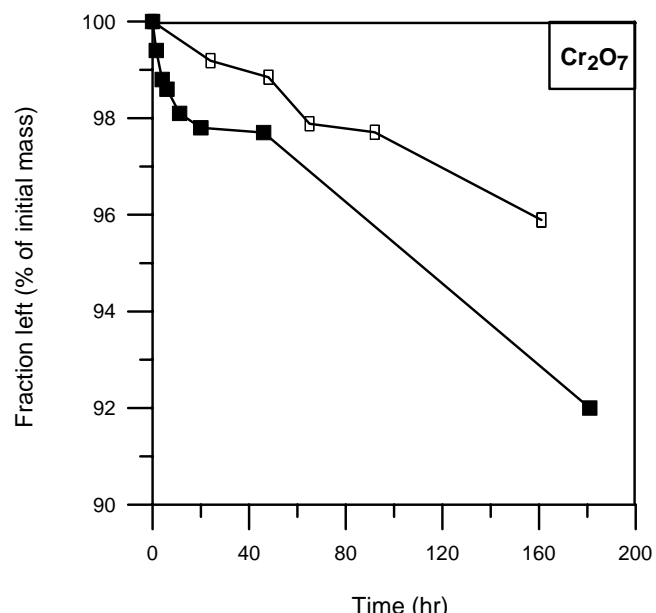


Figure 3-4: Dichromate oxidation of the lithogenic graphite used in this study (white squares), compared to the BC standard used by Wolbach and Anders (1989)(dark squares).

silica-matrices containing some synthetic graphite and charcoal. The carbon contents measured before and after the rinsing steps show that the rinsing steps did not affect the carbon content (tables 3-8 a and b), indicating that the carbon was well retained by the silica-matrix during centrifugation and rinsing.

a) Gte stc 0.86; SiO₂ 99.14 % %OC measured	
Before rinsing	After rinsing
0.835	0.889
0.837	0.828
0.861	0.853
0.895	
0.857 (0.028)	0.857 (0.030)

b) Charcoal 0.77; SiO₂ 99.23 % %OC measured	
Before rinsing	After rinsing
0.629	0.648
0.637	0.631
0.640	0.626
0.638	
0.636 (0.005)	0.635 (0.011)

Tables 3-8 a and b: Carbon contents (% OC) measured before and after the rinsing steps, on 10-20 mg of synthetic samples containing a) graphite and b) charcoal (after acidification HCl 2M).

For the BC experiment, we prepared seven synthetic matrices composed of SiO₂ and CaCO₃, in which we added one carbonaceous standard. To evaluate the potential interference of organic matter, we added acetanilide into two matrices containing synthetic graphite (table 3-9). OC and BC theoretical contents were calculated from the initial weight proportion of the standards in the matrices and their carbon content (TC, table 3-1). The percentage of charred BC is the carbon which survives the combined oxidation (% charred BC = 100 x BC_{measured} /BC_{theoretical}). The results are presented in detail in table 3-9 and summarized in table 3-10. The reliability of the BC extraction is discussed in the following part.

Hc acid 5.167 ; CaCO ₃ 79.82; SiO ₂ 15.00 %	Total mass of matrice = 1004.10 mg
mass (mg)	% C
Sample	C
164.30	0.044
295.79	0.160
220.42	0.057
n=3; mean (SD)	0.036 (0.018)

Gte stc 0.423 ; CaCO ₃ 89.50; SiO ₂ 10.08 %	Total mass of matrice = 1004.56 mg
mass (mg)	BC m
Sample	BC th
229.78	0.974
267.76	1.135
n=2;	mean 0.307

Gte stc 0.466 ; CaCO ₃ 87.05; SiO ₂ 9.87 ; Acet 2.61 %	Total mass of matrice = 1012.99 mg
mass (mg)	BC m
Sample	BC th
235.99	1.102
246.21	1.150
243.31	1.136
n=3;	mean (SD) 0.368 (0.008)

Gte lito 0.735 ; CaCO ₃ 88.95; SiO ₂ 10.3 %	Total mass of matrice = 1000.03 mg
mass (mg)	BC m
Sample	BC th
321.49	2.369
325.42	2.398
n=2;	mean (SD) 0.598 (0.018)

Gte lito 0.112 ; CaCO ₃ 94.72; SiO ₂ 5.16 %	Total mass of matrice = 1995.57 mg
mass (mg)	BC m
Sample	BC th
514.27	0.591
429.59	0.494
485.87	0.559
510.77	0.587
n=4;	mean (SD) 0.086 (0.010)

Table 3-9 : Estimation of the carbon loss associated with the thermal and chemical treatments on synthetic mixtures of known composition (weight %). Carbon (C) content (%C), BC theoretical (BC th) and measured (BC m), number of replicate analyses (n); mean carbon content and standard deviation (SD) in bold characters.

	% OC theoretical	% BC _{th} theoretical	% BC _m measured	SD	n	Charred BC % (BC _m /BC _{th} × 100)
Humic acids	1.974	—	0.036	0.018	3	1.81 ^a
Synthetic graphite	1.262	1.262	1.092	0.039	3	86.53
Synthetic graphite	4.754	1.243	1.020	0.031	4	82.06
Synthetic graphite	0.421	0.421	0.307		2	72.92
Synthetic graphite	2.321	0.463	0.368	0.008	3	79.48
Lithogenic graphite	0.730	0.730	0.598		2	81.92
Lithogenic graphite	0.111	0.111	0.086	0.010	4	77.48
						mean (SD) 80.06 (4.63)

a. % Charred BC = 100 × BC measured / OC theoretical

Table 3-10 : Results of the thermo/chemical oxidative treatment on synthetic matrices. OC and BC theoretical contents were calculated knowing the initial proportion of standards in the matrices (%weight) and their carbon content (%TC; table 3-1).

3.5 Discussion

3.5.1 Reliability of the TRC extraction

The results of the TRC extraction indicated that acetanilide and charcoal carbon were more labile than humic acids carbon because the TRC measured on the former samples was below the L_Q. This suggested that OC and charcoal would be removed by the single thermal treatment at 375°C. Humic acids carbon was more resistant, with 70% of charred TRC. This indicated that the thermal treatment at 375°C allows to distinguish between labile and refractory OC compounds, and that the thermal behavior of the highly polymerized compounds (humic acids) compared with that of the “soot carbon” compounds.

Preliminary tests are thus highly recommended to choose the more adequate method for soot determination. Although the TRC method is quick and consumes less sediment, this method provides a relatively high L_Q, because of limited sample size. Considering that the soot concentration in pelagic sediments is inferior to 0.1% of bulk dry sediment (Smith *et al.*, 1973), a

preliminary enrichment in soot carbon is needed to perform reliable TRC measurements. Moreover, the influence of the sedimentary environment on the deposition and preservation of some highly oxidation-resistant compounds should be systematically considered to apprehend TRC as biomass burning record. In this context, the coupling of physical (charcoal) or chemical (BC) analyses is strongly recommended (chapter 4 and 5).

3.5.2 Reliability of the BC extraction

Results of BC experiment suggested that the vast majority of refractory carbon was removed by the combined thermo/chemical procedure, since humic acids charred BC accounted for less than 2% (table 3-10). As evidenced by the matrices containing similar synthetic graphite quantity \pm acetanilide, the presence of acetanilide in the samples did not biased the BC content (table 3-10).

The correlation between the graphite added (% graphite weight) and the BC measured (BC_m) is remarkable (figure 3-5, $r^2 = 0.99$, $n=18$). The reproducibility of the BC determinations (<0.1%) demonstrates the applicability of the BC method to synthetic matrices containing silicates, carbonates, and OC.

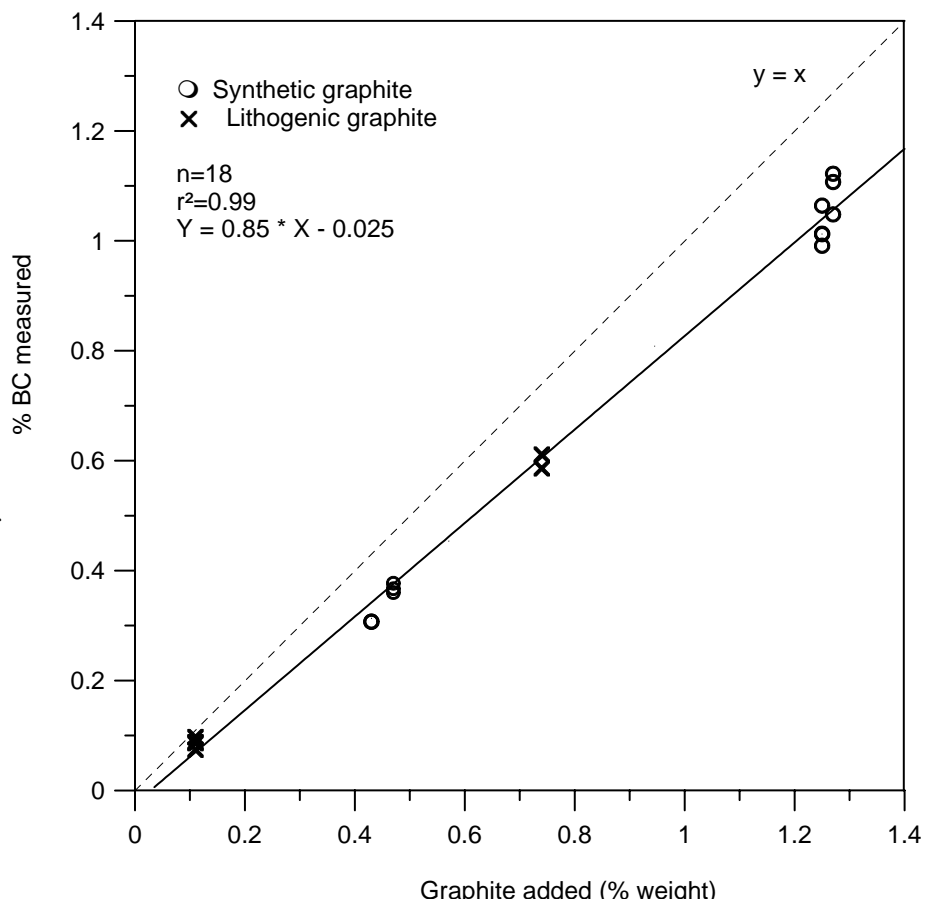


Figure 3-5: % BC measured as a function of graphite added (% weight). Synthetic graphite (circles), lithogenic graphite (crosses); $n=18$, $r^2 = 0.99$.

The recovery of the method is estimated by the mean charred BC, accounting for *ca.* $80.06 \pm 4.63\%$ of the theoretical charred BC (table 3-10). Individual charred BC results are presented on figure 3-6 as a function of the graphite added (% carbon). The larger spread towards the lower concentration of carbon, is presumably due to the much lower elemental carbon levels in these samples.

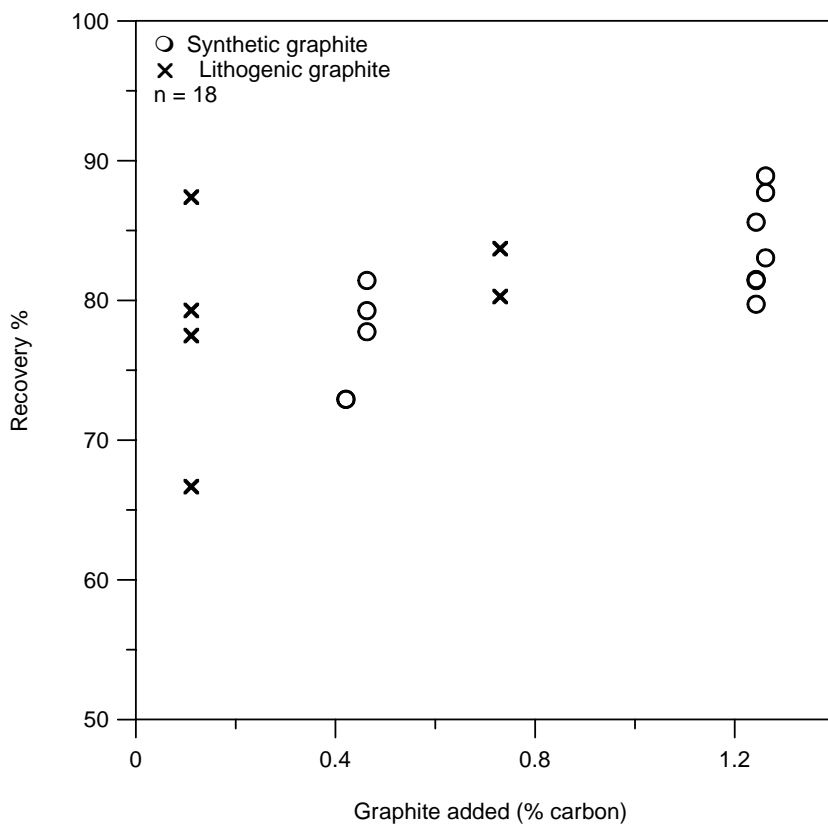


Figure 3-6: The recovery of the BC extraction as a function of graphite added (% carbon). Synthetic graphite (circles), lithogenic graphite (crosses); $n=18$.

The BC method was finally applied on two natural lacustrine (core MM8) and marine (core MD40) sediment samples, adding lithogenic graphite (tables 3-11 a and b, figure 3-7). The sedimentary intrinsic BC (BC_0) was determined and subtracted to the BC measured, yielding a recovery of *ca.* 81 and 95 % in the lacustrine and marine sediment, respectively (tables 3-11 a and b). Such difference between the recovery of the BC experiment in lacustrine and marine sediment, likely suggests that effect of grain-size, terrigenous fraction, especially clay content, has an effect on reducing loss of graphite during the filtration/rinsing steps of the procedure.

a) Gte lito 0.177; SiO₂ 4.97; MM8 sediment 94.85 %, BC₀ = 0.023					
Mass (mg)			BC %	BC – BC₀ %	Charred BC %
Sample	BC lito	BC m			
445.89	0.789	0.682	0.153	0.130	74.00
484.32	0.857	0.768	0.159	0.136	77.42
545.58	0.965	0.873	0.160	0.137	77.98
475.96	0.842	0.907	0.191	0.168	95.63
n=4; mean (SD)		0.166 (0.017)		0.143 (0.017)	81.26 (9.74)

b) Gte lito 0.113; SiO₂ 4.79; MD40 sediment 95.09 %, BC₀ = 0.016					
Mass(mg)			BC %	BC – BC₀ %	Charred BC %
Sample	BC lito	BC m			
516.44	0.580	0.694	0.134	0.118	105.21
451.82	0.508	0.586	0.130	0.114	101.64
538.43	0.605	0.534	0.099	0.083	74.01
437.64	0.492	0.556	0.127	0.111	98.97
n=4; mean (SD)		0.123 (0.016)		0.107 (0.016)	94.96 (14.20)

Tables 3-11 a and b: BC lithogenic mass added (BC_{lito}), BC measured mass (BC_m), BC content measured (%BC), and intrinsic BC (BC₀).

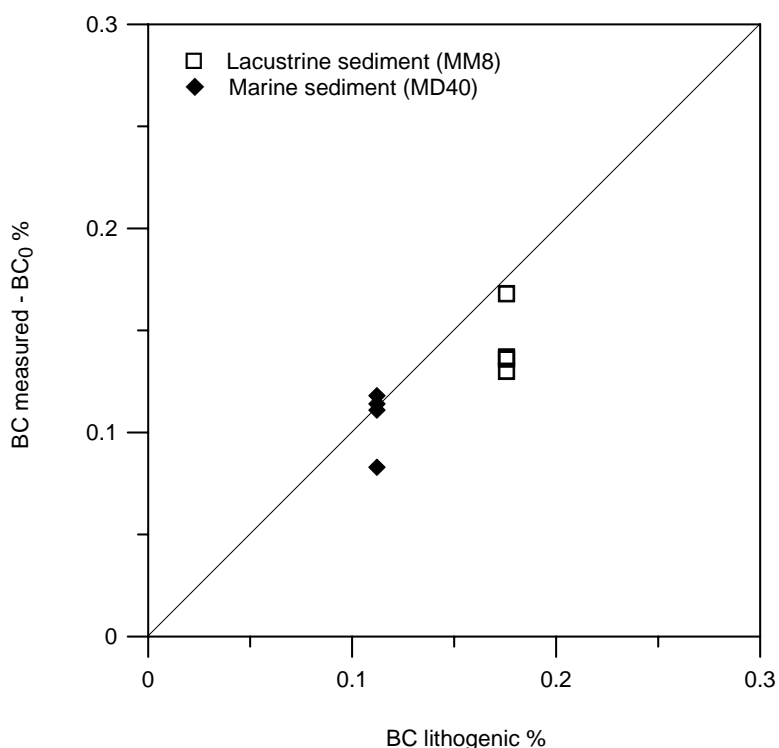


Figure 3-7: BC measured mass as a function of BC lithogenic mass added in lacustrine sediment (squares), and in marine sediment (lozenges).

This experimental loss of carbonaceous standard might also affected the synthetic matrices. As shown on figure 3-8, the recovery of the BC on synthetic matrices (from table 3-10) decreases while CaCO_3 proportion increases in the matrices (figure 3-8). This suggests that the remaining matrices (synthetic silica or natural clay) reduce the loss of BC during rinsing and filtration steps.

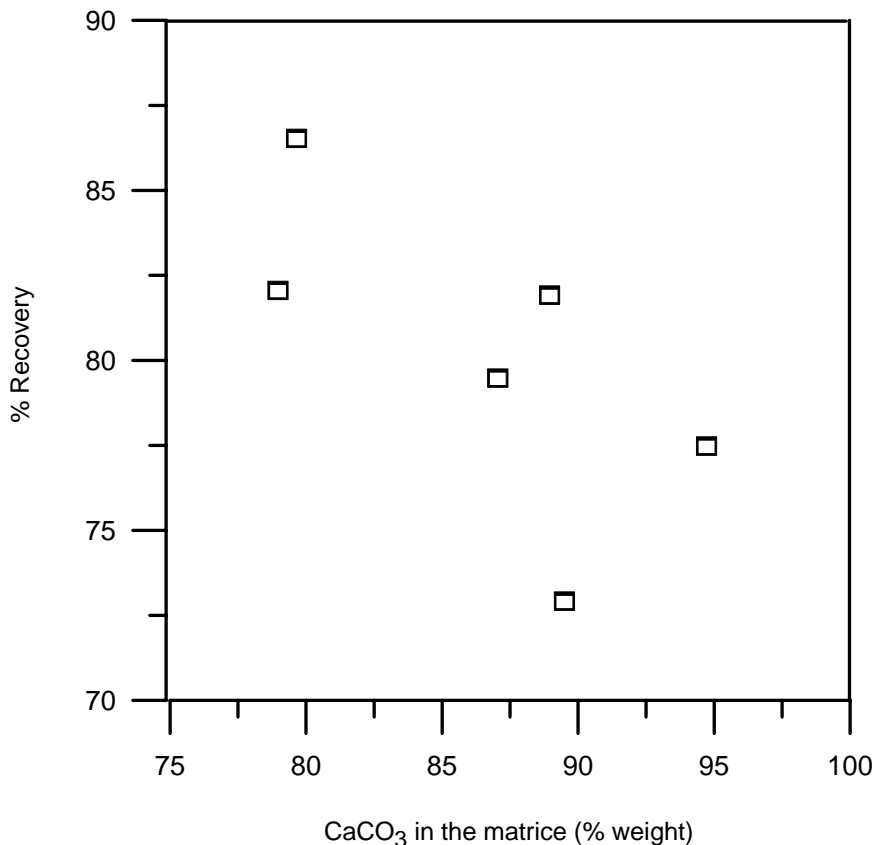


Figure 3-8: BC recovery as a function of CaCO_3 content in synthetic matrices.

3.6 Conclusion

In this study, we established an experimental method for quantifying sedimentary carbonaceous aerosols. Application of a single thermal treatment (375°C during 24h) to synthetic samples removed organic labile and charcoal carbon, preserving most of the BC and refractory carbon compounds which formed natural soot. However, because the refractory carbon compounds such as humic acids were not completely removed (charred TRC *ca.* 70%), the extraction of soot with a thermal method in sediments should be interpreted with caution.

Coupling thermal and acidic oxidative procedures was required to remove refractory carbon. The results indicate a satisfactory reproducibility of the method in application to synthetic and natural matrices. Results therefore suggested that the BC extraction would efficiently remove the most refractory contaminating materials, such as those derived from the degradation of leave or wood and/or from soil maturation. Moreover, the BC extraction which is performed in polyethylene test tubes, is not limited by the initial mass of the sample. Therefore, this procedure could be applied to a wide variety range of BC-poor natural materials.

The graphite standards were resistant to the thermal and chemical treatments (loss <3%), while the mean charred BC in synthetic matrices accounted for *ca.* $80 \pm 5\%$. This experimental loss of BC (rinsing/filtration) does not biased the accuracy of the method. However, the applicability of the BC extraction to clayey-poor sediments should be undertaken with caution. Further inter-calibrations using natural (aerosols) and commercial BC standards are needed to further improve the sedimentary records of biomass burning, and to establish the contribution of BC in the global cycle of carbon.

4. A 360 kyr record of carbonaceous biomass burning proxies from core MD972140, West Equatorial Pacific: Sedimentary, climate and human implications

4.1 Introduction

Biomass burning in the tropics releases today about one third of annual anthropogenic CO₂ emissions and large amounts of aerosol particles playing an important contribution to atmospheric chemistry and climate (chapter 1) (Seiler and Crutzen, 1980; Crutzen and Andreae, 1990; Hao *et al.*, 1990). Despite such major environmental effects, the dynamics of tropical fires, however, is still poorly documented and understood for the past, especially at the scale of global, glacial-interglacial climate cycles (Verardo and Ruddiman, 1996; Bird and Cali, 1998).

The aim of this chapter is to provide a Late Pleistocene multiproxy record of biomass burning from the West Pacific-East Asian region, a fire-sensitive region where present-day devastating forest fires are triggered and sustained by the combination of landuse practices, and regional changes in length and intensity of the dry season, in association with the El Niño-Southern Oscillation (ENSO) (Goldamer and Seibert, 1990; Goldamer, 1997).

To date, most marine sedimentary records of past biomass burning have been reconstructed by using physical analysis (microcharcoal counting) and/or chemical analysis (analysis of Oxydo-Resistant Elemental Carbon or OREC, Black Carbon or BC) of carbonaceous products (Bird and Cali, 1998; Gustafsson and Gschwend, 1998; Moss and Kershaw, 2000; van der Kaars *et al.*, 2000; Beaufort *et al.*, in press). Given the complex sources and behavior of carbonaceous material in sedimentary environments (chapter 2), and the lack of intercalibration between such methods, we combined OREC analysis, BC analysis, and charcoal counting on the same cored sequence to improve the reliability of biomass fire reconstruction.

To reconstruct past emissions of pyrogenic products and fire activity in the West Pacific-East Asian region, we investigated a 360 kyr pelagic sedimentary record from the Western Pacific Warm Pool (WPWP), North of Papua New Guinea.

4.2 General setting

Present-day oceanography and climate in the West Pacific Warm Pool area

The WPWP occupies the East Indian–West Pacific areas and is centered at the Equator, northeast of Papua New Guinea, close to the MD972140 coring site. The WPWP region contains the warmest surface waters of the global ocean. At annual scale, the precipitation pattern over the region is tied to the seasonal shift of the Intertropical Convergence Zone (ITCZ) and the trans-equatorial cold surge of the northern winter monsoon (An, 2000). The resulting Australian summer monsoon and summer rainfall affect an area which includes Indonesia, Papua New Guinea, and northern Australia. In the central highlands of Papua New Guinea, a double rainfall maximum occurs around March and September/October of each year (Haberle *et al.*, 1998), approximately in phase with the two insolation maxima at the Equator (spring and autumn equinoxes). Previous regional studies have shown that biomass burning in the region is closely controlled by the seasonal distribution of rains, and by its orbital (precession) forcing (Haberle and Ledru, 2001).

At interannual scale, zonal changes of the WPWP associated with ENSO-like oscillations cause dramatic changes in duration and regional extent of the dry season: at the onset of “warm” ENSO events (El Niño), the WPWP surface waters are driven eastward by the near-equatorial westerly winds associated to the East Asian winter monsoon. In the far western Pacific, concurrent upwelling and vertical mixing result in a cooling of sea surface temperatures (SSTs) (Perks and Keeling, 1998). Consequently, atmospheric convection and rainfall dramatically weaken above the tropical rainforests of the East Indian-West Pacific area. The recent massive fires that occurred in Indonesia were caused by the association between such dry, ENSO-driven conditions, and human forest clearing and occupation. It has thus been suggested that similar dramatic events possibly occurred during the Late Pleistocene (Goldamer, 1993; Goldamer, 1999; Haberle and Ledru, 2001; Siegert *et al.*, 2001).

Depositional setting of core MD972140

The 37.4 meter-long core MD972140 (2°N, 142°E; 2547m water depth) was collected on the southwestern slope of the NNE-SSW trending Eauripik ridge, during the IPHIS-IMAGE III cruise of the R.V. Marion Dufresne, in 1997. The coring site is located *ca.* 400 km North off Papua New Guinea in the Caroline Basin. Because it is separated from the continent by the New Guinea trench, the coring site is relatively isolated from the influence of terrigenous inputs from

Papua New Guinea, which scavenge in the deep hemipelagic region through a very narrow shelf (Woolfe and Lacombe, 1998).

The Caroline Basin (maximum depth: *ca.* 5000m) is isolated from the western North Pacific by a rise including the Sonsorol and Caroline Islands, and the Eauripik Rise (figure 4-1). This basin is located at the western end of the flow path of bottom waters from the equatorial Pacific. Below *ca.* 3000 m water depth, poor preservation of carbonates in the western Caroline Basin is found and may be caused by a strengthened alkalinity and carbon dioxide enrichment of bottom waters, in response to the isolation of the Caroline basin (Kawahata *et al.*, 1997).

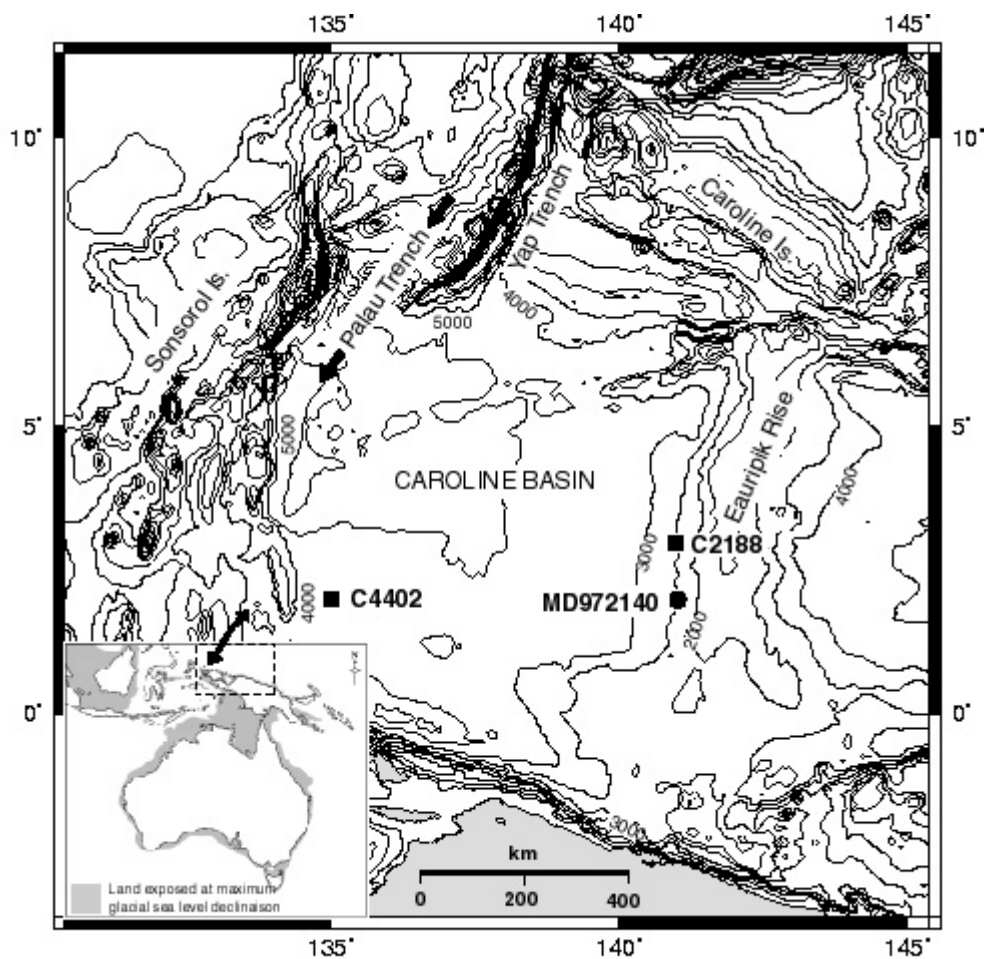


Figure 4-1: Regional map of the Papua New Guinea and Northern-Australian region with ancient exposed land shaded (Sahul), and bathymetric map of the West Caroline Basin showing the location of the core used in this study: dark circle represents MD972140 at 2547 m of 2°N and 141°E. The black square represents the core cited in this study: C4402 at 4402 m of 2°N and 135°E, and C2188 at 2188 m of 3°N and 141°E. The dark arrow identifies the predicted primary flow path of the Pacific bottom and deep waters into the West Caroline Basin (modified from Kawahata *et al.*, 1997).

4.3 Lithology, stratigraphy and sampling

The core MD972140 sediment consists in bioturbated, olive-grey nannofossil ooze. Like most pelagic carbonate sequences from the tropics, low amplitude changes in volume magnetic susceptibility κ (shipboard measurements) indicate a cyclic dilution of the carbonates by dominantly paramagnetic clays (Yamazaki and Loka, 1997).

A well-constrained oxygen isotope chronostratigraphy of core MD972140 has been established from the $\delta^{18}\text{O}$ record of *Globigerinoides ruber* (planktonic foraminifera) by de Garidel-Thoron et al. (in prep). For the upper part of the core (i.e. above the isotope stage 3-2 transition), the depth-age model was obtained by correlation with the radiocarbon-dated *Globigerinoides ruber* isotopic record of the neighboring core MD972138. Correlation with the SPECMAP stack (Imbrie *et al.*, 1984) was used for the bottom part of the record. The resulting depth-age curve (figure 4-2) locates the upper 14 meters of the core in the last 350 kyr, from Marine Isotope Stage (MIS) 10.

One striking feature of the depth-age relationship is the general upcore increase in mean apparent deposition rate, from *ca.* 1.6 cm.kyr⁻¹ at the bottom of the record to *ca.* 6 cm.kyr⁻¹ at the top (figure 4-3). This increase most probably reflects the elongation of the upper cored sediments in the Calypso piston corer, as previously reported from i) core sub-sampling observations and ii) measurements of the sediment magnetic fabric (Thouveny *et al.*, 2000).

For the purpose of this study, the upper 13.5 meters of the core were sub-sampled at 5cm depth-interval and stored at -20°C until analysis in CEREGE laboratories. The sampling interval yielded a resolution of 0.8-3 kyr

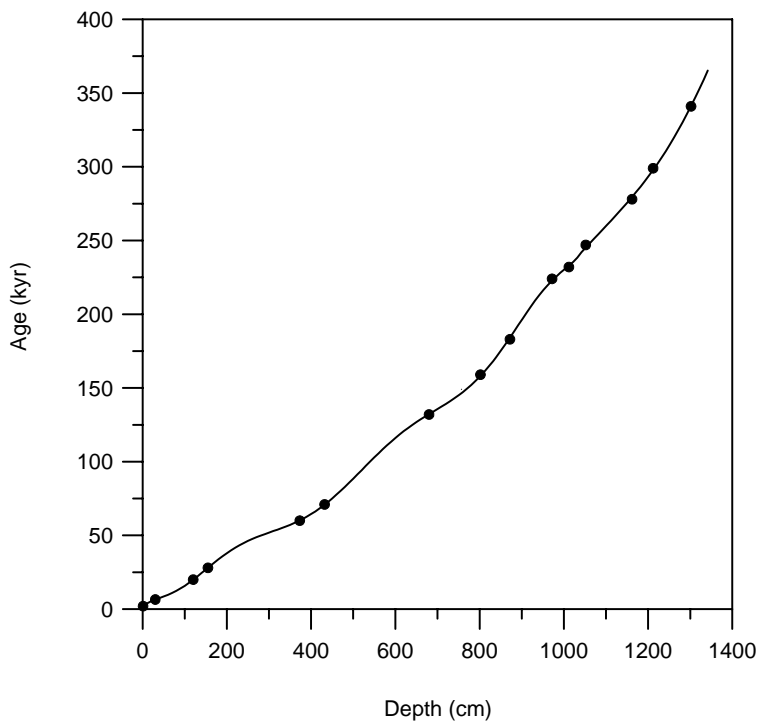


Figure 4-2: Age-depth relationship in core MD972140.

4.4 Methods

Physical and chemical techniques have been developed to characterize biomass-burning fingerprints. The plant-derived material partially altered and blackened by fire is generally referred as charred by microscopic or chemical characteristics (Jones *et al.*, 1997): i) Small charcoal particles are formed in fuel by low-temperature pyrolysis processes, and carried out with smoke emissions. ii) Soot particles (submicrometer or up to less than 1 µm size) are emitted with smoke and form via gas-phase processes, and gas-to-particle conversion. iii) During a fire at high temperature and intense flaming combustion, more carbon is reduced nearly its elemental state and referred as Black Carbon (BC) (Cofer *et al.*, 1997). The fire-originating aromatic to graphitic carbon particulate fraction (0.01 - 1 µm size range) is primarily produced in fire-altered material or smoke particulate (Penner *et al.*, 1992; Jacobson, 2001).

To improve the detection of fire-originating products, we combined the chemical extraction of elemental carbon, and charcoal counting. The analysis of organic and inorganic carbon (carbonate) was performed to reconstruct the general variability of deposition at the coring site, and to ensure that the charred determination was not biased by these carbonaceous components.

4.4.1 Organic Carbon (Corg) and calcium carbonate (CaCO_3) analyses

Sediment samples were taken at 5 cm depth interval along the upper 13.5 meters of the core, and stored at -20°C until analysis in CEREGE laboratories. The samples were lyophilized and grounded into a fine powder with an agate mortar. Carbon measurements were performed by using the automatic NA-1500 Elemental Analyzer. Total carbon (Ctotal) was measured on *ca.* 10 mg of bulk sediment within Sn caps (3x5 mm). Organic carbon (Corg) was determined on *ca.* 15 mg samples, after removing carbonate by acidification (2 N HCL) in Ag caps (3x5 mm). Ctotal and Corg experimental blank values did not differ significantly, yielding determination limit (L_Q) of *ca.* 1.6 and 4.3 µg-carbon (10 times the standard deviation of the mean blank value; Currie, 1968), and relative L_Q of 0.016 and 0.029%, respectively. The carbonate (CaCO_3) concentration was then calculated as the difference between Ctotal and Corg contents (Verardo *et al.*, 1990). Data are listed in table 4-1.

Table 4-1 : Organic (Corg) and mineral (CaCO_3) carbon, Oxidant Resistant Elemental Carbon (OREC), Black Carbon (BC), and charcoal for core MD972140.

Depth (cm)	Age (kyr)	Corg (%)	CaCO_3 (%)	OREC (%)	BC (%)	Charcoal (mm ² /g)
1	1.98	0.29	61.76	0.024	0.014	2.96
6	3.00	0.26	57.29	0.032	0.019	4.62
11	4.02	0.23	60.11	0.027	0.011	2.28
16	4.77	0.21	60.03	0.027	0.009	3.29
21	5.49	0.23	62.69	0.031	0.014	0.96
26	6.08	0.18	64.84	0.017	0.011	1.53
31	6.64	0.19	62.90			
36	7.15	0.25	60.64	0.021	0.009	2.47
41	7.65	0.19	59.82			
46	8.16	0.20	60.45			
51	8.67	0.18	60.74	0.027	0.012	1.80
56	9.21	0.19	59.38			
61	9.79	0.24	55.29			
66	10.39	0.28	53.39	0.031	0.021	2.91
71	11.06	0.40	51.73	0.045	0.024	2.77
76	11.74	0.50	52.77	0.059	0.028	3.18
81	12.52	0.59	51.08	0.073	0.031	3.43
86	13.29	0.58	50.14	0.081	0.013	3.32
91	14.17	0.64	47.13	0.067	0.015	1.85
101	16.01	0.69	47.62	0.106	0.013	2.09
106	16.99	0.66	46.79	0.101	0.013	2.88
111	18.02	0.54	46.38	0.075	0.014	2.01
116	19.08	0.51	47.07	0.089	0.017	3.16
121	20.17	0.58	47.54	0.076	0.013	4.14
126	21.29	0.63	48.33	0.066	0.012	4.21
131	22.42	0.58	47.69		0.011	
136	23.58	0.56	46.05			
141	24.74	0.69	45.35	0.062	0.012	2.26
146	25.92	0.60	47.29		0.010	
151	27.09	0.52	49.53	0.060	0.015	2.38
156	28.27	0.51	49.96			
161	29.44	0.46	51.25	0.051	0.018	2.82
166	30.59	0.46	53.54			
171	31.74	0.47	56.26			
176	32.86	0.50	56.99	0.050	0.014	2.85
181	33.98	0.52	58.75			
186	35.05	0.45	59.41	0.045	0.017	2.39
191	36.12	0.41	60.03			
196	37.14	0.46	61.00	0.053	0.021	2.46
201	38.15	0.42	59.66			
206	39.11	0.42	61.00			
211	40.06	0.43	59.88	0.050	0.014	3.55
216	40.96	0.44	60.70	0.048	0.016	1.99
221	41.83	0.39	58.53		0.006	
226	42.67	0.38	58.96	0.038	0.030	2.27
231	43.47	0.41	62.01			
236	44.26	0.40	60.90			
241	44.99	0.44	59.33	0.047	0.027	2.31
246	45.71	0.42	59.27			
251	46.38	0.45	59.44			

Table 4-1 (continued)

Depth (cm)	Age (kyr)	Corg (%)	CaCO ₃ (%)	OREC (%)	BC (%)	Charcoal (mm ² /g)
256	47.05	0.42	60.19	0.045	0.025	4.08
261	47.66	0.47	60.66		0.007	
266	48.27	0.49	61.36	0.055	0.016	2.08
271	48.85	0.48	57.79		0.009	
276	49.41	0.50	58.01	0.045	0.042	1.53
281	49.95	0.38	59.17			
286	50.48	0.35	59.82	0.040	0.034	1.74
291	51.00	0.37	60.04			
296	51.51	0.46	60.57	0.037	0.039	3.82
306	52.51	0.32	62.25	0.038	0.026	2.42
316	53.50	0.36	64.09		0.006	
326	54.51	0.31	65.35	0.031	0.008	3.05
336	55.57	0.33	66.35		0.006	
346	56.68	0.34	65.62	0.033	0.007	1.28
356	57.88	0.36	63.26			
366	59.17	0.46	59.43	0.046	0.008	2.33
376	60.57	0.47	54.80			
386	62.09	0.50	51.65	0.053	0.009	
396	63.74	0.58	47.99	0.054	0.015	3.74
406	65.53	0.59	46.45	0.069	0.012	2.72
416	67.46	0.47	43.95	0.052	0.011	2.95
426	69.53	0.37	52.15	0.039	0.008	2.76
436	71.74	0.35	54.48	0.035	0.010	2.12
446	74.09	0.24	57.41	0.036	0.010	
456	76.55	0.27	66.17			0.37
466	79.13	0.24	70.81	0.026	0.004	
476	81.80	0.45	57.11			
486	84.55	0.26	61.23	0.034	0.009	1.70
496	87.37	0.32	61.00			
506	90.23	0.29	60.40	0.039	0.008	1.21
516	93.11	0.35	60.88	0.039	0.009	0.32
526	96.01	0.28	58.38			
531	97.46	0.32	60.30	0.045	0.007	0.68
536	98.90	0.29	59.83			
541	100.34	0.25	59.70			
546	101.76	0.25	60.32	0.029	0.004	0.58
551	103.17	0.24	62.82			
556	104.57	0.29	58.67			
561	105.96	0.24	65.07	0.035	0.010	2.72
566	107.33	0.24	66.51			
571	108.68	0.30	66.34	0.033	0.007	0.65
576	110.01	0.24	63.67	0.033	0.007	0.89
581	111.31	0.23	60.09	0.088	0.010	1.40
586	112.61	0.24	58.55	0.034	0.014	2.04
591	113.86	0.28	60.13			
596	115.11	0.24	58.33	0.058	0.016	2.28
601	116.31	0.28	55.29			
606	117.51	0.26	55.68	0.032	0.009	
611	118.65	0.24	56.86			
616	119.80	0.23	57.57	0.039	0.011	1.75
621	120.90	0.26	60.72			

Table 4-1 (continued)

Depth (cm)	Age (kyr)	Corg (%)	CaCO ₃ (%)	OREC (%)	BC (%)	Charcoal (mm ² /g)
626	121.98	0.19	66.11			
631	123.03	0.16	68.16	0.026	0.004	0.62
636	124.07	0.19	67.32			
641	125.07	0.17	67.86			
646	126.06	0.23	61.63	0.027	0.006	0.87
651	127.02	0.18	67.34			
656	127.96	0.24	56.39	0.026	0.006	0.44
661	128.89	0.30	54.78			
666	129.80	0.32	60.57	0.040	0.009	2.94
671	130.70	0.41	53.07	0.073	0.011	0.79
676	131.57	0.54	53.45	0.073	0.014	1.42
681	132.45	0.48	51.39	0.069	0.007	0.60
686	133.31	0.44	55.92			
691	134.17	0.42	53.73	0.079	0.009	0.76
696	135.03	0.51	54.32		0.013	
701	135.89	0.46	57.58	0.074		1.87
706	136.75	0.52	56.67	0.038	0.008	1.38
711	137.62	0.45	58.18			
716	138.50	0.43	58.97	0.056	0.007	1.26
721	139.39	0.41	60.16			
726	140.30	0.37	62.15	0.053	0.009	1.21
731	141.23	0.40	63.83			
736	142.18	0.44	62.68			
741	143.15	0.45	58.41	0.048	0.009	
751	145.20	0.36	58.22	0.058	0.009	1.47
756	146.26	0.37	53.45	0.071	0.008	1.53
761	147.38	0.43	54.68	0.079	0.009	1.71
766	148.51	0.46	55.24			
771	149.72	0.42	55.89	0.064	0.013	1.15
776	150.93	0.41	58.96			
781	152.23	0.40	58.71	0.115	0.011	4.68
786	153.54	0.33	51.15			
791	154.94	0.36	55.51	0.062	0.007	4.04
796	156.35	0.31	61.80			
801	157.85	0.26	66.16	0.036	0.008	3.02
806	159.37	0.22	62.18	0.035	0.009	
811	160.97	0.27	69.89			
816	162.60	0.27	71.78	0.039	0.007	3.90
821	164.29	0.27	59.09			
826	166.04	0.30	68.14			
831	167.82	0.30	60.19	0.042	0.007	1.36
836	169.67	0.31	65.73	0.053	0.011	2.53
861	179.50	0.38	55.98	0.050	0.010	1.71
866	181.59	0.37	56.50	0.070	0.009	4.16
871	183.68	0.41	53.84	0.094	0.009	2.16
876	185.80	0.39	55.04	0.047	0.010	3.49
881	187.94	0.28	54.95	0.067	0.013	1.81
886	190.09	0.27	58.73	0.118	0.010	5.03
891	192.24	0.24	58.29	0.038	0.009	
896	194.39	0.21	61.11			
901	196.53	0.24	66.00	0.037	0.005	4.90

Table 4-1 (continued)

Depth (cm)	Age (kyr)	Corg (%)	CaCO ₃ (%)	OREC (%)	BC (%)	Charcoal (mm ² /g)
906	198.66	0.25	69.64			
911	200.77	0.20	68.60			
916	202.86	0.17	69.00	0.027	0.007	1.63
921	204.91	0.16	65.24			
926	206.93	0.18	61.18	0.028	0.008	1.40
931	208.89	0.25	61.57			
936	210.83	0.25	62.52	0.044	0.009	2.35
941	212.67	0.21	64.19			
946	214.51	0.19	62.55	0.096	0.011	2.54
951	216.23	0.25	70.03	0.096	0.008	1.80
956	217.94	0.15	67.19	0.017	0.010	0.86
961	219.52	0.15	71.26			
966	221.09	0.14	68.84	0.017	0.006	0.61
971	222.55	0.17	69.47			
976	223.97	0.22	71.51	0.030	0.003	1.40
981	225.32	0.23	68.44	0.035	0.006	0.98
986	226.62	0.24	65.72			
991	227.87	0.28	66.17			
996	229.08	0.21	64.94	0.036	0.006	0.80
1001	230.28	0.24	60.40			
1006	231.46	0.24	60.59	0.028	0.005	1.15
1011	232.66	0.20	65.08			
1016	233.90	0.16	66.99	0.017	0.004	1.31
1021	235.17	0.13	70.62		0.008	
1026	236.60	0.19	71.27	0.017	0.006	1.09
1031	238.05	0.20	66.94		0.008	
1036	239.84	0.16	67.83	0.026	0.006	2.22
1041	241.62	0.23	60.54			
1046	243.46	0.23	59.68	0.031	0.005	1.76
1051	244.95	0.32	62.82			
1056	246.44	0.32	62.95			
1061	247.94	0.29	63.35	0.053	0.005	2.84
1066	249.45	0.28	64.30			
1071	250.96	0.27	68.29	0.034	0.004	0.33
1076	252.47	0.24	67.36			
1081	253.99	0.20	66.35			
1086	255.51	0.25	69.21			
1091	257.03	0.24	71.08	0.024	0.004	0.13
1096	258.56	0.24	70.27			
1101	260.09	0.32	67.08			
1106	261.63	0.26	64.27			
1111	263.17	0.30	66.92			
1116	264.72	0.27	59.60			
1121	266.28	0.31	50.12	0.041	0.004	0.65
1126	267.85	0.31	57.41			
1131	269.43	0.28	61.05			
1136	271.02	0.18	65.33	0.025	0.004	2.32
1141	272.62	0.20	68.09			
1146	274.24	0.17	73.25			
1151	275.88	0.18	75.40			
1156	277.53	0.14	75.22	0.021	0.003	

Table 4-1 (continued)

Depth (cm)	Age (kyr)	Corg (%)	CaCO ₃ (%)	OREC (%)	BC (%)	Charcoal (mm ² /g)
1161	279.20	0.19	76.95			
1166	280.90	0.21	75.74			
1171	282.62	0.22	72.86			
1176	284.36	0.23	72.17			
1181	286.13	0.24	68.92	0.029	0.004	0.88
1186	287.93	0.16	69.82			
1191	289.77	0.16	71.32		0.003	
1196	291.63	0.17	72.98			
1201	293.53	0.21	73.44			
1206	295.46	0.26	72.76			
1211	297.43	0.17	74.55	0.021	0.003	1.93
1216	299.44	0.17	73.37			
1221	301.49	0.32	66.19			
1226	303.59	0.20	61.50	0.047	0.007	1.72
1231	305.72	0.21	62.95			
1236	307.91	0.24	65.03			
1241	310.13	0.18	64.41	0.037	0.004	3.62
1246	312.41	0.29	64.44			
1251	314.73	0.14	65.38			
1256	317.10	0.15	65.99			
1261	319.52	0.13	73.80	0.013	0.003	0.58
1266	321.99	0.16	72.93			
1271	324.50	0.15	57.99			
1276	327.07	0.18	57.66	0.023	0.006	1.47
1281	329.69	0.21	59.27			
1286	332.36	0.35	59.07			
1291	335.07	0.31	58.66			
1296	337.84	0.24	58.07	0.044	0.010	1.53
1301	340.65	0.26	61.70			
1311	346.41	0.22	65.70	0.038	0.006	3.46
1321	352.34	0.33	67.92	0.034	0.012	2.52
1331	358.43	0.18	58.46	0.028	0.006	3.01
1341	364.65	0.21	68.23	0.026	0.007	0.87
1346	367.80	0.19	66.59		0.007	

4.4.2 Oxidant Resistant Elemental Carbon (OREC) and Black Carbon (BC) analyses

Two methods (OREC and BC extractions) were used to remove mineral and organic carbon compounds, and to concentrate the elemental refractory carbon components. The OREC method has been previously applied to extract the elemental carbon (soot, charcoal) in sample of the Cretaceous-Tertiary boundary clay (Wolbach and Anders, 1989). However, Bird and Gröcke (1997) and Bird et al. (1999) suggested that an additional peroxide or thermal oxidation step can improves the removal of any remaining refractory organic carbon.

Oxidant Resistant Elemental Carbon (OREC) extraction and measurement was performed on *ca.* 500 mg bulk sediment samples by using the method of Wolbach and Anders (1989). The samples were placed into centrifugation tubes, and first treated by 3 treatments with 3*M* HCl and 10*M* HF/1*M* HCl, and 10*M* HCl, respectively. The following step consisted in oxidation during 65 h into a sulfo-dichromate solution maintained at 55°C (0.1*M* K₂Cr₂O₇ in a 2*M* solution of H₂SO₄), which removed organic compounds. Finally, the remaining insoluble residue was filtered with a vacuum pump on a pre-cleaned silica filter (heated at 550°C for 10 hours) and the resulting OREC was measured by elemental analysis within big Sn caps (10x10 mm).

The BC extraction was also performed on *ca.* 500 mg bulk sediment samples. The samples were first treated by thermal oxidation (375°C, 24h) before chemical oxidation in sulfo-dichromate (OREC extraction). Eventually, a peroxide treatment (33% H₂O₂, 24h) removed any remaining refractory carbon (Bird and Gröcke, 1997).

Although the L_Q of OREC or BC measurements (*ca.* 7.8 µg-carbon) was slightly higher than for Ctotal and Corg measurements, the treatment of *ca.* 500 mg samples allowed the applicability of the method to marine sediments (relative L_Q of 0.001%).

4.4.3 Microscopic charcoal counting

This method is based on the automated counting of microcharcoal particles as isolated by the image analysis of microscopic slides (Beaufort *et al.*, in press). To avoid contaminating opaque organic matter in microscopic preparations, three successive treatments were performed on 50-60 mg dry sediment samples to remove carbonate (15 ml of 3*M* HCl, one hour), pyrite (15 ml of HNO₃, one day), and organic material (15 ml of H₂O₂ 33%, three days), respectively. The resulting solution was filtered on a cellulose membrane mounted on a slide with Canada balm. For each slide, 100 digitized images (1.7 mm² area per image) were acquired under a light microscope by using a digitized camera coupled to the SYRACO software (SYstème de Reconnaissance Automatique de Coccolithes; Dolfus and Beaufort, 1999). The images were then analyzed using the Scion Image software (<http://www.scioncorp.com>). Identification (and analysis) of the black particles was made by isolating the particles with a gray-level (GL) value above a chosen threshold. The letter typically lies above 200, but still depends on the average lightning/GL value of the image. The results were then expressed in charcoal area per gram of initial sediment (mm²/g) (table 4-1).

4.5. Results

4.5.1 Organic and mineral carbon records

Although carbonate and Corg exports to marine sediments are partly driven by the surface biological productivity, the relative changes of these components in sediments also originate from additional processes such as the export of terrestrial organic matter to the sediments, changes in plankton communities (e.g., carbonate coccolithophorids and siliceous radiolarians and diatoms), and/or biogenic carbonate dissolution in the water column or in bottom sediments. The CaCO₃ and Corg records of core MD972140 show opposite changes over the whole record ($r = -0.74$ for the entire data set) (figures 4-11 and 4-12), with CaCO₃ values ranging between 40 and 75%, and Corg values ranging between 0.15 and 0.7%. Such pattern strongly contrasts with neighboring, shallower sediments of the Eauripik ridge (core C2188, 2188 m water depth, figure 4-1), where high and constant carbonate concentrations (*ca.* 80%) exclude significant effects of carbonate dissolution (Kawahata and Eguchi, 1996; Kawahata, 1999). As observed at deeper water depth (e.g. core C4402, 4402 m water depth figure 4-1) (Kawahata *et al.*, 1997), the negative correlation between Corg and CaCO₃ (figure 4-4) is consistent with the combined effects of i) dilution of organic matter by carbonate in variable productivity conditions, and ii) dissolution of carbonate in oxygen-deficient conditions.

Both CaCO₃ and Corg records are roughly connected with glacial-interglacial changes as reconstructed from the $\delta^{18}\text{O}$ isotope stratigraphy, with minimum carbonate values (maximum Corg values) during glacial MIS 2, 4, 6, and 8. High-frequency *ca.* 20 kyr changes are especially observed on the CaCO₃ record, suggesting that low-latitude insolation forcing strongly affects the carbonate record. Given the relatively finer grain size fraction of organic particulate matter, and the higher residence time, mixing, and bioturbation depth of the fine fraction in surficial sediments (Bard, 2001), a relative attenuation of high frequency changes in the Corg record should be ruled out.

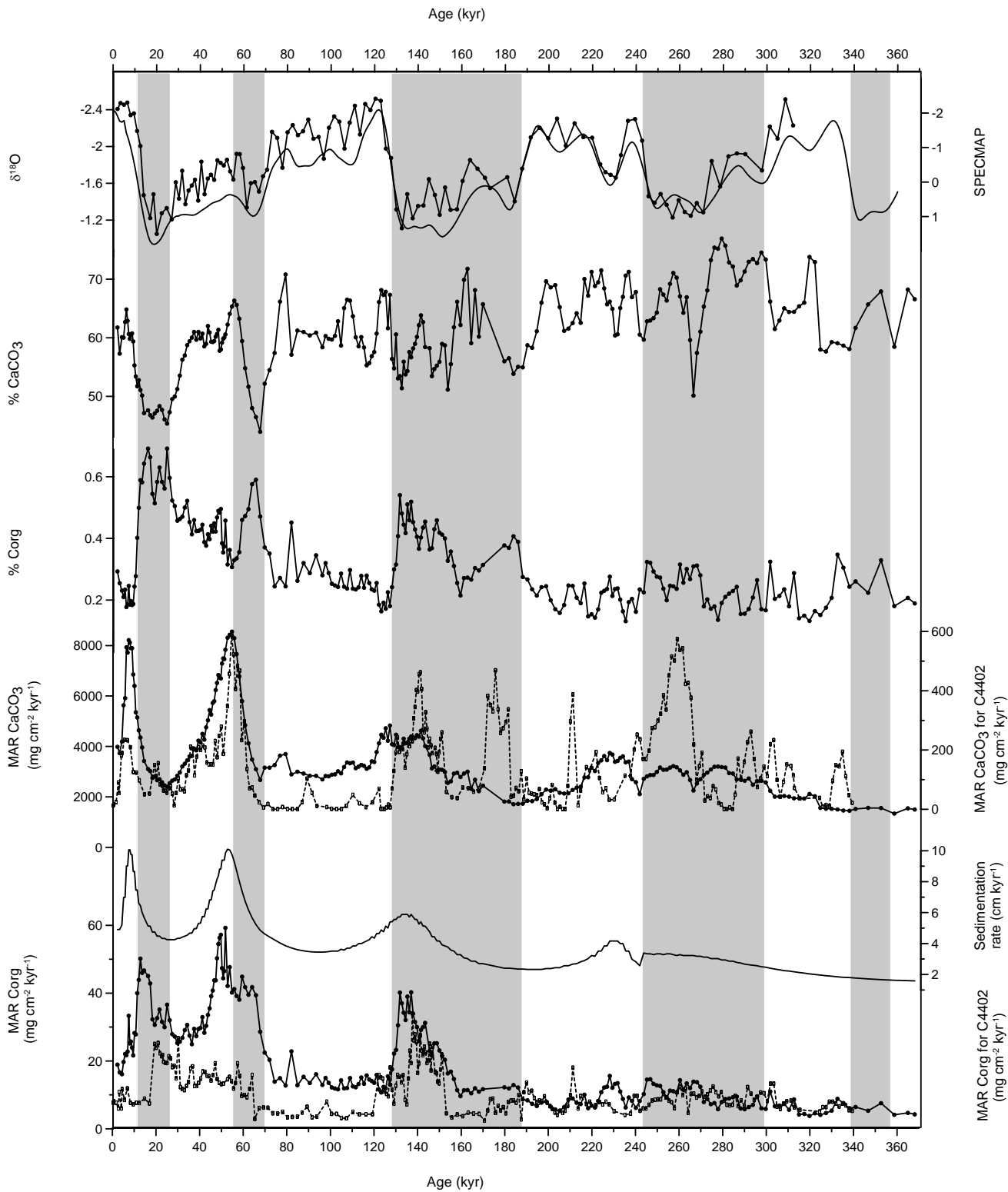


Figure 4-3: $\delta^{18}\text{O}$ (‰), CaCO_3 and Corg contents versus age (kyr) for core MD972140, compared to SPECMAP stack $\delta^{18}\text{O}$ record. Sedimentation rate of core MD972140, mass accumulation rates (MARs) of CaCO_3 and Corg in cores MD972140 (solid lines) and C4402 (dashed lines, Kawahata et al., 1998). Shaded areas indicate the glacial periods, unshaded areas indicate interglacial periods.

To further investigate the effects of accumulation rate, the Corg and CaCO₃ concentrations were converted to Mass Accumulation Rate (MAR) by using the following equation :

$$\text{MAR (mg cm}^{-2} \text{kyr}^{-1}\text{)} = 1000 \times \text{concentration (wt\%)} \times \text{sedimentation rate (cm kyr}^{-1}\text{)} \times \text{density (g cm}^{-3}\text{)}$$

In lack of dry bulk density measurements, we used the wet bulk density (WBD) in the calculation of MAR values. As shown on figure 4-5, the distributions of MAR(CaCO₃) and MAR (Corg) values are positively correlated along the record ($r = 0.68$), indicating that the MAR values are strongly controlled by the *ca.* 4 fold changes in Mean Apparent Sedimentation Rate (MASR). The general upcore increase in MAR values (figure 4-3) is strongly constrained by the elongation of the upper cored deposits (see paragraph 4.3). Despite such bias, the major increases in MAR-Corg and MAR-CaCO₃ generally correspond to carbonate-poor deposition (e.g., glacial MIS 6, 4, and 2), indicating that carbonate production does not solely control the apparent accumulation rate at the MD972140 coring site. In the same way, high-frequency “precessional” fluctuations are very poorly recorded in the MAR records. The MASR maxima and the resulting MAR estimates actually encompass the end of glacial stages and the

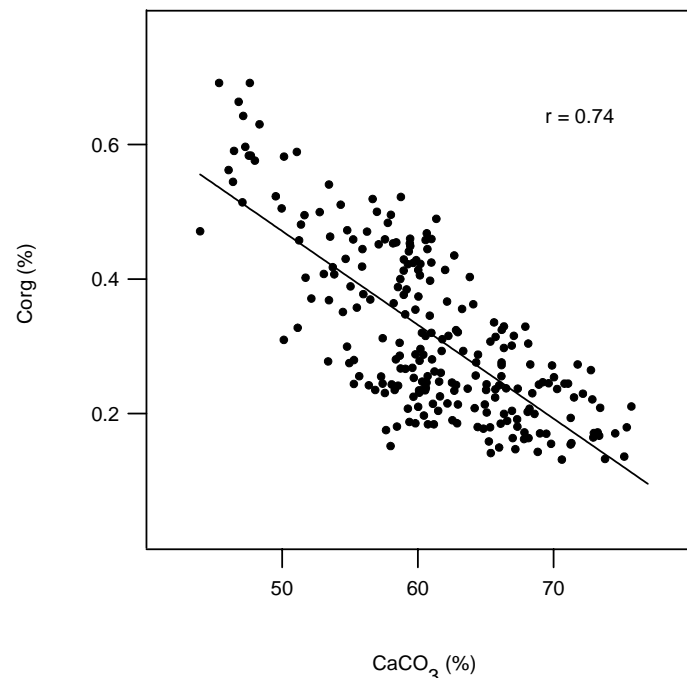


Figure 4-4: Corg content versus CaCO₃ content for core MD972140.

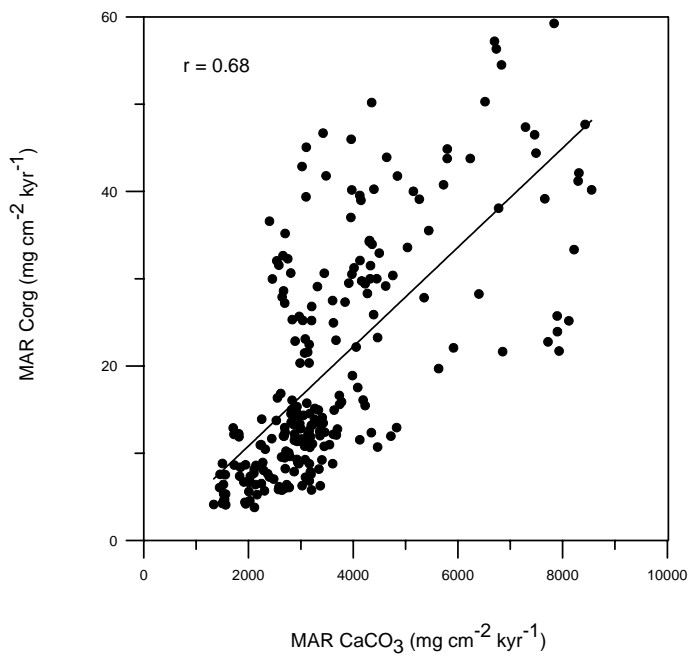


Figure 4-5: Corg MAR versus CaCO₃ MAR for core MD972140.

glacial-interglacial transitions 6/5 (Termination II), 4/3, and 2/1 (Termination I), pointing out a dominant control by sea-level change, as observed in many hemipelagic areas.

Interestingly, the pattern of $\text{MAR}_{\text{CaCO}_3}$ and MAR_{Corg} changes as recorded in core MD972140 is roughly similar to the core C4402 deep sea record (2°N, 135°E, 4402 m water depth) of the West Caroline Basin (Kawahata *et al.*, 1997) (figure 4-3). The carbonate content of core C4402 has been interpreted as a dissolution signal affected by deep seawater chemistry (inflow of bottom water into the West Caroline Basin) (Kawahata *et al.*, 1997). The similarity of the MD972140 and C4402 MAR records therefore suggests that changes in carbonate preservation (West Caroline Basin) and/or deposition rate (Eauripik ridge) were roughly synchronous, increasing dramatically during periods of low and/or rapidly changing sea-level.

4.5.2 Oxidant resistant carbonaceous particle records

The concentration changes in Corg, Oxidant Resistant Elemental Carbon (OREC), Black Carbon (BC), and charcoal are shown in figure 4-6. The charcoal area was converted in Charcoal Accumulation Rate (CHAR):

$$\begin{aligned} \text{CHAR} (\text{mm}^2 \text{ cm}^{-2} \text{ ky}^{-1}) = \\ \text{charcoal area} (\text{mm}^2 \text{ g}^{-1}) \times \text{sedimentation rate} (\text{cm ky}^{-1}) \times \text{density} (\text{g cm}^{-3}) \end{aligned}$$

The range of OREC values (from 0.013 to 0.117%) lies above the relative L_Q (0.001). The records of Corg, OREC and charcoal present similar low frequency changes, with relatively higher values in carbonate poor, glacial MIS (8) 6, 4 and 2. A positive correlation ($r = 0.85$) is especially observed between OREC and Corg values, suggesting either that “soot” carbon was not uniquely isolated during the OREC extraction procedure, or a common behavior of OREC and Corg in the pelagic depositional environment. The latter case should not be excluded, since OREC (and, to a lesser extent, microcharcoal and BC) and Corg belong to the fine organic particulate material, which is partly stored in the Dissolved Organic Carbon (DOC) reservoir (Masiello and Druffel, 1998). Because the deposition of DOC is strongly constrained by absorption on fine, clayey material (Premuzic *et al.*, 1982; Ogawa *et al.*, 2001), the Corg and OREC correlation possibly results from increased deposition and preservation of DOC in rapidly deposited (high MASR), carbonate-poor environments. This is further supported by the similarity between OREC (charcoal) and MAR_{OREC} (CHAR) profiles, which indicate a positive relationship between the carbonaceous particulate content and the mean apparent sedimentation rate.

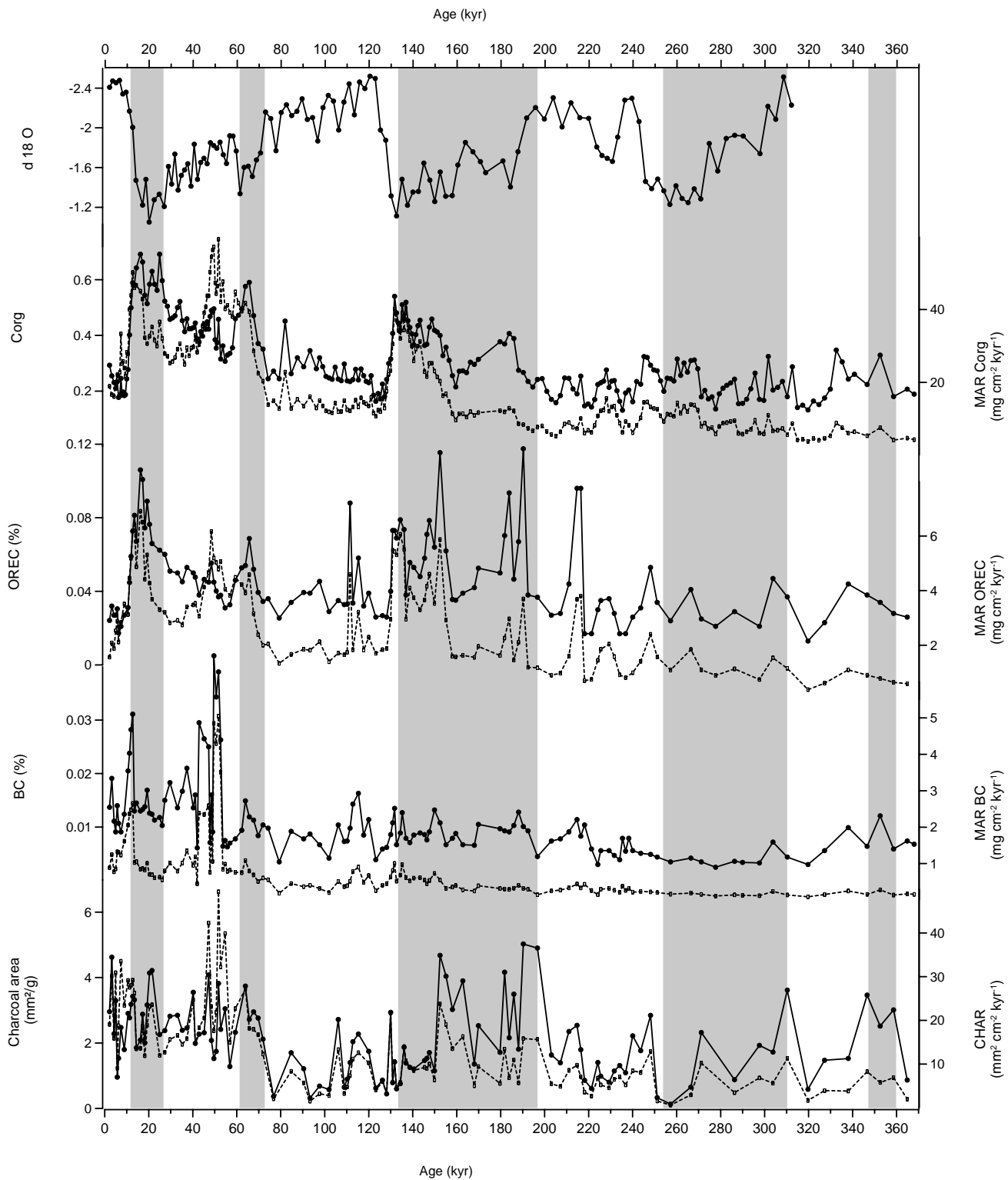


Figure 4-6: $\delta^{18}\text{O}$ (‰), and time series records of contents (plain lines) and MARs (dashed lines) of Corg, Oxidant Resistant Elemental Carbon (OREC), Black Carbon (BC), micro-charcoal area, versus age in core MD972140. Shaded areas indicate the glacial periods, unshaded areas indicate interglacial periods.

Compared to the magnitude of Corg variation (a factor 4 at most), however, the higher amplitude of OREC change (*ca.* one order of magnitude) suggests a higher sensitivity of carbonaceous particulate material to climate forcing. Such sensitivity is further observed on the charcoal and BC records, which especially present high amplitude and short duration cycle or events. Charcoal (CHAR) values range from 0.1 to 5 mm²/g, and show several high amplitude and short duration increases during the last 350 kyr, especially at 54- 47 kyr BP and after 12 kyr BP.

BC values range between *ca.* 0.003 to 0.042%, with abrupt BC (and MAR_{BC}) spikes at *ca.* 52-43 and 12-10 kyr BP, i.e. at the same time interval as major charcoal “events”. In contrast with the OREC and charcoal records, however, the BC record shows little change (range 0.003-0.015%) before the critical age of 52 kyr BP. Moreover, for the whole 330-220 kyr BP time-interval, the BC values (*ca.* 0.005%) lie near the relative L_Q (0.001%). Our data suggest that input in BC was not significant until *ca.* 220 kyr (MIS 7) in the region, and increased dramatically at 52 and at 12 kyr. Similar results are documented in Indonesia and Northern Australia, suggesting a regional increase in burning during these periods (Wang *et al.*, 1999; van der Kaars *et al.*, 2000; Beaufort *et al.*, in press).

Although the *ca.* 220 kyr BP increase in BC might reflect a regional trend in carbonaceous transportation processes and/or in fire intensity and frequency, the late 52 and 12 kyr increases correspond respectively and remarkably with i) the earliest major migration of *Homo sapiens* from Asia to Sahul (Australia and Papua New Guinea joined when sea levels were lower), between 60 and 50 kyr BP (Roberts *et al.*, 1994; Turney *et al.*, 2001), and ii) the Early Holocene major colonization of non-coastal areas, associated with a change in regional vegetation (Hope and Tulip, 1994; Haberle, 1998).

4.5.3 Frequency domain comparisons

Classically, the spectral signature of most paleoceanographic Pleistocene records shows major periods of 100, 41 and 23 to 19 kyr, which correspond to the general response of ice-sheet dynamics to orbital forcing (respectively eccentricity, tilt and precession; Imbrie *et al.*, 1984). The occurrence of such frequencies in the MD972140 carbon records was tested by performing a cross-spectral analysis (Blackman-Tuckey) between the carbon tracers and the δ¹⁸O global ice-volume proxy. This analysis was performed over the last 240 kyr time interval, where the oxidant resistant carbonaceous data are reliable. This choice obviously restricted an accurate analysis of the 100 kyr cycles. The spectral analysis was computed by using the Analyseries software (Paillard *et al.*, 1996).

CaCO_3 and Corg records

As already suggested from the direct comparison of vertical profiles (see paragraph 4.5.1), the cross-spectral analysis between i) $\delta^{18}\text{O}$ and CaCO_3 and ii) $\delta^{18}\text{O}$ and Corg shows that changes in carbonate and organic carbon are highly coherent with changes in global ice-volume ($\delta^{18}\text{O}$) at the three major 100-kyr, 41-kyr, and 23-kyr periodicities (figure 4-7). For these three major frequencies, Corg and maximum ice-volume (high $\delta^{18}\text{O}$ values) are in phase ($\phi < 10^\circ$), while CaCO_3 and maximum ice-volume are anticorrelated ($\phi > 140^\circ$; figure 4-8). Such results suggest that high latitude forcing, through glacial/interglacial changes in ice-volume may be the principal trigger of CaCO_3 and Corg concentration changes in the deep sea sediments of the Caroline Basin.

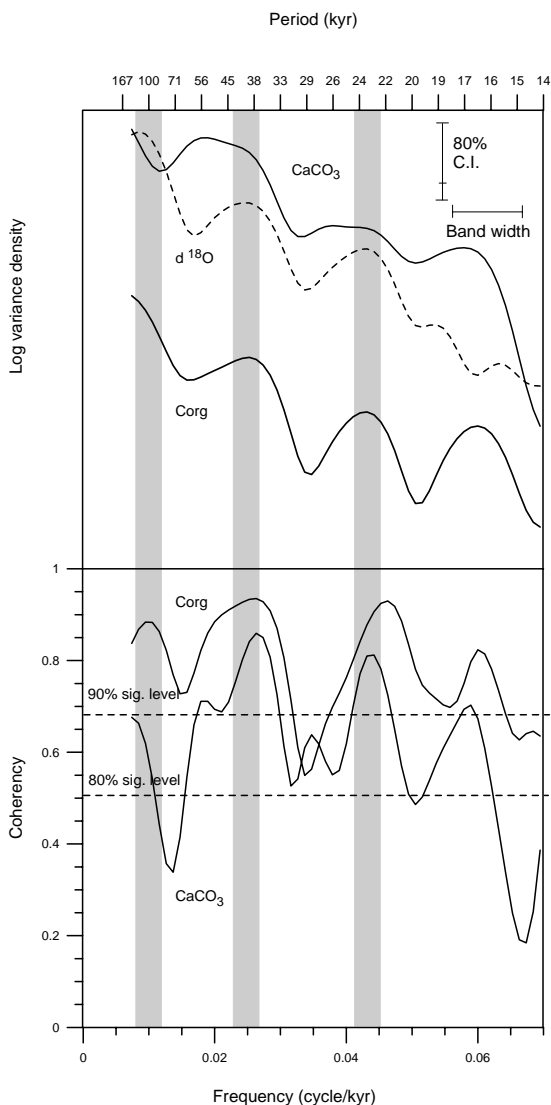


Figure 4-7: Cross-spectral (Blackman-Tuckey) analysis between Corg and CaCO_3 contents versus $\delta^{18}\text{O}_{G. ruber}$

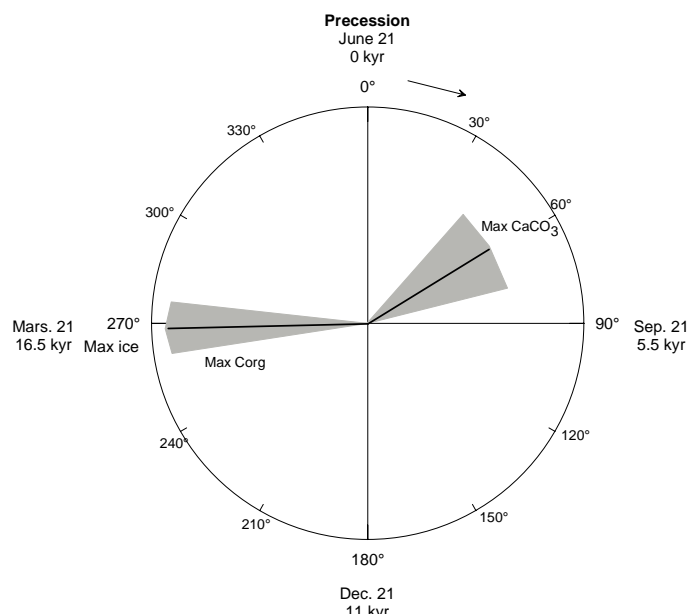


Figure 4-8: Phase diagram of Corg and CaCO_3 contents versus $\delta^{18}\text{O}$ for the precession band. The origin corresponds to the summer solstice in the northern hemisphere (21 June), and the $\delta^{18}\text{O}$ precession peak was set at 270° (21 March) (Beaufort et al., 1997).

Carbonaceous biomass burning particle records

The cross-spectral analysis of the carbonaceous biomass burning proxies with the $\delta^{18}\text{O}$ indicates different spectral content for OREC and for charcoal and BC, respectively (figures 4-9 and 4-10). The OREC signal shows a similar variability as Corg, i.e. a correlation with $\delta^{18}\text{O}$ for the obliquity and precession bands, which confirms the association between OREC and organic matter deposition processes, with a strong control of sea-level and/or deep sea circulation.

In contrast, charcoal and BC show only little coherency with the $\delta^{18}\text{O}$ in the obliquity band, but significant coherency in the precession band. Phase analysis indicates that charcoal and BC maxima lead the ice volume maxima by *ca.* 100° (or *ca.* 6 kyr).

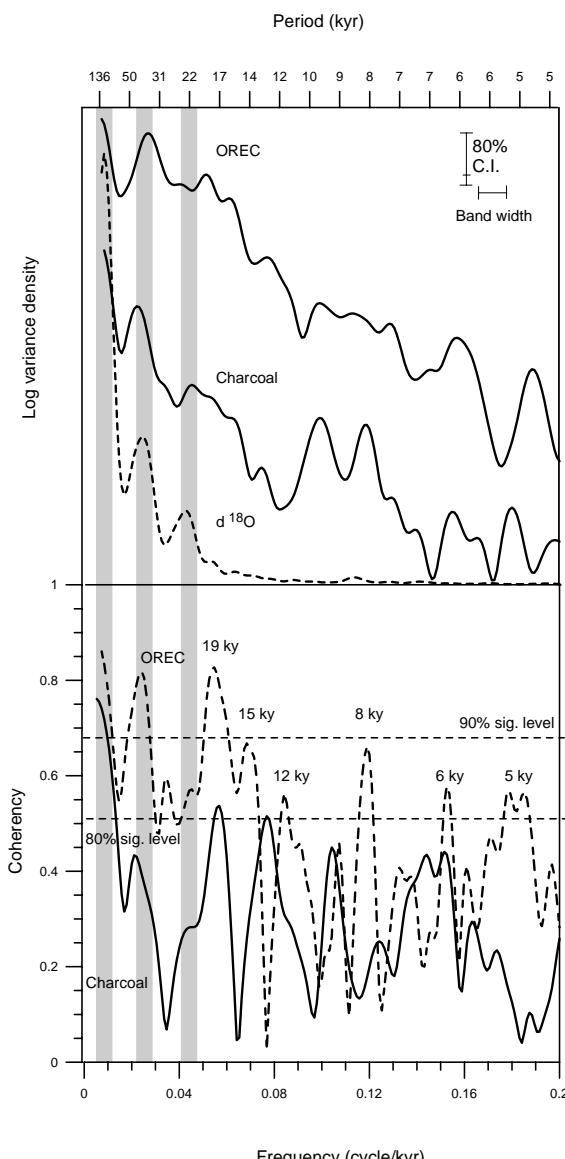


Figure 4-9: Cross-spectral (Blackman-Tuckey) analysis between $\delta^{18}\text{O}$ and OREC, BC and charcoal contents versus $\delta^{18}\text{O}_{G.\text{rub}}.$

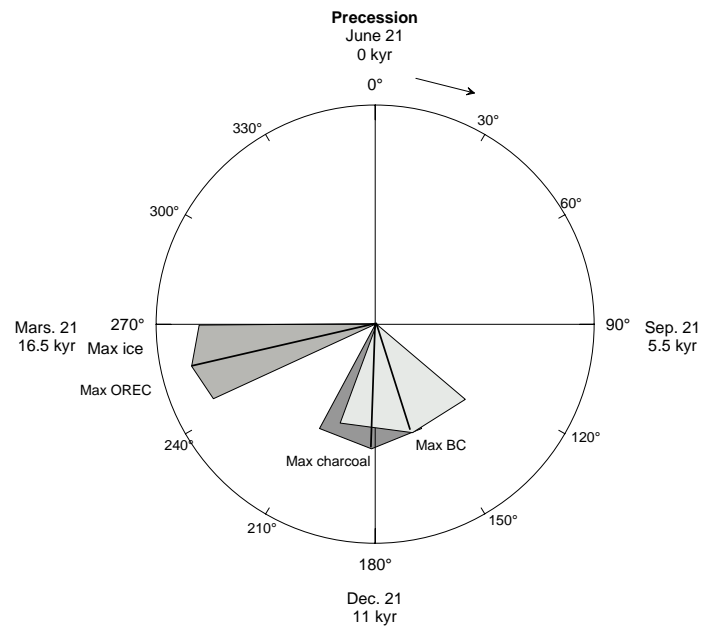


Figure 4-10: Phase diagram of OREC, BC and charcoal versus $\delta^{18}\text{O}$ for precession.

These results suggest that high frequency BC and charcoal changes do not solely respond to mineral or organic carbon accumulation, and provide a more reliable proxy of biomass fire than OREC in core MD972140. The *ca.* 100° lead of BC and charcoal maxima in the precession band locates such signals around mid-December. As suggested by Beaufort *et al.* (in press), charcoal or BC inputs are therefore probably strongly constrained by the intensity of the East-Asian winter monsoon, which variability is today connected to ENSO events (see discussion).

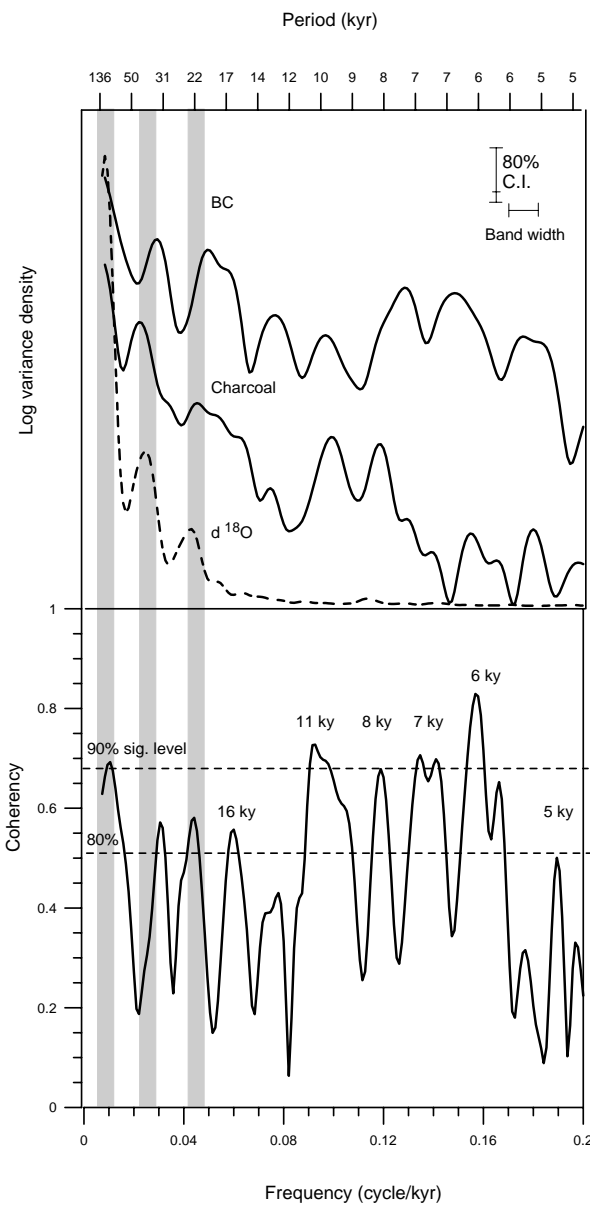


Figure 4-11: Cross-spectral (Blackman-Tuckey) analysis between BC and charcoal.

Because the charcoal and BC records likely contain a specific biomass burning signal, we performed a cross-spectral analysis between BC and charcoal (figure 4-11). In addition to the *ca.* 23 kyr precession band, charcoal and BC are coherent for several periods, especially 33 kyr, and 11, 7.4 and 5.3 kyr, respectively. These observations suggest that BC and charcoal biomass fire proxies in core MD972140 are strongly constrained, by low-latitude, precession-controlled insolation change, and monsoon dynamics. Indeed, the *ca.* 30 kyr cycle has been connected with the strength of the Boreal Summer Monsoon (BSM), and was identified in the primary productivity record of core MD972140 and in numerous records from the Indo-Pacific area as an ENSO-like signal (Beaufort *et al.*, 2001). By ENSO-like, we mean zonal gradient of thermocline depth or pressure, equivalent to ENSO, but on a longer time scale.

The 11, 7.4 and 5.3 kyr correspond to precessional harmonics ($p^2 = 11.5$ and 9.5 ; $p^3 = 7.3$; $p^4 = 5.5$ kyr; Pokras and Mix, 1987). The 11.5 kyr cycle especially corresponds to the twice-yearly insolation

maximum at the Equator, which strongly controls convection and rainfall over Papua New Guinea (Short *et al.*, 1991).

In addition to the precession control, the highest coherency between BC and charcoal change is found at 6.4-6 kyr. The *ca.* 6 kyr period has been identified as one of the main frequency domain of submillennial variability of the East Asian winter monsoon in the Sulu Sea, and might reflect an association with the dominant *ca.* 6 kyr pacing of the northern hemisphere climate and iceberg discharges in the North Atlantic (Bond *et al.*, 1993; Porter and Zhisheng, 1995; Bond *et al.*, 2001; de Garidel-Thoron *et al.*, 2001).

4.6 Discussion

Mean Accumulation Rates (MAR) and sea-level change in the Caroline basin

Although the MAR calculations provide “true” apparent accumulation rates of different sedimentary components, the MAR values of sedimentary/climate proxies still strongly depend on the relative magnitude of changes in mean apparent sedimentation rate (MASR). This is most especially the case for sedimentary components showing relatively lower magnitude change than MASR, such as the CaCO₃ content in the carbonate ooze of core MD972140. The MAR_{CaCO₃} record of core MD972140 is mostly controlled by factor *ca.* 4 changes in MASR as deduced from the oxygen isotope stratigraphy. Excluding the effect of core elongation, the main changes in MASR occur during glacial or deglaciation periods, and a significant contribution of erosion and transportation processes, coupled with variable carbonate dissolution rates, should not be ruled out at such periods of time. As a result, the MAR_{CaCO₃} profile unlikely reflects changes in primary carbonate production. The most significant components of the CaCO₃ or Corg signals may disappear upon convolution by MASR, due to their relatively low amplitude compared to MASR. This is especially observed for the precession-like periodic component of the CaCO₃ signal, one of the major cycle of primary biogenic carbonate production in the WPWP area (Beaufort *et al.*, 2001).

Alternatively, however, a significant correlation between the original signal and its corresponding MAR profile improves the interpretation in terms of primary input and/or production. In core MD972140, this actually occurs either when the original signal is strongly correlated to MASR (e.g., Corg and OREC), or when the magnitude of the original signal significantly exceeds the magnitude of MASR (e.g. BC and charcoal). For example, synchronous, abrupt increases in BC (charcoal) and in MAR_{BC} (CHAR) at 54-52 kyr testify the occurrence of a major input of carbonaceous, fire-originating particles.

Reliability and significance of carbonaceous biomass burning proxies

Although OREC, BC and charcoal are primarily emitted by biomass fire during the combustion process, their significance in the MD972140 environment need to be discussed.

The similar behaviors of i) OREC and Corg, and ii) BC and charcoal, respectively, suggest that OREC is associated with organic deposition and organic content. Given the complex origin of pelagic organic matter (Meyers-Schulte and Hedges, 1986), the chemical extraction of soot carbon (OREC) was probably not completed without including any additional thermal treatment. The resulting bias on OREC data would especially occur if the MD972140 organic matter contains significant contributions of i) oxidized, soil-originating organic matter such as humic acids, or ii) marine, bacterially oxidized organic matter (Masiello and Druffel, 1998). Further analyses are therefore needed to better understand the similarity between OREC and Corg records.

Charcoal and BC data show a relatively independent behavior from $\delta^{18}\text{O}$, with strong responses to the 54-52 kyr event or to the ENSO-like *ca.* 30 kyr period. This strongly suggests that the input of biomass fire products is dominantly constrained by local climate, independently from glacial-interglacial variability.

Atmospheric transport and fallout of particulate products by fire are strongly affected by atmospheric circulation and precipitation patterns, and the biomass burning relationship to the stratigraphic record largely differs with each sedimentary environment (Garstang *et al.*, 1997; Novakov *et al.*, 1997; Stocks and Kauffman, 1997). Indeed, the fire-signal can be biased through secondary remobilization of material remaining on the ground after a fire by wind, and/or by redistribution from terrestrial soils and sediment through erosion and runoff processes (Griffin and Goldberg, 1975; Andreae *et al.*, 1984; Emerson and Hedges, 1988). Smoke particulate emissions mostly consist in BC-like carbonaceous species, fine particulate carbon in the submicrometer-size range accounting for 50-80% of the total particulate carbon concentration (Cachier *et al.*, 1985). In fact, the gaseous and particulate composition, as well as the grain-size distribution of particulate carbon, strongly depend on the importance of the ratio of flaming to smoldering combustion, and to the type of burned vegetation i.e. plants, wood or fossil fuel (Cachier, 1989; Lobert and Warnatz, 1993).

Consequently, similar changes in BC and charcoal likely originate from the input of smoke particulate emissions, while different BC and charcoal features likely result from independent processes (e.g., intensity of combustion, soil erosion and runoff). Based on such criteria, major smoke emissions probably occurred at 54-52 and 12 kyr BP, respectively, and at

the precession-originating frequencies which control the rainfall distribution and the resulting probability of fires (Haberle and Ledru, 2001) over Indonesia, Papua New Guinea and Northern Australia. Alternatively, the lack of obliquity (41 kyr) signal in the BC record suggest that *ca.* 41 kyr changes in charcoal rather originated from changes in ice-volume and sea-level.

High latitude forcing on pelagic deposition and atmospheric circulation in the Caroline basin

Although numerous low-latitude pelagic and terrestrial records show a connection with high-latitude, glacial-interglacial climate, the connection between major, low-latitude atmospheric circulation features (such as monsoon or ENSO) and glacial-interglacial changes still needs better understanding. This is especially the case in the marine realm, where glacial-interglacial changes in global sea-level and bottom circulation strongly constrain the global depositional environment, with major effects of continental shelf erosion, bottom ventilation, and associated carbonate and organic matter preservation processes. This is observed in the MD972140 record, where the Corg and carbonate records are respectively correlated and anticorrelated with the *ca.* 100 and *ca.* 41 kyr glacial cycles. At the scale of precession, cross-spectral analysis and phase relationships are often used to decipher between low-latitude circulation features (e.g., seasonal wind and/or depth of the thermocline) and high-latitude ice-volume forcing (Beaufort *et al.*, 1997). Given the centimeter-scale of the phase-lags involved in such observations, however, it has to be assumed or proven that deep-sea sediment mixing between large and fine particles (Bard, 2001) have no or little effect on the above phase-lag relationships.

In this context, the identification, in core MD972140, of high-frequency smoke emissions that present the same timing as high-latitude Dansgaard-Oeschger cycles (*ca.* 6kyr) provides an additional but direct, independent evidence of a coupling between high and low-latitude atmospheric circulation patterns (de Garidel-Thoron *et al.*, 2001). Taken together, the i) present-day association between biomass fire and ENSO-originating droughts in the study area, and ii) past association between monsoon circulation and BC/charcoal inputs strongly suggest that, during the Late Pleistocene, high latitude forcing on the East-Asian winter monsoon strongly affected aridity over the region, likely through ENSO-like patterns, with potentially dramatic consequences over most tropical regions.

Late Pleistocene-Early Holocene Human-induced changes in fire activity

Despite the apparent climatic control over fire activity, human colonization and social change was almost everywhere marked by a new fire regime (Pyne and Goldamer, 1990).

Natural fires occur when the fuel is dry, while most human fires are ignited while the fuel is moist: as a result, a shift in fire regime can double or even triple the emissions of non-CO₂ emissions (such as microcharcoal or BC)(Saarnak, 2001). This should be considered to explain the two major (factor 3-4) increases in charcoal and BC from *ca.* 53 kyr and 12 kyr BP, respectively. Migration of *Homo sapiens* from Asia to northern Australia occurred prior or around 50 kyr (Roberts *et al.*, 1990). From that time, higher burning levels are supported by palynological data, assessing the impact of Aboriginal people on the vegetation and landscape (Kershaw, 1986). Archaeological sites and artifacts show that Sahul was colonised by people adapted to a coastal way of life, with initial colonising routes located around the coasts and then up the major river systems. Non-aquatic adaptations, such as desert and montane economies, came relatively late in the archaeological record, from *ca.* 12-10 kyr BP (Bowdler, 1977; Haberle, 1998).

Such observations therefore suggest that the two major charcoal and BC peaks of core MD972140 at 54-52 and 12 kyr BP closely correspond to the main Late Pleistocene/Early Holocene periods of human colonisation and practices.

Peculiarly, both 54-52 and 12 kyr events also occur during relatively cold glacial events of the last climatic cycle in the Greenland-North Atlantic region (Dansgaard *et al.*, 1993). The 54-52 kyr event would locate between warm Dansgaard-Oeschger (DO) events 16 and 14, while the 12 kyr BP event would correspond to the Younger Dryas. Both events clearly belong to the *ca.* 6 kyr periodic component of the DO record (de Garidel-Thoron *et al.*, 2001). Taken together, such data therefore suggest that strengthened smoke emissions and fire activity, at the time of major human colonisation events, did not occurred independently of relatively dry, ENSO-like conditions.

4.7 Conclusion

Our study provides a preliminary pelagic record of carbonaceous biomass burning proxies in the West pacific Warm Pool, north of Papua New Guinea. Several conclusions are stressed from this work:

- 1) Except from the BC record, the MD972140 record of biomass fire proxies is strongly constrained by depositional changes as coupled to global, dominantly *ca.* 100 and *ca.* 41 kyr changes in ice-volume. This confirms the tremendous effects of global changes in ice-volume and sea-level on i) the continental surface of this equatorial region, and the resulting inputs of terrestrial matter by (shelf) erosion, and ii) deep sea chemistry and circulation in relatively closed

“glacial” basins such as the Caroline basin. In contrast with cores located above the Carbonate Compensation Depth (CCD) such as core C2188 (2188 m above the Eauripik Rise) (Kawahata *et al.*, 1997), opposite changes in organic carbon and carbonate content at 2547m (our record) are probably strongly constrained by variable carbonate preservation.

2) The concentration of organic carbon which survives to chemical oxidation (OREC) shows a strong association with the Corg content. The OREC record thus encompasses variable forms and sources of organic carbon and poorly depends on the input of biomass fire products.

3) In contrast with Corg and OREC, the independent and coherent changes in BC and charcoal content consistently reflect the regional emission of smoke carbonaceous particulate material.

4) The BC/charcoal record shows a close relationship with precession-originating insolation change. This suggests that biomass burning emissions, associated with drought and ENSO-like conditions over Papua New Guinea and Northern Australia, were strongly constrained by monsoon circulation (most especially the Summer Boreal Monsoon and the East Asian winter monsoon). Additional semi precessional periods in such records further suggest that the insolation in the equatorial band strongly controlled aridity.

5) The high BC/charcoal coherency around *ca.* 6kyr periods suggest that the northern hemisphere climate dynamics as recorded in Greenland ice-cores is connected with monsoon dynamics and ENSO-like patterns in the Indo-Pacific region.

6) The major Late Pleistocene/Early Holocene periods of human colonization in Indonesia, Papua New Guinea and Australia at *ca.* 54-52 kyr and *ca.* 12 kyr BP, respectively, resulted in dramatic increases in emission of carbonaceous aerosols in the environment. Although such events still belong to the *ca.* 6kyr periodic component of biomass burning emission, amplitude of such events likely illustrate the consequence of a shift from natural to human fire regime.

5. A Late Holocene charcoal record from Lake Masoko, SW Tanzania: Climatic and anthropologic implications *

5.1 Introduction

Vegetation fires occur frequently in Africa (Delmas *et al.*, 1991; Lacaux *et al.*, 1993). African savanna and bush fires account currently for almost one third of the global emissions from vegetation burning, and largely control the equilibrium of tropical systems (Hao *et al.*, 1990; Andreae, 1991). However, prehistoric fire activity in Africa and its connection with past climate and vegetation changes remains poorly documented. The aim of this study is to establish a record of fire activity through the Late Holocene in the strongly fire-sensitive Zambezian woodlands (“Miombo”), the second largest phytogeographical region in Africa ($\sim 2.7 \cdot 10^6 \text{ km}^2$)

* Florian Thevenon, David Williamson, Annie Vincens, Maurice Taieb, Ouassila Merdaci, Michel Decobert and Guillaume Buchet. *The Holocene* 13, 5 (2003).

Abstract: Charcoal analysis from a short core in a small tropical crater lake (Lake Masoko, SW Tanzania) reveals changes in charred particle deposition and properties, consistent with high climate variability for the last 4,200 years. This is evidenced by automated image analysis of charcoal size distributions, thermally refractory carbon (soot) and black carbon elemental analysis. Charcoal particle transport in the lake decreases during dry spells, and increases with stronger runoff regime in the catchment area under humid periods and/or during abrupt low-stands of the lake. However, between 1830 and 1560 cal. yr B.P., charcoal distribution variability and abrupt increase in particulate carbonaceous particles, testifies regional emissions from forest fires and atmospheric transport. This event was followed by a prolonged period of material accumulation but regional climatic drying. After 1560 cal. yr B.P., large charcoal fragment accumulation and a rise in the length:width ratio of micro-charcoal, indicate fires closer to the lake and the opening of the local woodland. These new data give evidence of large-scale fire development just prior to a pollen-inferred vegetation change and Late Iron Age activity in the area, which probably coincide with an altered fire regime. In fact, charcoal-size distribution and particulate carbon elemental analysis constrain the sources of fossil carbonaceous particles, and provide an accurate proxy of fire and climatic change in southern Tropical Africa.

after the Sahara (White, 1983; Campbell *et al.*, 1996).

In Southern Tanzania, fire is widely used for a series of purposes, and considered an important ecological factor in Zambezian woodlands, resulting in various communities (Kikula, 1986; Frost, 1996; Chidumayo and Frost, 1996). Burning generally occurs throughout the dry season from June to November, with the availability of dry fuel and of high burning efficiency. It favors the increase in soil surface nutrients and the re-growth of plants at the onset of the rain (Pielou, 1952). Fire is also started early in the dry season in order to burn agricultural wastes that remain after the harvest, as control of which largely damage the grass cover but bush fires are less destructive to the woody plants (Trapnell, 1959; Chidumayo *et al.*, 1996). Slash-and-burn land-clearing activities serve for preparation of agricultural pastoral practices, stimulate the growth of new grass species, and act as a pest control. Fire is also used for clearing paths, hunting, and smoking bee hives for honey collection. Last but not least, extensive woodcutting and gathering provide charcoal and fuel wood for cooking and heating.

Although today almost all fires are induced by humans, the fire regime is closely controlled by the cycle of precipitation. The latitudinal movement of the Intertropical Convergence Zone (ITCZ) produces a climate wet enough to grow combustible vegetation and then dry enough for them to burn (Pyne, 2001). The intensity of a resulting fire is determined by the accumulation of fire potential and natural fire frequency. However, human colonization is often marked by an alteration of the fire regime, as reflected in fossil charcoal horizons (Pyne and Goldamer, 1990; van Wilgen *et al.*, 1990). Charring, which is the generation of particulate pyrogenic products, depends on the type of plant-derived material and the degree of combustion. Elemental carbon or Black Carbon (BC) particles ($<1\mu\text{m}$) are formed at high temperatures ($>600^\circ\text{C}$) as fire-altered material or smoke particulate; while small charcoal particles ($1\mu\text{m}$ to several mm size) are produced at lower temperatures as fuel and are carried out with smoke emissions (Jones *et al.*, 1990). Finally, soot particles ($<1\mu\text{m}$) are exclusively emitted as smoke and are produced *via* gas phase processes, encompassing a complex mixture of organic matter along with pure BC (Cachier *et al.*, 1989). Most of the fire-originated particulate carbon is in the sub-micrometer-size range, which is eventually trapped into the sediment consistent with atmospheric particle emission processes (Cachier *et al.*, 1985; Clark, 1988a). Moreover, the chemical resistance of charred products to biodegradation provides a potential tracer of past fire activity (Goldberg, 1985; Clark and Patterson, 1997; Clark *et al.*, 1998). Thereby, estimating fossil charcoal distribution by categorizing particles in several size-classes can provide a local signature of a regional background burning and/or variations in charcoal transport pathways (Patterson *et al.*, 1987; Blackford, 2000; Carcaillet *et al.*, 2001). Furthermore, distribution of

charcoal morphology in sediments should provide an indicator of the vegetation type, because micro-charcoal derived from grasses has a higher length:width ratio than particles derived from leaves or wood (Umbanhowar and McGrath, 1998). However, visual identification of the charred material (Wooller *et al.*, 2000) or chemical determination is generally necessary to explain charcoal representation in lake sediments.

The main difficulty in extracting particulate products of biomass combustion is to ensure the removal of unburned organic matter (Kuhlbusch, 1995). Smith *et al.* (1975) first performed oxidation of kerogen from marine sediments with hydrogen peroxide. Thermal techniques (340–375°C) have then been performed to oxidize Organic Carbon (OC) for analyzing soot carbon, which is unaffected by the thermal treatment (Cachier *et al.*, 1989; Gustafsson *et al.*, 1997). Soot and elemental carbon have also been separated from organic matter of Cretaceous-Tertiary boundary clays, by using a prolonged oxidation time in a dichromate solution (Wolbach *et al.*, 1988; Lim and Cachier, 1996).

Paleoenvironmental studies of charcoal data demonstrate that selected size-classes are required to distinguish fire products from soil contribution and charcoal redistribution by surface runoff (Emerson and Hedges, 1988; Pitkänen *et al.*, 1999; Blackford, 2000). Thin-section analysis of undisturbed lake sediments indicates charcoal transport and local sources, but particle shape and orientation tend to bias the estimate of area because charred particles do not have the same area in all planes (Clark, 1988b). The combination of this method with particle counting on pollen slides is then necessary to explain the charcoal representation and to identify regional sources (Clark, 1988a; Clark and Royall, 1995; Tinner *et al.*, 1998). Pollen slides are prepared for visual identification of opaque organic matter and particles. However, the preparation of pollen slides generally restricts the analysis of confident charcoal to diameters greater than 10 µm (Clark and Hussey, 1996; Clark, 1984; MacDonald *et al.*, 1991). In addition, repeated rinsing and centrifugation during pollen extraction may damage the charcoal representation (Patterson *et al.*, 1987; Rhodes, 1998).

5.2 The study site

Lake Masoko (9°20'S, 33°45'E, 770 m a.s.l., SW Tanzania) lies in a maar-type volcanic crater formed ~50,000 years ago in the Rungwe Volcanic Province, between Lakes Rukwa and Nyasa, in the East African Rift system (figure 5-1) (Williamson *et al.*, 1999). The maximum depth of the lake is about 39 m for a diameter of 700 m. The basin surface is about 0.5 km². The uppermost basin rim around Lake Masoko is 8.5 m above the present-day lake-level. The total

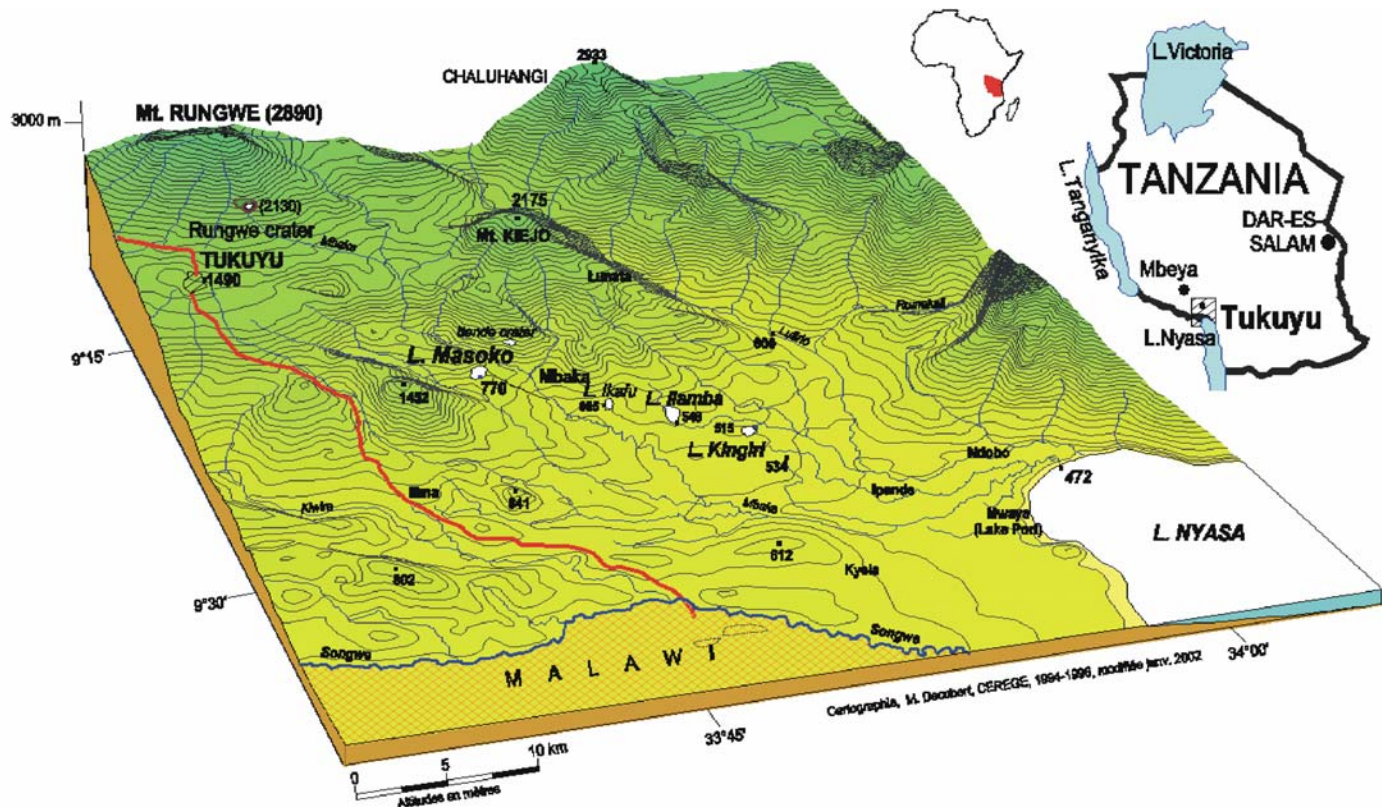


Figure 5-1: Topographical map of the Rungwe Volcanic Province showing the position of Lake Masoko.

mean annual rainfall between December and June exceeds 2500 mm in the area, following the trade wind regimes and the path of the ITCZ (Nicholson, 2000). Precipitation in the surrounding region is also influenced by Lake Nyasa (Malawi), from where winds carry moisture into the highlands. The lake level fluctuates by 1-2 m at seasonal/interannual scale. In fact, the lake level is supported by a regional aquifer that flows southward from the Rungwe mountain into Lake Nyasa (473 m), feeding a range of small crater-lakes (Masoko, Ikafu, Ilamba, Kingiri) and Mbaka river (Bergonzini *et al.*, 2001) (figure 5-1). The local vegetation is dominated by wet Zambezian woodlands of the Miombo type, while Afromontane formations are present on the surrounding highlands (White, 1983). *Brachystegia/Uapaca* woodland dominates in Lake Masoko catchment area. Some recent forest clearance has taken place in the surroundings, and the summit of the rim and southern depression crater is cultivated by local people.

5.3 Sediment stratigraphy

A 275 centimeter-long piston core (core MM8, spanning the last 4200 cal. yr B.P.) has been collected from the deepest part of the lake using a Mackereth corer, during the EC-RUKWA expedition in 1994. Six AMS ^{14}C dates have been obtained on Total Organic Matter

Depth in core (cm)	Type	Laboratory code (Orsay)	Measured ^{14}C age (yr BP)	Calibrated age (cal. yr BP)	$\delta^{13}\text{C}$ (‰)
2	TOM	H1832	270 ± 50	300	-28.9
19	TOM	H1836	400 ± 50	475	-25.9
42	TOM	H1655	965 ± 70	920	-24.7
143	Charcoal	H992	1610 ± 60	1520	-26.5
228	Wood	H1172	2940 ± 70	3070	-27.3
258	Wood	H1173	3750 ± 70	4090	-27.8

Table 4-13: Radiocarbon chronology from core MM8 (Gibert *et al.*, 2002). Calendar ages are calibrated using the program CALIB 3.0 (Stuiver and Reimer, 1993).

(TOM), charcoal and wood fragments (Gibert *et al.*, 2002) (table 4-13). The ^{14}C ages have been calibrated to give calendar years BP using the program CALIB 3.0 (Stuiver and Reimer, 1993). The sediment mostly consists of homogeneous silt-sized gyttja with interbedded ash layers pointing to a regional volcanic event at 108-85 cm, *ca.* 1200 cal. yr B.P. (figure 5-2). This tephra possibly corresponds to one of the last explosions of the Rungwe volcano, dated from outcrops at 800 years ago (Ebinger *et al.*, 1989; Lenck-Santini, 1996). It may be also correlated with the pumice layer of Lake Rukwa which occurred between 2 and 1.4 cal. kyr BP (Thevenon *et al.*, 2002). Between 261-255 and 228-216 cm downcore, centimeter-scale sandy-silt layers with a high low-field magnetic susceptibility (χ_{lf}) and a low Organic Carbon (Corg) likely reflect erosional events (Williamson *et al.*, 1999) (figure 5-4). The latter sandy-silt layer (228-216 cm) contains a large wood fragment which may testifies to the strength of such detrital inputs, possibly including the erosion of littoral deposits during an abrupt low stand of the lake.

5.4 Methods

Forty sediment samples were taken at 5 cm depth-interval along the MM8 cored sequence and subjected to charcoal, TRC and BC analyses. The charred particle record is compared with previous rock-magnetic, organic matter, and palynological studies. The method for organic

carbon analysis is described in Merdaci (1998) and those used for pollen and magnetic data follow Vincens *et al.* (1998) and Williamson *et al.* (1998).

Chemical extraction of Thermally Refractory Carbon (TRC) and Black Carbon (BC)

Two oxidative procedures were used to remove organic carbon (Corg) compounds. A schematic flow diagram of the method is shown in figure 5-2. About 15-20 mg (for the analysis of TRC) and 100-300 mg (for the analysis of BC) of dry powdered sediment from each sample was each placed into porcelain crucibles and heated in a furnace at 375°C for 24 hours. In the TRC experiment, cooled residues were sub-sampled and 5-10 mg weighed into prepared silver capsules for use in a Na-1500 Elemental Analyzer, after in situ acidification (HCl 3M).

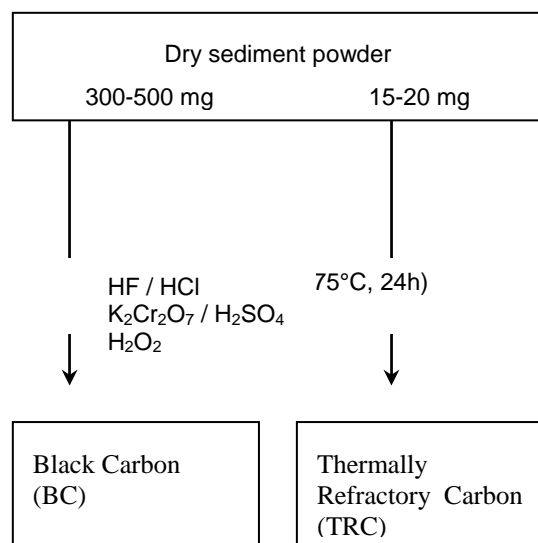


Figure 5-2: Schematic flow diagram showing Thermally Refractory Carbon (TRC) and Black Carbon (BC) extractions.

In the BC extraction, the cooled residues were transferred in test tubes and acid treated. HF (10M)/HCl (1M) and HCl (10M) were successively used for 24 hours to remove carbonates and silicates, which highly concentrates the BC. Corg was then removed by sulfo-dichromate oxidation (0.1 M K₂Cr₂O₇/2 M H₂SO₄) for 65 hours while a water bath maintained at 56°C (Wolbach and Anders, 1989). Hydrogen peroxide (33% H₂O₂) was finally used to destroy any residual form of Corg (Bird and Gröcke, 1997). The residual BC was filtered onto a glass microfibre filter (GF/C Whatman) and analyzed in the Elemental Analyzer.

Optical counting of macro and micro-charcoal particles

Because the particles were to be quantified in size classes, the sample preparation procedure has to ensure that little particle fragmentation occurred (Rhodes, 1998). Three successive acid treatments were applied on 500 mg dried sediment samples, without any centrifuging or rinsing, in order to minimize particle fragmentation: 1) 15 ml of hydrochloric acid (HCl 3M) 2) 15 ml of concentrated nitric acid (Winkler, 1985) and 3) 30 ml of hydrogen peroxide (33% H₂O₂). These steps digest organic material, carbonate and pyrite minerals. Opaque microfragments that remain to the chemical procedure were considered as charcoal. Macro-charcoal fragments were separated by using a 150 µm sieve. The macro charcoal was then observed through a binocular microscope (at 65× magnification). Distilled water was added to the residual solution to adjust the total volume to 500 ml. 10 ml of this solution was filtered onto a nucleopore filter (0.47 µm nominal porosity and 45 mm of diameter). A part of the cellulose membrane was then mounted on a slide using Canadian balsam. The automated acquisition of 150 fields of view (2.6 mm²) was conducted using a transmitted light microscope equipped with a 50× objective and a digital camera, driven by SYRACO software, SYstème de Reconnaissance Automatique de Coccolites (Dolfus and Beaufort, 1999). The automated measurements on the selected dark particles was performed with the Scion Image analysis software. The microscopic charcoals were isolated by thresholding the gray-level images (figure 5-3).

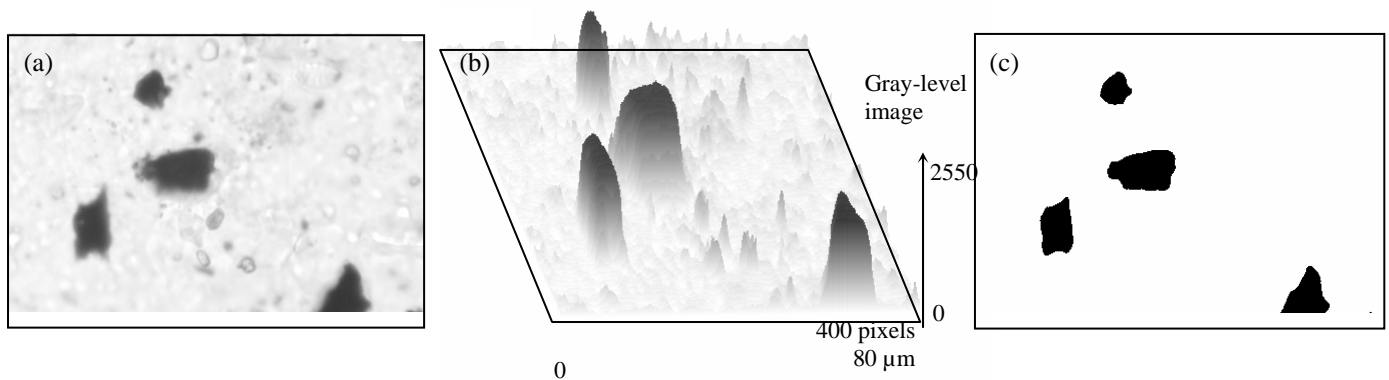


Figure 5-3: An example to illustrate automated measurements of charcoal area. Enhanced threshold of the gray-level image (a and b) allows to isolated charcoal particles (c).

The results were given as the total surface (mm^2) occupied by dark particles (microscopic charcoal) per gram of sediment. Four size classes were arbitrary defined to characterize the charcoal distribution: ultra-fine (0.2-1 μm) which may includes a part of the soot fraction, fine (1-63 μm), medium (63-150 μm) and coarse ($>150 \mu\text{m}$). Morphological parameters (perimeter, length and width) were calculated on the medium-sized particles to determine microscopic charcoal-shape variability. Results were expressed in $\mu\text{m}/\text{particle}$.

5.5 Results

The charred-particle distribution clearly show two well-defined units (zones 3 and 1), separated by a transition zone (zone 2) between 163 and 109 cm downcore (figures 5-4, 5-5 and 5-6).

Zone 3 (269-163 cm; 4180-1,880 cal. yr B.P.)

Charred-particle distributions show a roughly similar pattern of fluctuation in this unit (figures 5-4, 5-5 and 5-6). Data also indicate that microscopic charcoal particles account for almost 90% of the total charcoal area (up to 300-400 mm^2/g). The medium-size class (63-150 μm), which represents more than a half of the total assemblage, shows a marked decrease between 237 and 211 cm (3310-2740 cal. yr B.P.). The morphological parameters of this dominant fraction indicate that relatively small and rounded particles prevail in this zone (figures 5-5 and 5-6). The ultra-fine fraction (0.2-1 μm) constitutes up to less than 1% of the total charcoal area (<1 to 2 mm^2/g) while the coarse fraction ($>150\mu\text{m}$) constitutes less than 10% (20-40 mm^2/g) (figure 5-4). The quantities of charcoal, Corg and BC are strongly variable in this unit, while the soot concentration (TRC) remains low and constant (figure 5-4). Although the abundance of charred-particles is relatively low in this zone, sharp peaks corresponding to silty layers occur around 257, 227, 208 and 180 cm (*ca.* 3850, 3050, 2700, 2200 cal. yr B.P.) (figures 5-4 and 5-6).

Zone 2 (160-109 cm; 1830-1320 cal. yr B.P.)

Zone 2 is defined by a sharp rise in the concentration of soot (TRC) and BC around 160 cm (1830 cal. yr B.P.) (figure 5-4). Synchronously, the total charcoal concentration drops while

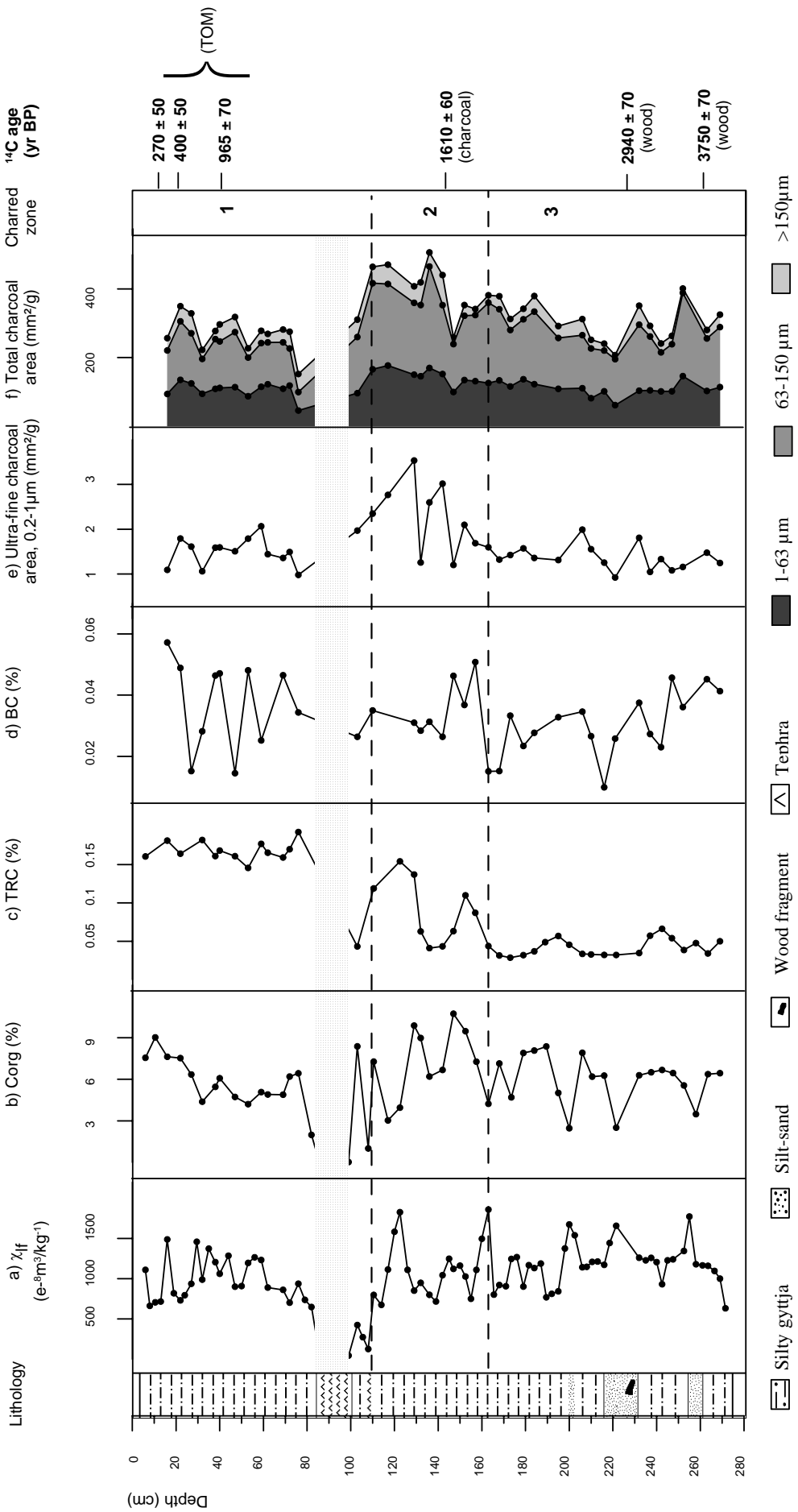


Figure 5-4: Magnetic susceptibility (χ_{lf}), Organic Carbon (Corg), Thermally Refractory Carbon (TRC) content, Black Carbon (BC), ultra-fine (0.2-1 μ m) charcoal area, and total charcoal size class distributions.

the shape of the particles changes (figure 5-5). A major increase in micro and macroscopic particles abundance takes place at *ca.* 145 cm (1560 cal. yr B.P.) (figure 5-4), associated with an increase in the perimeter and length:width ratio (figure 5-6). The change in the charred-particle distribution starts at *ca.* 15 cm (*ca.* 270 years) before a major change in the physiognomy of the local vegetation, as registered in the AP/NAP ratio (arboreal/non-arboreal pollen) near 145 cm (1560 cal. yr B.P.) (figure 5-6).

Zone 1 (106-16 cm; 1300-440 cal. yr B.P.)

The mean size of charcoal decreases above 106 cm (1300 cal. yr B.P.), where significant numbers of tephra shards first appear in the sediments (figure 5-4), and remains relatively low until 71 cm (1090 cal. yr B.P.), while the shape of particles remains thinner and longer than in zone 3 (figure 5-5). The total area of charcoal decreases until 71 cm (1090 cal. yr B.P.) (figure 5-4). The tephra horizon deposited at *ca.* 1200 cal. yr B.P. does not appear to affect significantly charred-particle distributions. As in the bottom zone, BC values show a strong variability in this unit, especially from 71 to 30 cm (1090-690 cal. yr B.P.) (figure 5-4).

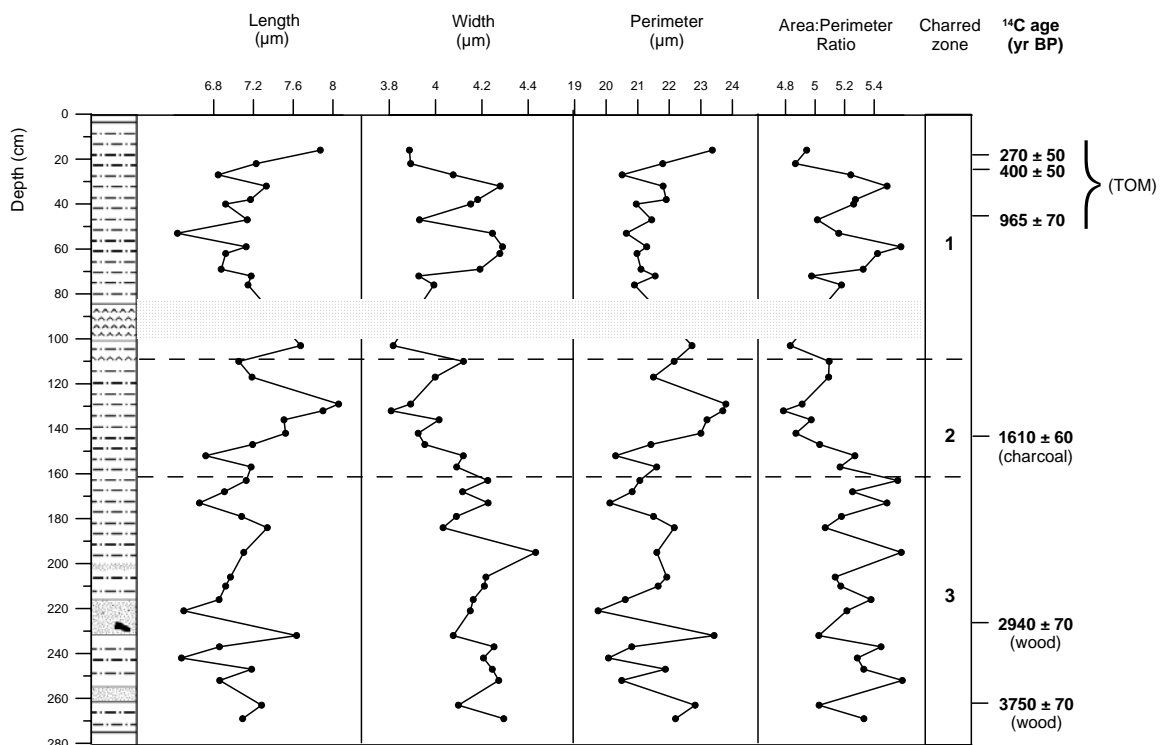


Figure 5-5: Morphological parameters of the medium-charcoal class (63-150 μm) : Length, width, perimeter and area:perimeter ratio.

The distributions of particle size and shape are highly variable during this interval (figure 5-5), whereas the soot proxy shows sustained high values (figure 5-4).

5.6 Discussion

From 4180 to 1880 cal. yr B.P., the distribution of charred particle is relatively conservative and dominated by the 63-150 μm sub-fraction. The abundance of charcoal and BC is relatively low and constant, although there are high values during the erosional events as evidenced by the increase in magnetite concentration (χ_{lf}) *ca.* 3850, 3050, 2700, 2200 cal. yr B.P. (figure 5-4). Between 3310 and 2740 cal. yr B.P., the charcoal content decreases synchronously with a short episode of woodland regression (AP decline; figure 5-6), and then increases when this vegetation-type re-expands from 2700 to 1800 cal. yr B.P. Moreover, relatively low abundance in charcoal $<1\mu\text{m}$ and in soot carbon (TRC) within this section of the core, combined with the relatively consistent morphology of the microscopic charcoal, do not evidence fire occurrence. Because settling is believed to be one of the important modes of particle removal at the large diameters ($>10\ \mu\text{m}$) (Clark and Hussey, 1996), these results suggest that charcoals in Lake Masoko are mainly transported by water and therefore subject to breakage (Patterson *et al.*, 1987). Micro-charcoal deposition in this interval therefore appears to be mostly controlled by the residual degradation of leaves or wood, as well as by saltation and redistribution of past-fires products, *i.e.* by the erosion of local woodland soils under relatively humid conditions as deduced from previous studies (Williamson *et al.*, 1999). Changes in charcoal deposition thus reflect rainfall variability, in good agreement with previous results from Intertropical Africa, showing high climatic instability post *ca.* 4000 B.P. and relatively drier conditions between *ca.* 3000 and 2000 yr cal. B.P. (Street and Grove, 1976; Vincens, 1993; Vincens *et al.*, 1998; Bonnefille and Chalié, 2000).

Zone 2 is characterised by a sudden shift in charred-particle distributions. The major increase in the content of TRC and BC may reflect a change in particle sources and transport (Clark *et al.*, 1998). The emission of fine atmospheric particulate carbon ($<1\mu\text{m}$) which are likely from regional and extra-local fires *ca.* 1830 cal. yr B.P., precedes the deposition of large fragments, which attests local burning *ca.* 1560 cal. yr B.P. The latter increase in coarse charcoal deposition and rise in the length:width ratio of the largest microscopic particles (figure 5-6) suggest a more open vegetation-type around lake Masoko. However, further improvements using carbon stable isotope analyses (Ficken *et al.*, 2002) or sub-fossil grass

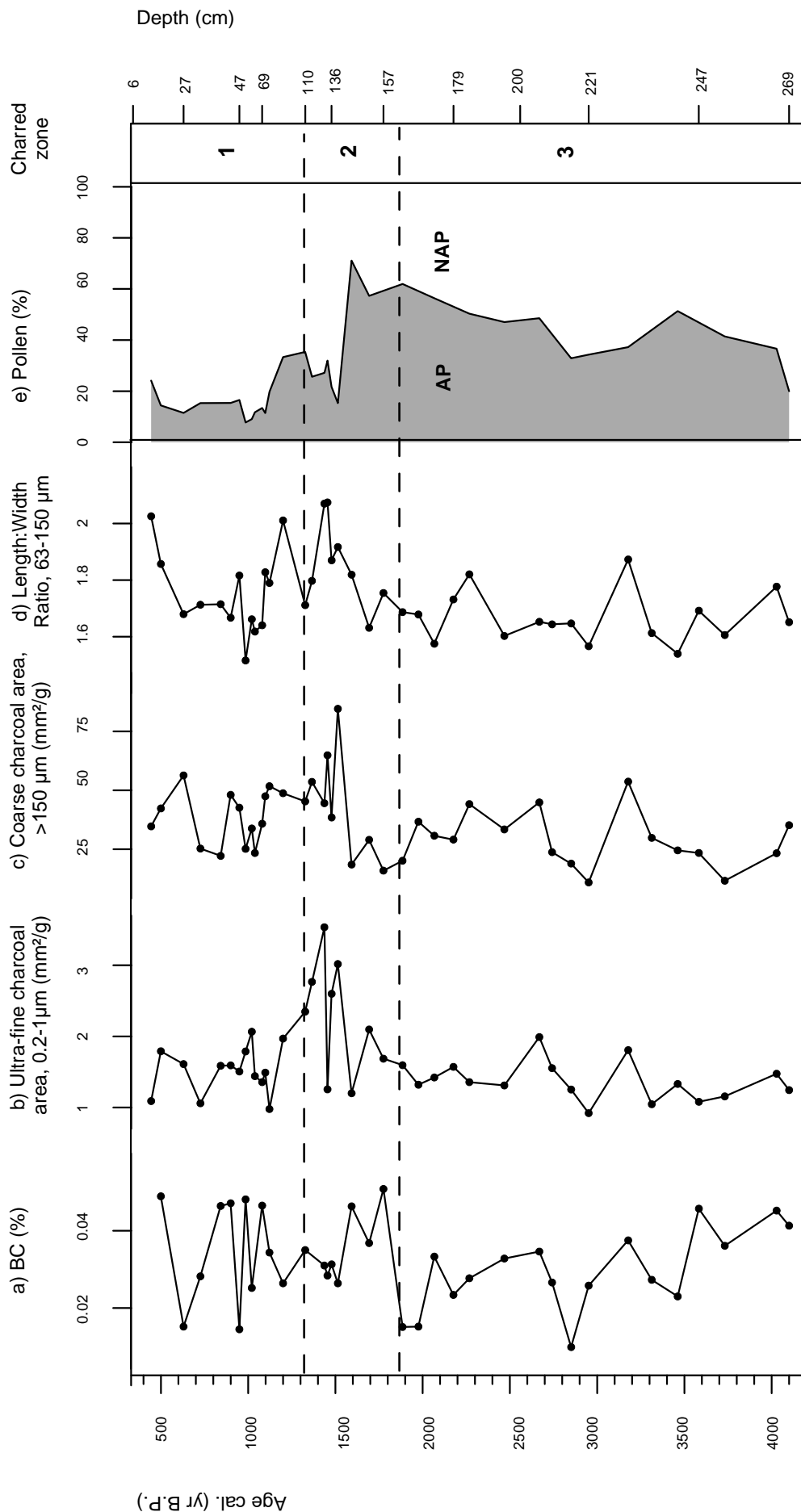


Figure 5-6: BC content, ultra-fine charcoal area ($0.2\text{-}1\mu\text{m}$), coarse charcoal area ($>150\mu\text{m}$), Length:Width ratio of the medium-charcoal class ($63\text{-}150\mu\text{m}$), and the Arboreal / Non-Arboreal Pollen ratio.

cuticle identification (Wooller *et al.*, 2000) should be used to confirm that length:width ratio can be used as a indicator of vegetation type in sedimentary records. This interpretation is strongly supported by the pollen record, which indicates the development of grasslands (NAP) at that time. Fires could have affected the arboreal strata in the Masoko area, as suggested by the large decrease in AP pollen following their appearance (figure 5-6). Pollen diagrams (Vincens *et al.*, in press) indicate a local woodland retreat at *ca.* 1650 cal. yr B.P., when *Uapaca* is partially replaced by *Macaranga*, a pioneer tree abundant after burning and a marker of vegetation opening (Jolly and Bonnefille, 1992). A gradual decline in montane forests and in water balance (Barker *et al.*, 2000) just prior that time suggests that regionally drier conditions could have favored the spread of fire. But the increase in *Ricinus communis* pollen above 1560 cal. yr B.P. could also attest an additional human impact.

Climatic drying, about 3000 years ago in Atlantic Central Africa, along with industrial innovations in the form of iron-working, facilitated the migration of people toward lower latitudes, with accompanying cultural changes *e.g.* cultivation (Schwartz, 1992; Taylor and Marchant, 1994-95). Many Early Iron Age industrial sites (between 2500 and 1500 B.P.) have been excavated by archeologists in the interlacustrine region (Schmidt and Childs, 1995; Van Noten and Raymaekers, 1988). Moreover, the technology of Late Iron Age furnaces developed by the Haya of northwestern Tanzania, more than 1500 years ago, may have evolved as an adaptation to the depletion of the rain forest resources (Schmidt and Avery, 1978). Early forest clearance and environmental degradation, as registered in East Africa, coincide with the engulfing of Khoisan herders and hunter-gatherers by the Bantu-speaking, iron-workers and agriculturists. Wet-climate crops inherited from West Africa or acquired in the Great Lakes region, combined with iron implements, allowed the Bantu to farm in wet areas of East Africa by clearing forest efficiently (Hamilton *et al.*, 1986; Philippson and Bahuchet, 1994-95). In Southern Tanzania, archeological investigations East of Lake Malawi proved that the region was settled by iron producing people *ca.* 1500 yr B.P. and the lack of previous archeological evidence in this area suggests that the environment was not attractive (Mapunda and Burg, 1991).

Between 1100 and 600 cal. yr B.P., the concentration of charred particles decreases, in consistence with a reduction of the woodland. The strong variability of BC and charcoal proxies in this interval suggests a high variability in the fire activity or in the transport mechanisms of charred particles. Previous studies on diatom assemblages and mineral-magnetic proxies indicate lower water levels and reduced runoff during this interval (Williamson *et al.*, 1999; Barker *et al.*, 2000). Reduced precipitation and plant material accumulation may have limited fire potential and particle redistribution. In addition, NAP largely extend at that time, and grassland fires,

which have much lower fuel loads than forests and higher levels of burning efficiency, yield low BC and charcoal formation (Ducret and Cachier, 1992; Kuhlbusch and Crutzen, 1995; Stocks and Kauffman, 1997). These results indicate that the production and deposition of charred products is primarily limited by climatic variability. Particle transport to the lake re-increased post 500 cal. yr B.P., supported by moister conditions and increased terrigenous contribution.

5.7 Conclusion

The measurement of morphological variability in the largest fraction of microscopic charcoal, and the quantification of the finest fraction has been achieved in this study. Additional chemical analyses of charred carbonaceous particles resulting from biomass burning decipher their redistribution. According to other paleoenvironmental proxies from the same core, our results suggest that runoff from local woodland soils can be the dominant process for charcoal particle transportation to the lake. Fire activity can be isolated from the background charcoal signal by a shift in particle distributions between 1830-1560 cal. yr B.P. In fact, the decrease in the dominant-size fraction and the increase in fine particulate carbon implies atmospheric emission and transport. After 1560 cal. yr B.P., deposition of well preserved fragments and changes in the shape of micro-charcoal indicate the occurrence of relatively local fires. This latter event is contemporaneous with the woodland degradation inferred from the pollen spectra. Moreover, this alteration in the fire regime coincides with the arrival of iron-age Bantu speaking people in the Great Lakes region, which profoundly modified the environment for iron smelting and farming. Independently of this probable human impact, the extent of the forest clearance and burning recorded in Lake Masoko may have involved relatively drier climatic conditions, and/or anomalies in the periodicity of rainfall events. Further paleoecological and archeological investigations are required to better estimate climate-landuse relationships during this period.

6. Conclusion générale et prospectives

L'objectif de cette étude était d'identifier les résidus carbonés traceurs de combustion de végétaux dans les sédiments. Nous avons pour cela développé des méthodes expérimentales physiques (comptage optique des charbons) et chimiques (teneur élémentaire en carbone réfractaire et BC). L'application de ces outils géochimiques aux séquences lacustres et océaniques offre de large perspectives de recherche sur l'impact climatique et anthropique de la dynamique des feux, mais aussi sur l'étude du réservoir global de carbone réfractaire.

6.1 Méthodologie

La méthode optique d'analyse d'image montre que l'oxydation modérée de la matière organique, l'absence de centrifugation, et le comptage automatisé permettent de quantifier l'abondance mais aussi la morphologie des charbons de façon très précise (résolution de 0.2 µm). Bien que cette méthode soit établie à partir de conditions expérimentales fiables (pesée du sédiment et taille limite de particules) cette méthode n'a pas été calibrée à l'aide de standards expérimentaux et reste descriptive. En effet, la chimie du sédiment et le choix de la valeur de seuillage des images peuvent influencer les résultats du point de vue quantitatif (partie 2.6.2).

La quantification du carbone élémentaire dans des matrices synthétiques montre que les standards carbonés réagissent différemment aux divers traitements. Le carbone minéral (CaCO_3) est complètement dissous par l'acidification. Le carbone organique labile et le charbon de bois sont oxydés par le traitement thermique (375°C pendant 24h), tandis que la majorité (70%) du carbone humique et la totalité du carbone graphitique résistent (partie 3.4.4). Puisque une partie de la matière organique est réfractaire au traitement thermique, la méthode d'extraction de la suie (par simple traitement thermique) n'est pas applicable à tous les environnements sédimentaires. De plus, la limite de détermination ($L_Q = 4.3 \mu\text{g}$) et la faible quantité de sédiment traité (5-20 mg) ne permettent pas d'appliquer ce protocole aux sédiments océaniques pauvres en carbone réfractaire (L_Q relative >0.02% ; partie 3.4.1). Il est donc recommandé de coupler l'analyse en TRC avec une méthode optique et/ou chimique.

La combinaison d'un traitement thermique à un traitement chimique (bichromate de potassium), sur des matrices synthétiques contenant un standard carboné, oxyde la quasi-totalité du carbone humique (<2%) et préserve *ca.* $80 \pm 5\%$ du carbone graphitique (partie 3.4.5). La

perte de graphite semble largement liée aux conditions expérimentales (rinçages/filtration) et n'affecte pas la précision des mesures (partie 3.5.2). Dans cette expérience, la limite de détection de l'analyseur est plus élevée que précédemment (7.8 µg), mais le traitement de 200-500 mg de sédiment enrichit le sédiment en carbone élémentaire (BC) et rend possible l'application de la méthode aux sédiments océaniques (L_Q relative >0.001% ; partie 3.4.1).

La diversité des méthodes d'oxydation et des techniques de mesure génère une certaine confusion dans l'étude des aérosols carbonés (Countess, 1990). Il n'y a pas de distinction franche entre les composés organiques charbonneux, réfractaires, et le BC, mais une résistance croissante à l'oxydation (partie 4). Afin de comparer les résultats avec ceux obtenus sur divers matériaux, il est indispensable de poursuivre la calibration des méthodes d'analyse avec des standards naturels et synthétiques disponibles dans le commerce (Gustafsson et al., 2001).

6.2 Les charbons, le carbone réfractaire, et le BC dans les sédiments

L'application des méthodes précitées aux sites lacustre et pélagique montre que 1) les sédiments Holocène du lac de cratère (MM8 ; 9°S, 33°E) contiennent 152-506 mm²/g de charbon, 0.03-0.19% de TRC, et 0.01-0.06% de BC ; 2) les sédiments pélagiques (MD40 ; 2°N, 141°E) du Pléistocène contiennent 0-5 mm²/g de charbon, 0.01-0.07% d'OREC, et 0-0.04% de BC. L'enregistrement d'OREC semble en partie contrôlé par les processus sédimentaires et ne peut pas être interprété de façon univoque comme traceur de feux.

Il est possible de convertir les résultats en flux si la densité sèche et le taux de sédimentation sont connus. Pour la carotte océanique, on ne dispose que des valeurs de densité humide, et les flux sont biaisés par l'augmentation apparente du taux de sédimentation (partie 4.5.1). Néanmoins, le flux moyen de BC océanique pour les derniers 360 ka est de 0.76 g/m²/an (équivalent au µg/cm²/an ou au t/km²/an), ce qui est cohérent avec les valeurs mesurées sur des sédiments de l'Océan Pacifique pélagique (0.001 à 3.6 g/m²/an)(Smith et al., 1973; Herring, 1985), qui sont utilisées pour estimer le flux de BC piégés par l'océan de surface (environ 7 ± 3 Tg BC/an) (Suman et al., 1997).

Le flux de BC continental du lac Masoko pour la période Holocène est compris entre 1.47 et 18.42 g/m²/an. Le flux moyen de BC est de 6.44 g/m²/an et celui de carbone réfractaire (TRC) de 20.78 g/m²/an, ce qui est proche de l'accumulation de carbone atmosphérique piégé par le lac Malawi pour la période Holocène (17 g/m²/an, soit 380 x 10³ t/an) (Einsele et al., 2001). Ces résultats soulignent l'importance de l'enfouissement de carbone réfractaire dans les lacs.

Toutefois, une part du TRC peut provenir des apports du bassin versant, et l'interprétation du TRC comme unique proxy de feu n'est pas fiable (partie 5.6).

Au lac Masoko, les apports en charbons augmentent en période humide avec le ruissellement sur les sols forestiers, ou lors d'événement érosifs importants (partie 5.6). Les sols et les sédiments exposés au ruissellement et à l'érosion sont donc les principales sources de charbons. La distribution par classes de taille et l'analyse morphologique montrent toutefois un changement de source et de mode de transport pour les charbon il y a 1,8-1,6 ka. L'introduction de charbons $>150\mu\text{m}$ atteste d'incendies locaux et l'augmentation du rapport longueur/largeur des charbons $>63\mu\text{m}$ suggère un changement de nature de combustible (partie 5.6).

La comparaison des résultats du comptage optique avec ceux de la méthode thermo/chimique suggère que les charbons pélagiques (partie 4.5.2) et les charbons lacustres $\leq 1\mu\text{m}$ (partie 5.5) sont associés à la fraction des aérosols carbonés extraite chimiquement (BC). Ces aérosols carbonés reflètent prioritairement la dynamique des feux régionaux car ils sont majoritairement transportés par voie aérienne. Les charbons micrométriques et le BC sont ainsi fortement contraints par la dynamique des feux, tandis que les macrocharbons et le carbone réfractaire (OREC ou TRC) sont d'avantage affectés par les apports terrigènes et/ou le système sédimentaire (partie 4.5.3). En effet, même si nos données suggèrent un lien entre l'activité des feux et OREC ou TRC, ces composés organiques réfractaires ne permettent pas de discriminer les feux de façon équivoque. Mais l'étude des composés organiques résistants à l'oxydation n'en demeure pas moins intéressante, car elle permet de mieux comprendre les processus sédimentaires et les échanges entre les différents réservoirs du cycle global du carbone.

6.3 La dynamique des feux tropicaux ; implications climatiques et anthropiques

Les données actuelles comme les modèles montrent que l'activité des feux dépend prioritairement de la longueur de la saison sèche (partie 1.3), mais aussi des activités humaines (parties 1.4 et 1.5). Comme le suggèrent les données obtenues dans l'Océan Pacifique Ouest Equatorial (partie 4), la variabilité des feux tropicaux au cours du Pléistocène est avant tout d'origine climatique. L'analyse fréquentielle des aérosols carbonés (microcharbons et BC) montre l'influence des cycles de précession et de ses harmoniques (Pokras and Mix, 1987) sur la dynamique des feux, associés aux changements de précipitation (Thevenon et al., 2002 ANNEXE; Trauth et al., 2003). De plus, l'émission accrue d'aérosols pendant les périodes froides de l'hémisphère Nord, y compris à l'échelle des cycles de Dansgaard-Oeschger (*ca.* 6kyr), implique un couplage entre les circulations atmosphériques de basses et hautes latitudes

(Porter and Zhisheng, 1995; de Garidel-Thoron et al., 2001). La dynamique des feux tropicaux est donc fortement liée aux variations d'insolation saisonnière à l'équateur, mais aussi au forçage des hautes latitudes sur la mousson qui entraîne des conditions de sécheresse sur le SE Asiatique. Une diminution des précipitations de mousson associée à une réduction de la convergence tropicale semble augmenter l'activité des feux.

En dépit du contrôle climatique de la dynamique des feux, cette étude a mis en évidence d'importants changements dans le régime des feux révélateurs de perturbations anthropiques. Le triplement des valeurs de BC entre 53-43 ka semble marquer la colonisation du continent australien par l'homme, *ca.* 55 ka (Roberts et al., 1994). L'augmentation des feux, enregistrée du NE de l'Australie à l'Indonésie, témoigne d'un évènement régional (Wang *et al.*, 1999; van der Kaars *et al.*, 2000; Beaufort *et al.*, in press). Ceci illustre certainement le passage d'un régime de feux contrôlés par le climat à un régime de feux contrôlés par l'homme (Saarnak, 2001) qui s'affranchit de paramètres climatiques indispensables (fréquence et longueur de la saison sèche, quantité et état du combustible). De même, l'augmentation du BC *ca.* 12-10 ka pourrait être attribuée à un changement culturel en Papouasie Nouvelle Guinée, avec l'apparition de l'agriculture dans la région (Hope and Tulip, 1994) et la colonisation des terres non côtières (Haberle, 1998).

La déforestation rapide enregistrée par les pollens du lac Masoko suite à l'extension de feux régionaux puis locaux autour de 1,8 et 1,6 ka BP, intervient dans un contexte régional de changement climatique soumis à de fortes fluctuations hydrologiques (lac Rukwa ; ANNEXE). Ces changements climatiques ont certainement facilité les migrations humaines, particulièrement celle du peuple Bantu qui s'étend alors dans la région des grands lacs Africains (Hamilton *et al.*, 1986). De plus, la déforestation enregistrée autour du Lac Victoria il y a 1,8 ka BP, est synchrone de la révolution de l'Age de Fer, et les premiers fours mis à jour au Sud de la Tanzanie datent d'environ 1,5 ka BP (Mapunda and Burg, 1991; Schmidt and Childs, 1995). La recrudescence des feux autour du lac Masoko intervient dans un contexte de changement de statut social des peuplements locaux (passage d'une société de chasseurs-cueilleurs à celle de cultivateurs maîtrisant la métallurgie du fer).

Ces résultats montrent que le régime des feux a considérablement changé au cours du dernier cycle climatique, notamment en relation avec les activités humaines (Goldamer and Seibert, 1990; Penner *et al.*, 2001). Nos observations suggèrent aussi que la dynamique des peuplements humains a été fortement contrainte par le climat, et probablement par la longueur de la saison sèche (parties 4 et 5).

6.4 Perspectives de recherche

Les feux de biomasse représentent une source importante de gaz à effet de serre et d'aérosols carbonés, leur étude s'intègre dans celle des réservoirs de carbone et du cycle global du carbone. Toutefois, ceci nécessite plus de travaux de calibration et d'inter-comparaison, grâce à de nouveaux standards et aux récentes techniques de chromatographie (Elias et al., 2001). La calibration de la méthode optique doit aussi être envisagée.

La caractérisation des résidus carbonés sédimentaires traceurs de feux (microcharbon et BC) offre de large perspectives de recherche sur les aérosols, grâce à des techniques quantitatives applicables aux sédiments lacustres, océaniques, et aux sols. En raison de la forte influence de la variabilité du bilan hydrique sur la dynamique des feux, il est nécessaire d'intégrer ce type d'études aux méthodes paléoclimatiques traditionnelles.

L'étude taphonomique des macrorestes de végétaux (Wooller et al., 2000) et surtout les analyses isotopiques en $\delta^{13}\text{C}$ des aérosols carbonés amèneraient des informations essentielles sur la nature de la végétation brûlée (Cachier, 1989; Bird and Gröcke, 1997). La destruction du carbone réfractaire offre aussi la possibilité de dater au radiocarbone des enregistrements sédimentaires de façon précise (Bird et al., 1999).

Les aérosols carbonés témoignent non seulement des interactions géosphère-atmosphère-biosphère, mais aussi de l'anthropisation des milieux naturels. Afin d'estimer l'importance de l'impact humain par rapport au changement climatique, il serait souhaitable que ce type d'étude soit appliqué aux enregistrements lacustres continus depuis le dernier maximum glaciaire (LGM), telle que la séquence du lac Masoko (Merdaci, 1998), ainsi qu'à d'autres enregistrements régionaux. Enfin, l'étude des aérosols carbonés qui actuellement jouent un rôle important dans le bilan radiatif terrestre et dans la circulation atmosphérique, permettrait d'affiner les modèles prédictifs de la dynamique du climat et de l'environnement.

LISTE DES FIGURES

Chapitre 1

- 1.1 Détection des feux actifs pour l'année 2000.
- 1.2 Historique de la fréquence des feux simulée par le modèle LPJ-DGVM pour la période 1901-98.
- 1.3 Types d'incendies naturels et sources de combustible.
- 1.4 Formation de BC mesurée après combustion expérimentale en fonction de degré de combustion pour les échantillons d'herbes (carrés et ligne noire) et pour deux échantillons de bois décidu.
- 1.5 Forçage radiatif moyen global du système climatique en l'an 2000 par rapport à 1750.
- 1.6 Modélisation de changements des précipitations d'été (mm/jour) dans le cas d'aérosols contenant du BC, Expérience A, et dans le cas d'aérosols blancs, Expérience B
- 1.7 Augmentation des rejets totaux annuels de carbone anthropique en Tg C (points noirs) et courbe mensuelle de CO₂ atmosphérique mesurée à Mona Loa (Hawaï) entre 1958 et 1995 en ppmv.
- 1.8 Cycle global du carbone (C) et du Black Carbon (BC). Pour le cycle du carbone, chiffres gris, les stocks de C sont en giga tonnes ($1 \text{ Gt} = 10^{15} \text{ g}$) de C et les échanges ou flux de C sont en Gt C/an. Pour les émissions des feux, les chiffres rouges sont en péta grammes de C ($1 \text{ Pg} = 10^{15} \text{ g}$). Pour le cycle du BC, chiffres noirs, les flux sont en terra grammes ($1 \text{ Tg} = 10^{12} \text{ g}$) de C/an.
- 1.9 L'extension de l'ITCZ et de l'IOC sur le continent Africain en janvier (à gauche) et en juillet (à droite).
- 1.10 La saisonnalité des feux sur le continent africain, avec les feux en janvier (à gauche) et en juillet (à droite).
- 1.11 Schéma représentant la circulation de surface et la position de la thermocline dans le Pacifique Ouest en situation normale (à gauche) et lors d'événements El Niño (à droite).

Chapitre 2

- 2.1 Images de charbons lacustres après oxydation de la matière organique par attaques à l'acide nitrique et eau oxygénée (Lac Masoko ; Tanzanie) a) macrocharbons au microscope binoculaire (après tamisage à 150 µm) b) microcharbons au microscope photonique.
- 2.2 Thermogrammes d'échantillons chauffés de 30 à 800°C sous oxygène a) les pics de cellulose et de lignine se recouvrent, et le pic de lignine peut inclure le BC. b) les pics de carbonates et BC peuvent chevaucher la perte d'eau des argiles.
- 2.3 Perte de masse (oxydation au bichromate de potassium) pour un échantillon de la limite Crétacée-Tertiaire, Woodside Creek 50A (carrés blancs) et pour un échantillon de graphite (Black Carbon, carrés noirs).
- 2.4 Comptage automatique des charbons par analyse d'image : Les images composées de 255 niveaux de gris sont ouvertes (a et b) puis seuillées à un niveau de gris défini (c). Les particules sont indexées et les paramètres choisis sont mesurés. Ici, les particules inférieures à 50 µm² et celles qui touchent le bord ont été ignorées.
- 2.5 Nombre de pixels en fonction du nombre images analysées (a) et du nombre de microcharbons (b) pour le même échantillon lacustre. Nombre de pixels de 3 échantillons lacustres pour une valeur de seuil variable (c).
- 2.6 Schéma de l'analyseur élémentaire CN (Fisons 1500).
- 2.7 Protocoles d'extraction chimique de OREC et de BC.

Chapitre 3

- 3.1 The sequence reaction scheme of the various elemental-carbon analyses: Total Carbon (TC), Organic Carbon (OC), Thermally Refractory Carbon (TRC; first experiment), and Black Carbon (BC; second experiment).
- 3.2 The concentration of carbon added from carbonaceous standards (excluding CaCO₃), as a function of the carbon measured after HCl acidification (% OC).
- 3.3 The behavior of the BC standards during an extended period of thermal oxidation.
- 3.4 Dichromate oxidation of the lithogenic graphite used in this study (white squares), compared to the BC standard used by Wolbach and Anders (1989)(dark squares).
- 3.5 % BC measured as a function of graphite added (% weight). Synthetic graphite (circles), lithogenic graphite (crosses); n=18, r² = 0.99.

- 3.6 The recovery of the BC extraction as a function of graphite added (% carbon). Synthetic graphite (circles), lithogenic graphite (crosses); n=18.
- 3.7 BC measured mass as a function of BC lithogenic mass added in lacustrine sediment (squares), and in marine sediment (lozenges).
- 3.8 BC recovery as a function of CaCO₃ content in synthetic matrices.

Chapitre 4

- 4.1 Regional map of the Papua New Guinea and Northern-Australian region with ancient exposed land shaded (Sahul), and bathimetric map of the West Caroline Basin showing the location of the core used in this study: dark circle represents MD972140 at 2547 m of 2°N and 141°E. The black square represents the core cited in this study: C4402 at 4402 m of 2°N and 135°E, and C2188 at 2188 m of 3°N and 141°E. The dark arrow identifies the predicted primary flow path of the Pacific bottom and deep waters into the West Caroline Basin.
- 4.2 Age-depth relationship in core MD972140.
- 4.3 δ¹⁸O (‰), CaCO₃ and Corg contents versus age (kyr) for core MD972140, compared to SPECMAP stack δ¹⁸O record. Sedimentation rate of core MD972140, mass accumulation rates (MARs) of CaCO₃ and Corg in cores MD972140 (solid lines) and C4402 (dashed lines). Shaded areas indicate the glacial periods, unshaded areas indicate interglacial periods.
- 4.4 Corg content versus CaCO₃ content for core MD972140.
- 4.5 Corg MAR versus CaCO₃ MAR for core MD972140.
- 4.6 δ¹⁸O (‰), and time series records of contents (plain lines) and MARs (dashed lines) of Corg, Oxidant Resistant Elemental Carbon (OREC), Black Carbon (BC), micro-charcoal area (CHAR) versus age in core MD972140. Shaded areas indicate the glacial periods, unshaded areas indicate interglacial periods.
- 4.7 Cross-spectral (Blackman-Tuckey) analysis between Corg and CaCO₃ contents versus δ¹⁸O_{G .ruber}.
- 4.8 Phase diagram of Corg and CaCO₃ contents versus δ¹⁸O for the precession band. The origin corresponds to the summer solstice in the northern hemisphere (21 June), and the δ¹⁸O precession peak was set at 270° (21 March).
- 4.9 Cross-spectral (Blackman-Tuckey) analysis between δ¹⁸O and OREC, BC and charcoal contents versus δ¹⁸O_{G .ruber}.

- 4.10 Phase diagram of OREC, BC and charcoal versus $\delta^{18}\text{O}$ for precession.
- 4.11 Cross-spectral (Blackman-Tuckey) analysis between BC and charcoal.

Chapitre 5

- 5.1 Topographical map of the Rungwe Volcanic Province showing the position of Lake Masoko.
- 5.2 Schematic flow diagram showing Thermally Refractory Carbon (TRC) and Black Carbon (BC) extractions.
- 5.3 An example to illustrate automated measurements of charcoal area. Enhanced threshold of the gray-level image (a and b) allows to isolated charcoal particles (c).
- 5.4 Magnetic susceptibility (χ_{lf}), Organic Carbon (Corg), Thermally Refractory Carbon (TRC) content, Black Carbon (BC), ultra-fine ($0.2\text{-}1\mu\text{m}$) charcoal area, and total charcoal size class distributions.
- 5.5 Morphological parameters of the medium-charcoal class ($63\text{-}150\mu\text{m}$) : Length, width, perimeter and area:perimeter ratio.
- 5.6 BC content, ultra-fine charcoal area ($0.2\text{-}1\mu\text{m}$), coarse charcoal area ($>150\mu\text{m}$), Length:Width ratio of the medium-charcoal class ($63\text{-}150\mu\text{m}$), and the Arboreal / Non Arboreal Pollen ratio.

Annexe

- 1 Geological and structural setting of Lake Rukwa.
- 2 Sedimentation rate and lithology of the core R96-I.
- 3 Photomicrographs of phytoliths, Mg-calcite, and volcanic ash debris.
- 4 The R96-I multiproxy depth record.
- 5 Mean grainsize and Mg profiles in core R96-I, as a function of calendar age; compared to the equinox insolation at the equator.

LISTE DES TABLEAUX

Chapitre 1

- 1.1 La consommation de bois combustible, charbon, et déchets agricoles dans les régions tropicales et extra-tropicales.
- 1.2 Les feux de biomasse en régions tropicales.
- 1.3 Estimations globales de la quantité annuelle de biomasse brûlée et du carbone émis dans l'atmosphère.
- 1.4 Contribution des feux de biomasse aux émissions globales (incluant les feux de biomasse).

Chapitre 2

- 2.1 Principales méthodes d'extraction des résidus traceurs de feux

Chapitre 3

- 3.1 The determination limit (L_Q) is approximated by multiplying the standard deviation (SD) of the mean blank value by 10.
- 3.2 Total Carbon content (%TC) measured on the bulk standard, mean, number of replicate analyses (n), standard deviation (SD).
- 3.3 Description of the carbonaceous standards. Mean Total Carbon (%TC), number of replicate analyses (n), standard deviation (SD) (see details in table 4-2).
- 3.4 Mass loss experiments of BC standards (% initial mass) during the thermal treatment.
- 3.5 Summary of the results from the first experiment (see details in table 4-6).
- 3.6 Estimation of the carbon loss associated with the thermal treatment procedure (375°C, 24h). Carbon (C) measurements were performed prior (OC) and after (TRC) the thermal treatment on synthetic mixture of known composition (weight %). Number of replicate analyses (n); mean and standard deviation (SD) in bold characters.
- 3.7 Dichromate oxidation of the lithogenic graphite used in this study compared to the BC standard used by Wolbach and Anders (1989).
- 3.8 a and b: Carbon contents (% OC) measured before and after the rinsing steps, on 10-20 mg of synthetic samples containing a) graphite and b) charcoal (after acidification HCl 2M).

- 3.9 Estimation of the carbon loss associated with the thermal and chemical treatments on synthetic mixtures of known composition (weight %). Carbon (C) content (%C), BC theoretical (BC th) and measured (BC m), number of replicate analyses (n); mean carbon content and standard deviation (SD) in bold characters.
- 3.10 Results of the thermo/chemical oxidative treatment on synthetic matrices. OC and BC theoretical contents were calculated knowing the initial proportion of standards in the matrices (%weight) and their carbon content (%TC; table 4-1).
- 3.11 a and b: BC lithogenic mass added (BC_{lito}), BC measured mass (BC_m), BC content measured (%BC), and intrinsic BC (BC_0).

Chapitre 4

- 4.1 Organic (Corg) and mineral ($CaCO_3$) carbon, Oxidant Resistant Elemental Carbon (OREC), Black Carbon (BC), and charcoal for core MD972140.

Chapitre 5

- 5.1 Radiocarbon chronology from core MM8. Calendar ages are calibrated using the program CALIB 3.0.

Annexe

- 1 Radiocarbon chronology of the TOM of R96-I sediments

BIBLIOGRAPHIE

- An, Z. (2000). The history and variability of the East Asian paleomonsoon climate. *Quaternary Science reviews* 19, 171-187.
- Andreae, M. O., Andreae, T. W., Ferek, R. J., and Raemdonck, H. (1984). Long-range transport of soot carbon in the marine atmosphere. *The science of the total Environment* 36, 73-80.
- Andreae, M.O. (1991). Biomass Burning: Its history, use, and distribution and its impact on environmental quality and global climate. In "Global Biomass Burning: Atmospheric, climatic, and biospheric implications". (J.S. Levine, Editor), The MIT Press, Cambridge, MA, pp. 3-21.
- Bard, E. (2001). Paleoceanographic implications of the difference in deep-sea sediment mixing between large and fine particles. *Paleoceanography* 16, 235-239.
- Barker, P., Telford, R., Merdaci, O., Williamson, D., Taieb, M., Vincens, A., and Gilbert, E. (2000). The sensitivity of a Tanzanian crater lake to catastrophic tephra input and four millennia of climate change. *The Holocene* 10, 303-310.
- Beaufort, L., Garidel, T., Linsley, B., Oppo, D., and Buchet, N. (in press). Continental biomass burning and oceanic primary production estimates in the Sulu record East Asian summer and winter monsoon dynamic for the last 380 kyr. .
- Beaufort, L., Garidel-Thoron, T., Mix, A. C., and Pisias, N. (2001). ENSO-like Forcing on Oceanic Primary Production During the Late Pleistocene. *Science* 293, 2440-2444.
- Beaufort, L., Lancelot, Y., Camberlin, P., Cayre, O., Vincent, E., Bassinot, F., and Labeyrie, L. (1997). Insolation cycles as a major control of equatorial Indian ocean primary productivity. *Science* 278, 1451-1454.
- Bergonzini, L., Gibert, E., Winckel, A., and Merdaci, O. (2001). Bilans hydrologique et isotopique (^{18}O et ^2H) du lac Massoko, Tanzanie. Quantification des échanges lac-eaux souterraines. *Comptes-Rendus de l'Académie des Sciences Paris* 333, 617-623.
- Bird, M. I., and Cali, J. A. (1998). A million-year record of fire in Sub-Saharan Africa. *Nature* 394, 767-769.
- Bird, M. I., and Gröcke, D. R. (1997). Determination of the abundance and carbon isotope composition of elemental carbon in sediments. *Geochimica et Cosmochimica Acta* 61, 3413-3423.
- Bird, M. I., Ayliffe, L. K., Fifield, L. K., Turney, C. S. M., Cresswell, R. G., Barrows, T. T., and David, B. (1999). Radiocarbon dating of "old" charcoal using a wet oxidation, stepped-combustion procedure. *Radiocarbon* 41, 127-140.

- Blackford, J. J. (2000). Charcoal fragments in surface samples following a fire and the implications for interpretation of subfossil charcoal data. *Paleogeography, Paleoclimatology, Paleoecology* 164, 33-42.
- Bond, G., Broecker, W., Johnsen, S., McManus, J., Labeyrie, L., Jouzel, J., and Bonani, G. (1993). Correlations between climate records from North Atlantic sediments and Greenland ice. *Nature* 365, 143-147.
- Bond, G., Kromer, B., Beer, J., Muscheler, R., Evans, M. N., Showers, W., Hoffmann, S., Lotti-Bond, R., Hajdas, I., and Bonani, G. (2001). Persistent solar influence on North Atlantic climate during the Holocene. *Science* 294, 2130-2136.
- Bonnefille, R., and Chalié, F. (2000). Pollen-inferred precipitation time-series from equatorial mountains, Africa, the last 40 kyr B.P. *Global and planetary change* 26, 25-50.
- Bowdler, S. (1977). "Sunda and Sahul: prehistoric studies in Southeast Asia, Melanesia and Australia." Academic Press, London.
- Bradbury, J. P. (1997). Reports of Working/Discussion Groups at NATO Workshop: Sediment records of Biomass Burning and Global Change. In "Sediment records of biomass burning and global change." (J. S. Clark, H. Cachier, J. G. Goldamer, and B. Stocks, Eds.), pp. 463-481. Springer, Berlin.
- Burney, D.A., 1987. Late quaternary stratigraphic charcoal records from Madagascar. *Quaternary Research*, 28: 274-280.
- Cachier, H. (1989). Carbonaceous aerosols from different tropical biomass burning sources. *Nature* 340, 371-373.
- Cachier, H. and Ducret, J. (1991). Influence of biomass burning on equatorial African rains. *Nature*, 352: 228-230.
- Cachier, H., Brémont, M. P., and Buart-Ménard, P. (1989). Determination of atmospheric soot carbon with a simple thermal method. *Tellus* 41B, 379-390.
- Cachier, H., Buart-Menard, P., Fontugne, M., and Rancher, J. (1985). Source terms and source strengths of the carbonaceous aerosol in the tropics. *Journal of Atmospheric Chemistry* 3.
- Cachier-Rivault, H. (1996). Les aérosols carbonés. *Dossier Pour la Science*, 7612 L'atmosphère: 119-121.
- Campbell, B., Frost, P., and Bryon, N. (1996). Miombo woodlands and their use: overview and key issue. In "The Miombo in transition: Woodlands and Welfare in Africa." (B. Campbell, Ed.), pp. 1-10. CIFOR, Indonesia.
- Carcaillet et al. (2002). Holocene biomass burning and global dynamics of the carbon cycle. *Chemosphere*, 49(49): 845-863.

- Carcaillet, C. and Richard, P.J.H. (2000). Holocene changes in seasonal precipitation highlighted by fire incidence in eastern Canada. *Climate Dynamics*, 16: 549-559.
- Carcaillet, C. and Thimon, M. (1996). Pedoanthracological contribution to the evolution of the upper treeline in the Maurienne Valley (north French Alps): Methodology and preliminary data. *Review of Paleobotany and Palynology*, 91: 399-416.
- Carcaillet, C., Bouvier, M., Frechette, B., Larouche, A. C., and Richard, P. J. H. (2001). Comparison of pollen-slide and sieving methods in lacustrine charcoal analyses for local and regional fire history. *The Holocene* 11, 467-476.
- Chameides, W.L. and Bergin, M. (2002). Soot takes center stage. *Science*, 297: 2214-2215.
- Chidumayo, E., and Frost, P. (1996). Population biology of miombo trees. In "The Miombo in transition: Woodlands and Welfare in Africa." (B. Campbell, Ed.), pp. 59-71. CIFOR, Indonesia.
- Chidumayo, E., Gambiza, J., and Grundy, I. (1996). Managing miombo woodland. In "The Miombo in transition: Woodlands and Welfare in Africa." (B. Campbell, Ed.), pp. 175-193. CIFOR, Indonesia.
- Clark, J. S. (1988a). Particle motion and the theory of charcoal analysis: Source area, transport, deposition, and sampling. *Quaternary Research* 30, 67-80.
- Clark, J. S. (1988b). Stratigraphic charcoal analysis on petrographic thin sections: Application to fire history in Northwestern Minnesota. *Quaternary Research* 30, 81-91.
- Clark, J. S., and Hussey, T. C. (1996). Estimating the mass flux of charcoal from sedimentary records: Effects of particle size, morphology, and orientation. *The Holocene* 6, 129-144.
- Clark, J. S., and Patterson, W. A. (1997). Background and local charcoal in sediments: Scales of fire evidence in the paleorecord. In "Sediment records of biomass burning and global change." (J. S. Clark, H. Cachier, J. G. Goldamer, and B. Stocks, Eds.), pp. 23-48. NATO, Berlin.
- Clark, J. S., and Royall, P. D. (1995). Particle-size evidence for source areas of charcoal accumulation in Late Holocene sediments of Eastern North American Lakes. *Quaternary Research* 43, 80-89.
- Clark, J. S., Lynch, J., Stocks, B. J., and Goldammer, J. G. (1998). Relationships between charcoal particles in air and sediments in west-central Siberia. *The Holocene* 8, 19-29.
- Clark, R. L. (1984). Effects on charcoal of pollen preparation procedures. *Pollen et spores* XXVI, 559-576.
- Cofer, W. R., Koutzenogii, K. P., Kokorin, A., and Ezcurra, A. (1997). Biomass burning emissions and the atmosphere. In "Sediment records of biomass burning and global change." (J. S. Clark, H. Cachier, J. G. Goldamer, and B. Stocks, Eds.), pp. 189-206. Springer, Berlin.

- Cope, M.J. and Chaloner, W.G. (1980). Fossil charcoal as evidence of past atmospheric composition. *Nature*, 283: 647-649.
- Countess, R. J. (1990). Interlaboratory analyses of carbonaceous aerosol samples. *Aerosol Science and Technology* 12, 114-121.
- Coutinho, L.M., 1990. Fire in the ecology of the Brazilian Cerrado. In "Fire in the tropical biota. Ecosystem processes and global challenges." (J.G. Goldamer, Editor), Springer, Berlin, pp. 82-105.
- Crutzen, P. J., and Andreae, M. O. (1990). Biomass burning in the tropics: Impact on atmospheric chemistry and biogeochemical cycles. *Science* 250, 1669-1677.
- Currie, L. A. (1968). Limits for qualitative detection and quantification determination: Application to radiochemistry. *Anal. Chem.* 40, 586-593.
- Dansgaard, W., Johnsen, S. J., Clausen, H. B., Dahl-Jensen, D., Gundestrup, N. S., Hammer, C. U., Hvidberg, C. S., Steffensen, J. P., Sveinbjörnsdottir, A. E., Jouzel, J., and Bond, G. (1993). Evidence for general instability of past climate from a 250-kyr ice-record. *Nature* 364, 218-220.
- de Garidel-Thoron, T., Beaufort, L., Linsley, B. K., and Dannenmann, S. (2001). Millenial-scale dynamics of the East Asian winter monsoon during the last 200,000 years. *Paleoceanography* 16, 491-502.
- Delmas, R., Loudjani, P., Podaire, A., and Menaut, J. C. (1991). Biomass burning in Africa: An assessment of annually burnt biomass. In "Global Biomass Burning: Atmospheric, climatic, and biospheric implications." (J. S. Levine, Ed.), pp. 126-133. The MIT Press, Cambridge, MA.
- Dolfus, D., and Beaufort, L. (1999). Fat neural network for recognition of position-normalised objects. *Neural Networks* 12, 553-560.
- Ducret, J., and Cachier, H. (1992). Particulate carbon content in rain at various temperate and tropical locations. *Journal of Atmospheric Chemistry* 15, 55-67.
- Ebinger, C., Deino, A. L., Drake, R. E., and Tesha, A. L. (1989). Chronology of volcanism and rift basin propagation: Rungwe volcanic province, East Africa. *Journal Geophysical Research* 94, 15,785-15,803.
- Einsele, G., Yan, J. and Hinderer, M. (2001). Atmospheric carbon burial in modern lake basins and its significance for the global carbon budget. *Global and Planetary Change*, 30: 167-195.
- Elias, V.O., Simoneit, B.R.T., Cordeiro, R.S. and Turcq, B. (2001). Evaluating levoglucosan as an indicator of biomass burning in Carajas, Amazonia: A comparison to the charcoal record. *Geochimica et Cosmochimica Acta*, 65(2): 267-272.

- Emeis, K.-C., Doose, H., Mix, A., and Schulz-Bull, D. (1995). Alkenone sea-surface temperatures and carbon burial at Site 846 (eastern equatorial Pacific Ocean): the last 1.3 m.y. In "Proc. ODP, Sci. Results." (N. G. Pisias, L. A. Mayer, T. R. Janecek, A. Palmer-Julson, and T. H. van Andel, Eds.), pp. 605-613. TX, College Station.
- Emerson, S. and Hedges, J.I. (1988). Processes controlling the organic carbon content of open ocean sediments. *paleoceanography*, 3(5): 621-634.
- Emiliani, C., Price, D.A. and Seipp, J., 1991. Is the postglacial artificial? *The Geochemical Society*, 3: 229-231.
- FAO, 1986. FAO Production Yearbook. FAO, Rome.
- FAO, 1989. Yearbook of forest products 1987 (1976-1987). FAO, Rome.
- Ficken, K. J., Wooller, M. J., Swain, D. L., Street-Perrott, F. A., and Eglinton, G. (2002). Reconstruction of a subalpine grass-dominated ecosystem, Lake Rutundu, Mount Kenya: a novel multi-proxy approach. *Paleogeography, Paleoclimatology, Paleoecology* 177, 137-149.
- Fosberg, M.A., Goldammer, J.G., Rind, D. and Price, C. (1990). Global Change: Effects on Forest Ecosystems and Wildfire Severity. In "Fire in the tropical biota. Ecosystem processes and global challenges." (J.G. Goldamer, Editor), Springer, Berlin, pp. 463-486.
- Frost, P. (1996). The ecology of Miombo woodlands. In "The Miombo in transition: Woodlands and Welfare in Africa." (B. Campbell, Ed.), pp. 11-56. CIFOR, Indonesia.
- Garstang, M., Tyson, P. D., Cachier, H., and Radke, L. (1997). Atmospheric transports of particulate and gaseous products by fires. In "Sediment records of biomass burning and global change." (J. S. Clark, H. Cachier, J. G. Goldamer, and B. Stocks, Eds.), pp. 207-250. Springer, Berlin.
- Gibert, E., Bergonzini, L., Massault, M., and Williamson, D. (2002). AMS ^{14}C chronology of continuous deposits from a crater lake (Lake Masoko, Tanzania): modern water balance and environmental implications. *Paleogeography, Paleoclimatology, Paleoecology* 187, 307-322.
- Gill, A.M., Hoare, J.R.L. and Cheney, N.P. (1990). Fire and their effects in the wet-dry tropics of Australia. In "Fire in the tropical biota. Ecosystem processes and global challenges." (J.G. Goldamer, Editor), Springer, Berlin, pp. 159-178.
- Goldamer, J. G. (1993). Historical Biogeography of Fire: Tropical and Subtropical. In "Fire in the environment. The Ecological, Atmospheric, and Climatic Importance of Vegetation Fires." (P. J. Crutzen, and J. G. Goldamer, Eds.), pp. 297-314. John Wiley and Sons Ltd., Chichester.

- Goldamer, J. G. (1997). Cooperation of the Paleofire Science Community with Interdisciplinary Fire Research Programs. In "Sediment records of biomass burning and global change." (J. S. Clark, H. Cachier, J. G. Goldamer, and B. Stocks, Eds.), pp. 483-489. Springer, Berlin.
- Goldamer, J. G. (1999). Forests on fire. *Science* 284, 178-283.
- Goldamer, J. G., and Seibert, B. (1990). The impact of drought and forest fires on tropical lowland rain forest of East Kalimantan. In "Fire in the tropical biota. Ecosystem processes and global challenges." (J. G. Goldamer, Ed.), pp. 11-31. Springer, Berlin.
- Goldamer, J.G. and Penafiel, S.R. (1990). Fire in the Pine-Grassland biomes of tropical and subtropical Asia. In "Fire in the tropical biota. Ecosystem processes and global challenges." (J.G. Goldamer, Editor), Springer, Berlin, pp. 45-62.
- Goldamer, J.G., 1999. Forests on fire. *Science*, 284: 178-283.
- Goldberg, E. D. (1985). "Black carbon in the environment." Wiley, J., New York.
- Griffin, J. J., and Goldberg, E. D. (1975). The fluxes of elemental carbon in coastal marine sediments. *Limnology and oceanography* 20.
- Gustafsson, O. and Gschwend, P.M. (1998). The flux of black carbon to surface sediments on the England continental shelf. *Geochimica et Cosmochimica Acta*, 62(3): 465-472.
- Gustafsson, O., Bucheli, T. D., Kukulska, Z., Andersson, M., Largeau, C., Rouzaud, J. N., Reddy, C. M., and Eglinton, T. I. (2001). Evaluation of a protocol for the quantification of black carbon in sediments. *Global Biogeochemical Cycles* 15, 881-890.
- Gustafsson, O., Haghseta, F., Chan, C., MacFarlane, J. and Gschwend, P.M. (1997). Quantification of the Dilute Sedimentary Soot Phase: Implications for PAH Speciation and Bioavailability. *Environmental Science Technologies*, 31: 203-209.
- Haberle, S. G. (1998). Late Quaternary vegetation change in the Tari Basin, Papua New Guinea. *Paleogeography, paleoclimatology, paleoecology* 137, 1-24.
- Haberle, S. G., and Ledru, M.-P. (2001). Correlations among Charcoal Records of Fires from the Past 16,000 Years in Indonesia, Papua New Guinea, and Central and South America. *Quaternary Research* 55, 97-104.
- Haberle, S. G., Hope, G. S., and van der Kaars, S. (1998). Biomass burning in Indonesia and Papua New Guinea: natural and human induced fire events in the fossil record. *Paleogeography, paleoclimatology, paleoecology* 171, 259-268.
- Hamilton, A., Taylor, D. and Vogel, J.C. (1986). Early forest clearance and environmental degradation in south-west Uganda. *Nature*, 320(6058): 164-167.
- Hao, W. M., Liu, M. H., and Crutzen, P. J. (1990). Estimates of annual and regional releases of CO₂ and other trace gases to the atmosphere from fires in the tropics, based on FAO statistics

- for the period 1975-1980. In “Fire in the Tropical Biota”. (J. G. Goldammer, Ed.), pp. 440-462.
- Heinselman, M.L. (1973). Fire in the Virgin forests of the boundary waters canoe area, Minnesota. *Quaternary Research*, 3: 329-382.
- Herring, J.R. (1985). Charcoal fluxes into sediments of the North Pacific Ocean: the Cenozoic record of burning. In “The carbon cycle and atmospheric CO₂: Natural variations, Archean to present”. (B.W. Sundquist ET, Editor), Amer Geophys Union, Washington DC, pp. 419-442.
- Hope, G. and Pask, J., 1998. Tropical vegetational change in the late Pleistocene of New Caledonia. *Paleogeography, Paleoclimatology, Paleoecology*, 1998: 1-21.
- Hope, G., and Tulip, J. (1994). A long vegetation history from lowland Irian Jaya, Indonesia. *Paleogeography, Paleoclimatology, Paleoecology* 109, 385-398.
- Imbrie, J., Hays, J. D., Martinson, D. G., McIntyre, A., Mix, A. C., Morley, J. J., Pisias, N. G., Prell, W. L., and Shackleton, N. J. (1984). The orbital theory of Pleistocene climate: Support from a revised chronology of the marine δ¹⁸O record. In “Milankovitch and Climate”. (A. L. Berger et al., Ed.), pp. 269-305. Reidel, D., Norwel, Mass.
- IPCC and Climat, (2001). Bilan 2001 des changements climatiques: Les éléments scientifiques. Rapport du groupe de travail I du Groupe d'Experts Intergouvernemental sur l'Evolution du Climat.
- Jacobson, M. Z. (2001). Strong radiative heating due to the mixing state of black carbon in atmospheric aerosols. *Nature* 409, 695-697.
- Jolly, D., and Bonnefille, R. (1992). Hisoire et dynamique du marécage de Ndurumu (Burundi), données polliniques. *Review of Paleobotany and Palynologie* 75, 133-151.
- Jones, T. P., Chaloner, W. G., and Kuhlbusch, T. A. K. (1997). Proposed bio-geological and chemical based terminology for fire-altered plant matter. In “Sediment Records of Biomass Burning and Global Change.” (J. S. Clark, H. Cachier, J. G. Goldamer, and J. G. Stocks, Eds.), pp. 9-22. Springer, Berlin.
- Kawahata, H. (1999). Fluctuations in the ocean environment within the western Pacific warm pool during the Pleistocene. *Paleoceanography* 14, 639-652.
- Kawahata, H., Ahagon, N., and Eguchi, N. (1997). Carbonate preservation in the Caroline Basin during the last 330 kyr. *Geochemical Journal* 31, 85-103.
- Kawahata, H., and Eguchi, N. (1996). Biogenic sediments on the Eauripik Rise of the western equatorial Pacific during the late Pleistocene. *Geochemical Journal* 30, 201-215.

- Kawahata, H., Suzuki, A., and Ahagon, N. (1998). Biogenic sediment in the West Caroline Basin, the western equatorial Pacific during the last 330,000 years. *Marine Geology* 149, 155-176.
- Keeling, C.D. and Whorf, T.P. (2002). Atmospheric CO₂ records from sites in the SIO air sampling network. In: O.R.N.L. Carbon Dioxide Information Analysis Center, U.S. Department of Energy, Oak Ridge, Tenn., U.S.A. (Editor), In Trends: A Compendium of Data on Global Change.
- Kershaw, A. P. (1986). Climatic change and Aboriginal burning in north-east Australia during the last glacial/interglacial cycles. *Nature* 322, 47-49.
- Kershaw, P., van der Kaars, S., Moss, P. and Wang, S. (2002). Quaternary Records of Vegetation, Biomass Burning, Climate and Possible Human Impact in the Indonesian-Northern Australian Region. In "The Environmental and Cultural History and Dynamic of the SE-Asian-Australian Region". (M. Rohdenburg, Editor), pp. 97.
- Kikula, I. S. (1986). The influence of fire on the composition of Miambo woodland of SW Tanzania. *Oikos* 46, 317-324.
- Koonce, A.L. and Gonzales-Caban, A. (1990). Social and ecological aspects of fire in central America. In "Fire in the tropical biota. Ecosystem processes and global challenges. Springer". (J.G. Goldamer, Editor), Berlin, pp. 135-158.
- Kuhlbusch, A.J. (1995). Method for determining black carbon in residues of vegetation fires. *Enviroment Sciences and Technologies*, 29: 2695-2702.
- Kuhlbusch, T. A. J., and Crutzen, P. J. (1995). Toward a global estimate of black carbon in residues of vegetation fires representing a sink of atmospheric CO₂ and a source O₂. *Global Biogeochemical Cycles* 9, 491-501.
- Kuhlbusch, T.A.J. et al. (1996). Black carbon formation by savanna fires: Measurements and implications for the global carbon cycle. *Journal of Geophysical Research*, 101(19): 23,651-23,665.
- Lacaux, J.-P., Cachier, H., and Delmas, R. (1993). Biomass burning in Africa: An overview of its impact on atmospheric chemistry. In "Fire in the environment. The Ecological, Atmospheric, and Climatic Importance of Vegetation Fires." (P. J. Crutzen, and J. G. Goldamer, Eds.), pp. 159-192. John Wiley and Sons Ltd., Chichester.
- Lenck-Santini, M. L. (1996). "Tephra dans les sédiments lacustres Est Africains (Programme Rukwa)". Universités d'Aix-Marseille III et INPL Toulouse III.
- Lim, B., and Cachier, H. (1996). Determination of black carbon by chemical oxidation and thermal treatment in recent marine and lake sediments and Cretaceous-Tertiary clays. *Chemical Geology* 131, 143-154.

- Lobert, J. M., and Warnatz, J. (1993). Emissions from the combustion process in vegetation. In "Fire in the environment. The Ecological, Atmospheric, and Climatic Importance of Vegetation Fires." (P. J. Crutzen, and J. G. Goldamer, Eds.), pp. 15-38. John Wiley and Sons Ltd.
- MacDonald, G. M., Larsen, C. P. S., Szeicz, J. M., and Moser, K. A. (1991). The reconstruction of boreal forest fire history from lake sediments: A comparison of charcoal, pollen, sedimentological, and geochemical indices. *Quaternary Science Reviews* 10, 53-71.
- Mapunda, B., and Burg, S. (1991). Preliminary report on archeological reconnaissance along the Ruhuhu river basin, Southern Tanzania. *Nyame Akuma* 36, 32-39.
- Marland, G., Boden, T.A. and Andres, R.J. (2002). Global, Regional, and National CO₂ Emissions. In Trends: A Compendium of Data on Global Change. In: O.R.N.L. Carbon Dioxide Information Analysis Center, U.S. Department of Energy, Oak Ridge, Tenn., U.S.A. (Editor).
- Masiello, C. A., and Druffel, E. R. (1998). Black Carbon in marine sediments. *Science* 280, 1911-1913.
- Menon, S., Hansen, J., Nazarenko, L., and Luo, Y. (2002). Climate effects of black carbon aerosols in China and India. *Science* 297, 2250-2253.
- Merdaci, O. (1998). "Changements climatiques au cours des 30 000 ans en Afrique Sud-Equatoriale (Tanzanie) par l'étude des pigments et phénols lacustres". Univ. Aix-Marseille III.
- Meyers-Schulte, K.J. and Hedges, J.I. (1986). Molecular evidence for a terrestrial component of organic matter dissolved in ocean water. *Nature*, 321: 61-62.
- Middelburg, J. J., Nieuwenhuize, J., and van Breugel, P. (1999). Black carbon in marine sediments. *Marine Chemistry* 65, 245-252.
- Moss, P. T., and Kershaw, A. P. (2000). The last glacial cycle from the humid tropics of northeastern Australia: comparison of a terrestrial and a marine record. *Paleogeography, Paleoclimatology, Paleoecology* 155, 155-176.
- Mworia-Maitima, J. (1997). Prehistoric fires and land-cover change in western Kenya: evidences from pollen, charcoal, grass cuticles and grass phytoliths. *The Holocene*, 7(4): 409-417.
- Nicholson, S. E. (2000). The nature of rainfall variability over Africa on time scales of decades to millennia. *Global and planetary change* 26, 137-158.
- Novakov, T., Cachier, H., Clarck, J. S., Gaudichet, A., Macko, S., and Masclet, P. (1997). Characterization of particulate products of biomass combustion. In "Sediment records of biomass burning and global change." (J. S. Clark, H. Cachier, J. G. Goldamer, and B. Stocks, Eds.), pp. 117-143. Springer, Berlin.

- Ogawa, H., Amagai, Y., Koike, I., Kaiser, K. and Benner, R. (2001). Production of refractory dissolved organic matter by bacteria. *Science*, 292: 917-920.
- Ogren, J.A. and Charlson, R.J. (1983). Elemental carbon in the atmosphere: Cycle and lifetime. *Tellus*, 35B: 241-254.
- Paillard, D., Labeyrie, L., and Yiou, P. (1996). Macintosh program performs time-series analysis. *Eos Trans. AGU* 77.
- Patterson, W. A., Edwards, K. J., and Maguire, D. J. (1987). Microscopic charcoal as a fossil indicator of fire. *Quaternary Science Reviews* 6, 3-23.
- Penner, J. E., Dickinson, R. E., and O'Neill, C. A. (1992). Effects of aerosol from biomass burning on the global radiation budget. *Science* 256, 1432-1433.
- Penner, J., Hegg, D. and Leaitch, R. (2001). Unraveling the role of aerosols in climate change. *Environmental Science and Technology*, August 1: 332-340.
- Penner, J.E., Eddleman, H. and Novakov, T. (1993). Towards the development of a global inventory of black carbon emissions. *Atmospheric Environment*, 27(A): 1277-1295.
- Perks, H. M., and Keeling, R. F. (1998). A 400 kyr record of combustion oxygen demand in the western equatorial Pacific: Evidence for a pressionally forced climate. *Paleoceanography* 13, 63-69.
- Philipsson, G., and Bahuchet, S. (1994-95). Cultivated crops and Bantu migrations in Central and Eastern Africa: A linguistic approach. *Azania XXIX-XXX*, 103-120.
- Pielou, E. C. (1952). Notes on the vegetation of the Rukwa Rift Valley, Tanganyika. *Journal of ecology* 40, 383-392.
- Pitkänen, A., Lehtonen, H., and Huttunen, P. (1999). Comparison of sedimentary microscopic charcoal particle records in a small lake with dendrochronological data: evidence for the local origin of microscopic charcoal produced by forest fires of low intensity in eastern Finland. *The Holocene* 9, 559-567.
- Pokras, E. M., and Mix, A. C. (1987). Earth's precession cycle and Quaternary climatic change in tropical Africa. *Nature* 326, 486-487.
- Porter, S. C., and Zhisheng, A. (1995). Correlation between climate events in the North Atlantic and China during the last glaciation. *Nature* 375, 305-308.
- Premuzic, E. T., Benkovitz, C. M., Gaffney, J. S., and Walsh, J. J. (1982). The nature and distribution of organic matter in the surface sediments of world oceans and seas. *Organic Geochemistry* 4, 63-77.
- Pyne, S. J. (2001). The fires this time, and next. *Science* 294, 1005-1006.

- Pyne, S. J., and Goldamer, J. G. (1997). The culture of fire: An introduction to Anthropogenic Fire History. In "Sediment records of biomass burning and global change." (J. S. Clark, H. Cachier, J. G. Goldamer, and J. G. Stocks, Eds.), pp. 71-115. Springer, Berlin.
- Pyne, S.J. (2001). The fires this time, and next. *Science*, 294: 1005-1006.
- Rhodes, A. N. (1998). Preparation and quantification of microscopic charcoal. *Holocene* 8, 113-117.
- Roberts, R. G., Jones, R., and Smith, M. A. (1990). Thermoluminescence dating of a 50,000-year-old human occupation site in northern Australia. *Nature* 345, 153-156.
- Roberts, R. G., Jones, R., Nigel, A., Spooner, N. A., Head, M. J., Murray, A. S., and Smith, M. A. (1994). The human colonization of Australia: Optical dates of 53,000 and 60,000 years bracket human arrival at Deaf Adder Gorge, Northern territory. *Quaternary Geochronology (Quaternary Science Reviews)* 13, 575-583.
- Saarnak, C. F. (2001). A shift from natural to human-driven fire regime: Implications for trace-gas emissions. *The Holocene* 11, 373-375.
- Schmidt, M. W., and Noack, A. G. (2000). Black carbon in soils and sediments: Analysis, distribution, implications, and current challenges. *Global Biogeochemical Cycles* 14(3), 777-793.
- Schmidt, P. R., and Childs, S. T. (1995). Ancient African iron production. *American scientist* 83, 524-533.
- Schmidt, P., and Avery, D. H. (1978). Complex iron smelting and prehistoric culture in Tanzania. *Science* 201, 1085-1089.
- Schwartz, D. (1992). Climatic drying about 3,000 B.P. and Bantu expansion in Atlantic Central Africa: some reflexions. *Bulletin de la Société Géologique de France* 163, 353-361.
- Scott, A.C. (1989). Observations on the nature and origin of fusain. *International Journal of Coal Geology*, 12: 443-475.
- Seiler, W., and Crutzen, P. J. (1980). Estimates of gross and net fluxes of carbon between the biosphere and the atmosphere from biomass burning. *Climatic Change* 2, 207-247.
- Short, D. A., Mengel, J. G., Crowley, T. J., Hyde, W. T., and North, G. R. (1991). Filtering of Milankovitch cycles by earth's geography. *Quaternary Research* 35, 157-173.
- Siegert, F., Ruecker, G., Hinrichs, A., and Hoffmann, A. A. (2001). Increased damage from fires in logged forests during droughts caused by El Niño. *Nature* 414, 437-440.
- Simoneit, B.R.T. et al., 1999. Levoglucosan, a tracer for cellulose in biomass burning and atmospheric particles. *Atmosph. Environ.*, 33: 173-182.
- Smith, D. M., Griffin, J. J., and Golberg, E. D. (1975). Spectrometric method for the quantitative determination of elemental carbon. *Analytical Chemistry* 47(2), 233-238.

- Smith, D. M., Griffin, J. J., and Goldbreg, E. D. (1973). Elemental carbon in marine sediments: a baseline for burning. *Nature* 241, 268-270.
- Stocks, B. J., and Kauffman, J. B. (1997). Biomass consumption and behavior of wildland and fires in Boreal, Temperate, and Tropical ecosystems: Parameters necessary to interpret historic fire regimes and future fire scenarios. In "Sediment records of biomass burning and global change". (J. S. Clark, H. Cachier, J. G. Goldamer, and B. Stocks, Eds.), pp. 169-188. NATO, Berlin.
- Stocks, B. J., and Kauffman, J. B. (1997). Biomass consumption and behavior of wildland and fires in Boreal, Temperate, and Tropical ecosystems: Parameters necessary to interpret historic fire regimes and future fire scenarios. In "Sediment records of biomass burning and global change". (J. S. Clark, H. Cachier, J. G. Goldamer, and B. Stocks, Eds.), pp. 169-188. NATO, Berlin.
- Strazzulla, J., 1991. Les incendies de forêt. Denoël, Paris, 239 pp.
- Street, F. A., and Grove, A. T. (1976). Environmental and climatic implications of late Quaternary lake-level fluctuations in Africa. *Nature* 261, 385-389.
- Stuiver, M., and Reimer, P. J. (1993). Extended ^{14}C database and revised CALIB 3.0 ^{14}C age calibration program. *Radiocarbon* 35, 215-30.
- Suman, O., Kuhlbusch, T. A. J., and Lim, B. (1997). Marine sediments: A reservoir for Black Carbon and their use as spatial and temporal records of combustion. In "Sediment records of biomass burning and global change." (J. S. Clark, H. Cachier, J. G. Goldamer, and B. Stocks, Eds.), pp. 271-294. Springer, Berlin.
- Suman, O., Kuhlbusch, T.A.J. and Lim, B. (1997). Marine sediments: A reservoir for Black Carbon and their use as spatial and temporal records of combustion. In "Sediment records of biomass burning and global change". (J.S. Clark, H. Cachier, J.G. Goldamer and B. Stocks, Editors), Springer, Berlin, pp. 271-294.
- Taylor, D., and Marchant, R. (1994-95). Human impact in the Interlacustrine region: long-term pollen records from the Rukiga Highlands. *Azania* XXIX-XXX, 283-295.
- Thevenon, F., Williamson, D. and Taieb, M. (2002). A 22-kyr BP sedimentological record of Lake Rukwa (8°S , S-W Tanzania): environmental, chronostratigraphic and climate implications. *Paleogeography, Paleoclimatology, Paleoecology*, 187(special issue: LENNOU, Brest 2000): 285-294.
- Thonicke, K.T., Venevsky, S., Stich, S. and Cramer, W. (2001). The role of fire disturbance for global vegetation dynamics: coupling fire into a Dynamic Global Vegetation Model. *Global Ecology & Biogeography*, 10: 661-677.

- Thouveny, N., Moreno, E., Delanghe, D., Candon, L., Lancelot , Y., and Shackleton, N. (2000). Rock magnetic detection of distal ice-rafted debries : clue for the identification of Heinrich events on the Portuguese margin. *Earth and Planetary Science Letters* 180, 61-75.
- Tinner, W., Conedera, M., Amman, B., Gäggeler, H. W., Gedye, S., Jones, R., and Sägesser, B. (1998). Pollen and charcoal in lake sediments compared with historically documented forest fires in southern Switzerland since AD 1920. *The Holocene* 8, 31-42.
- Trapnell, C. G. (1959). Ecological results of woodland burning experiments in Northern Rhodesia. *Journal of ecology* 47, 129-168.
- Trapnell, C.G., 1959. Ecological results of woodland burning experiments in Northern Rhodesia. *Journal of ecology*, 47: 129-168.
- Trauth, M.H., Deino, A.L., Andreas, G.N., Bergner, G.N. and Strecker, M.R. (2003). East African climate change and orbital forcing during the last 175 kyr BP. *Earth and Planetary Science Letters*, 206: 297-313.
- Turney, C. S. M., Bird, M. I., Fifield, L. K., Smidt, M., Dortch, C. E., Grün, R., Lawson, E., Ayliffe, L. K., Miller, G. H., Dortch, J., and Cresswell, R. G. (2001). Early human occupation at Devil's Lair, Southwestern Australia 50,000 years ago. *Quaternary Research* 55, 3-13.
- Umbanhowar, J., C.E., and McGrath, M. J. (1998). Experimental production and analysis of microscopic charcoal from wood, leaves and grasses. *The Holocene* 8, 341-346.
- van der Kaars, S., Wang, X., Kershaw, P., Guichard, F., and Setiabudi, D. S. (2000). A Late Quaternary paleoecological record from the Banda Sea, Indonesia: patterns of vegetation, climate and biomass burning in Indonesia and northern Australia. *Paleogeography, Paleoclimatology, Paleoecology* 155, 135-153.
- Van Noten, F., and Raymaekers, J. (1988). Les débuts de la métallurgie en Afrique centrale. *Pour la Science* 130, 38-45.
- van Wilgen, B. W., Everson, C. S., and Trollope, W. S. W. (1990). Fire management in Southern Africa: Some exemples of current objectives, practices and problems. In "Fire in the tropical biota. Ecosystem processes and global challenges." (J. G. Goldamer, Ed.), pp. 179-215. Springer, Berlin.
- Verardo, D. J., and Ruddiman, W. F. (1996). Late Pleistocene charcoal in tropical Atlantic deep-sea sediments: Climatic and geochemical significance. *Geology* 24(9), 855-857.
- Verardo, D. J., Froelich, P. N., and McIntyre, A. (1990). Determination of organic carbon and nitrogen in marine sediments using the Carlo Erba NA-1500 Analyzer. *Deep-Sea Research* 37, 157-165.

- Verardo, D.J., 1997. Charcoal analysis in marine sediments. *Limnology and Oceanography*, 42(1): 192-197.
- Vincens, A. (1993). Nouvelle séquence pollinique de Lac Tanganyika: 30,000 ans d'histoire botanique et climatique du bassin nord. *Review of Paleobotany and Palynology* 78, 381-394.
- Vincens, A., Schwartz, D., Bertaux, J., Elenga, H., and C., d. N. (1998). Late Holocene climatic changes in Western Equatorial Africa inferred from pollen from Lake Sinnda, Southern Congo. *Quaternary Research* 50, 34-45.
- Vincens, A., Williamson, D., Thevenon, F., Taieb, M., Buchet, G., Decobert, M., and Thouveny, N. (2003). Pollen-inferred vegetation changes in Southern Tanzania during the last 4200 years: climate and/or human impact. *Paleogeography, Paleoclimatology, Paleoecology*.
- Wang, X., Kaars, v.d., Kershaw, P., Bird, M. and Jansen, F., 1999. A record of fire, vegetation and climate through the last three glacial cycles from Lombok Ridge core G6-4, eastern Indian Ocean, Indonesia. *Paleogeography, Paleoclimatology, Paleoecology*, 147: 241-256.
- Ward, D.E. et al. (1996). Effect of fuel composition on combustion efficiency and emission factors for African savanna ecosystems. *Journal of Geophysical Research*, 101(D19): 23,569-23,576.
- White, F. (1983). The vegetation of Africa. A descriptive memoir to accompany the UNESCO/AETFAT/UNSO vegetation map of Africa (UNESCO, Ed.), pp. 356 pp., Paris.
- Wilgen, B.W., Everson, C.S. and Trollope, W.S.W. (1990). Fire management in southern Africa: some examples of current objectives, practices, and problems. In "Fire in the tropical biota. Ecosystem processes and global challenges". (J.G. Goldamer, Editor) Springer, Berlin, pp. 179-215.
- Williams, P.M. and Druffel, E.R.M. (1987). Radiocarbon in dissolved organic matter in the central North Pacific Ocean. *Nature*, 330: 246-248.
- Williamson, D., Jackson, M. J., Banerjee, S. K., Marvin, J., Merdaci, O., Thouveny, N., Decobert, M., Gibert-Massault, M., Massault, M., Mazaudier, D., and Taieb, M. (1999). Magnetic signatures of hydrological change in a tropical maar-lake (Lake Massoko, Tanzania): Preliminary results. *Phys. Chem. Earth (A)* 24, 799-803.
- Williamson, D., Jelinowska, A., Kissel, C., Tucholka, P., Gibert, E., Gasse, F., Massault, M., Taieb, M., Van Campo, E., and Wieckowski, K. (1998). Mineral-magnetic proxies of

- erosion/oxidation cycles in tropical maar-lake sediments (Lake Tritrivakely, Madagascar): paleoenvironmental implications. *Earth and Planetary Science Letters* 155, 205-19.
- Winkler, M.G. (1985). Charcoal analysis for paleoenvironmental interpretation: A chemical assay. *Quaternary Research*, 23: 313-326.
- Wolbach, W. S., and Anders, E. (1989). Elemental carbon in sediments: Determination and isotopic analysis in the presence of kerogen. *Geochimica et Cosmochimica Acta* 53, 1637-1647.
- Wolbach, W. S., Gilmour, I., Anders, E., Orth, C. J., and Brooks, R. R. (1988). Global fire at the Cretaceous-Tertiary boundary. *Nature* 334, 665-669.
- Wolbach, W.S., Lewis, R.S. and Anders, E. (1985). Cretaceous extinctions: Evidence for wildfires and search for meteoric material. *Science*, 230: 167-172.
- Woolfe, K., and Laccombe, P. (1998). Tropical River-Ocean Processes in Coastal Settings. In "Contrasting styles of sedimentation on tropical shelves of NE Australia and Papua New Guinea". (A. O. Sciences, Ed.), pp. 1330, San Diego, California.
- Wooller, M. J., Street-Perrot, F. A., and Agnew, A. D. Q. (2000). Late Quaternary fires and grassland paleoecology of Mount Kenya, East Africa: evidence from charred grass cuticles in lake sediments. *Paleogeography, Paleoclimatology, Paleoecology* 164, 233-246.
- Yamazaki, T., and Loka, N. (1997). Environmental rock-magnetism of pelagic clay: Implications for Asian eolian input to the North Pacific since the Pliocene. *Paleoceanography* 12, 111-124.
- Zep, R.G. and Macko, S.A., 1997. Polycyclic Aromatic Hydrocarbons in Sedimentary Records of Biomass Burning. In "Sediment Records of Biomass Burning and Global Change". (J.S. Clark, H. Cachier, J.G. Goldamer and J.G. Stocks, Editors), Springer, Berlin, pp. 145-166.



ELSEVIER

PALAEO

Palaeogeography, Palaeoclimatology, Palaeoecology 187 (2002) 285–294

www.elsevier.com/locate/palaeo

A 22 kyr BP sedimentological record of Lake Rukwa (8°S, SW Tanzania): environmental, chronostratigraphic and climatic implications

F. Thevenon *, D. Williamson, M. Taieb

CEREGE, BP 80, 13545 Aix-en-Provence Cedex 4, France

Received 23 March 2000; received in revised form 2 February 2001; accepted 10 July 2002

Abstract

The sedimentological study of a 12.8 m long core (R96-I) from Lake Rukwa (Tanzania, 8°S) provides a new record of past lake-level fluctuations that took place in response to changes of the regional climate since the last glacial period. From 21 to 15 cal kyr BP, nearshore and swamp/marsh environments are evidenced from clastic deposition, macrophytes debris and Ca–Mg carbonate enrichments. A transgressive sequence, starting around 15 cal kyr BP, lead to the humid lacustrine optimum between 15 and 7 cal kyr BP. From 12 to 10 cal kyr BP, anoxic lake bottom environments were favored by the concomitant effects of high primary productivity, increased subsidence and inputs of volcanic ash in the lake. The Middle Holocene (7–3 cal kyr BP) is characterized by high concentrations of silt, carbonates, and low organic content, which indicate the occurrence of relatively oxic, shallow and saline depositional environments, especially around 7 and 3.4 cal kyr BP. Although grainsize and TOC profiles suggest that shallow environments likely persisted in the Upper Holocene, low Mg concentration values for the last 3 kyr may indicate a trend toward relatively more dilute environments. The two main Lake Rukwa low-stand periods, at 21–15 and 7–3 cal kyr BP, correspond remarkably well with the insolation maximum at the Equator, which occurred at 17 kyr BP for the spring equinox, and at 6 kyr BP for the autumn equinox, respectively. We suggest that, during these periods of minimum inter-hemispheric insolation gradients, monsoon circulation weakened in south equatorial regions, and the ITCZ was located north of 8°S in east Africa.

© 2002 Elsevier Science B.V. All rights reserved.

1. Introduction

One of the most striking features of climate change in the tropics is the regional increase in moisture across equatorial and north tropical Africa (9°S–30°N) between ca. 15 and 5.8 cal

kyr BP (Haberyan, 1987; Street-Perrott and Perrott, 1993). This feature has been readily explained by an intensified summer monsoon, a consequence from the amplified seasonal cycle of solar radiation in the Northern Hemisphere during the Early and Mid-Holocene (e.g. Kutzbach et al., 1993). Nevertheless, the significance of low-latitude orbital forcing on the tropical climate is still questioned (COHMAP members, 1988; Kutzbach and Street-Perrott, 1985). This is because (i) the general lack of continuous paleoclimate

* Corresponding author. Tel.: +33-4 42 97 15 781;
Fax: +33-4 42 97 1 78.

E-mail address: thevenon@cerege.fr (F. Thevenon).

records covering the last precession cycle(s) across the Equator (especially in the southern tropics) prevents the control of insolation to be assessed more accurately, while (ii) the evidences of strong climate variations at sub-millennial scale (especially during the last deglaciation period) suggest a direct connection between the tropical climate and ice-sheet dynamics (e.g. Broecker et al., 1998). In this context, the Late Quaternary record of hydrological change in Lake Rukwa (southern Tanzania) would be especially relevant to test such hypothesis.

Previous diatom (Haberyan, 1987) and organic carbon (Talbot and Livingstone, 1989) studies as performed on a discontinuous sedimentary record taken from the shallow part (2 m water depth) of this lake, evidenced relatively deep (meromictic or monomictic) lake environments during the Early Holocene (ca. 15–5.2 kyr BP). However, no paleohydrological record was available prior to 15 kyr BP, and the chronology of the observed changes needed to be improved with additional AMS ^{14}C dates. Therefore, we took a new core (R96-I) in the deepest part of Lake Rukwa, in the framework of the EC-Rukwa project. In this paper, we describe the 22 kyr depositional record of this core.

2. General setting

Lake Rukwa is a large ($120 \times 16 \text{ km}^2$) and shallow lake (maximum depth ~ 14 m), lying along a half-graben basin which forms a NW–SE trending segment of the western branch of the East African Rift system (Morley et al., 2000). The basin is bounded by the Lupa border fault and the Tanzanian craton on the northeastern side, and by the Ufipa uplifted block on the southwestern side (Delvaux et al., 1998) (Fig. 1). Lake Rukwa is now a closed hydrologic system which mostly receives the inflows of the Rungwa River in the north and the Songwe River in the south. Most precipitation ($\sim 1000 \text{ mm/yr}$) on the $78\,200 \text{ km}^2$ watershed occurs from November to April. At inter-annual scale, however, highly variable ($P-E$) water balances result in considerable changes of the lake surface (Bergonzini, 1997; Rogers, 1982; Talbot and Livingstone, 1989).

Low lake-stands during the first half of the nineteenth century and high-stands during the 1880's indicate that the closed Lake Rukwa shows an immediate response to changes in rainfall. Such historical records also show that the lake may become almost totally desiccated in some years (Nicholson, 1999). Thus, the occurrence of periods of desiccation and pedogenesis in the shallow part of Lake Rukwa during the Late Holocene does not come as a surprise (Talbot and Livingstone, 1989). In contrast, two radiocarbon dates on charcoals (ca. 10.8 cal kyr BP) and mollusc shells (ca. 8.9 cal kyr BP) from ancient shoreline deposits indicate that the Early Holocene level of Lake Rukwa was located ~ 200 m above its present-day level. During this period, Lake Rukwa likely overflowed into Lake Tanganyika, via Ilyandi watershed, north of the Ufipa plateau (Delvaux et al., 1998; Haberyan, 1987).

3. Coring, sampling and measurements

In the framework of the EC-Rukwa project, a high resolution seismic investigation was carried out at Lake Rukwa in October 1994 in order to describe the general architecture of the lake deposits (Ceramicola et al., 1997b). A coring site was chosen along a seismic transect showing a nearly continuous depositional sequence, in the deepest part of the lake (Fig. 1). The corresponding core (R96-I, 12.8 m length, $8^\circ 25' \text{S}$, $32^\circ 43' \text{E}$, 14 m water depth) was collected in October 1996, using a Sedidrill piston corer mounted on a large platform. Although the sediment recovery was only 68% of the cored sedimentary sequence, the major lithological units show good preservation for detailed studies. The 1 m long section cores (70 mm diameter) were transported to Aix-en-Provence and stored in the CEREGE cold room before being subsampled for a wide range of studies including radiocarbon chronology, rock magnetism, sedimentology, diatom (Barker et al., 2002) and pollen. Sediment subsamples were taken at 5–10 cm intervals.

Grainsize distributions (Malvern laser granulometer) between 0.1 μm and 1 mm were determined after removing organic matter using hydro-

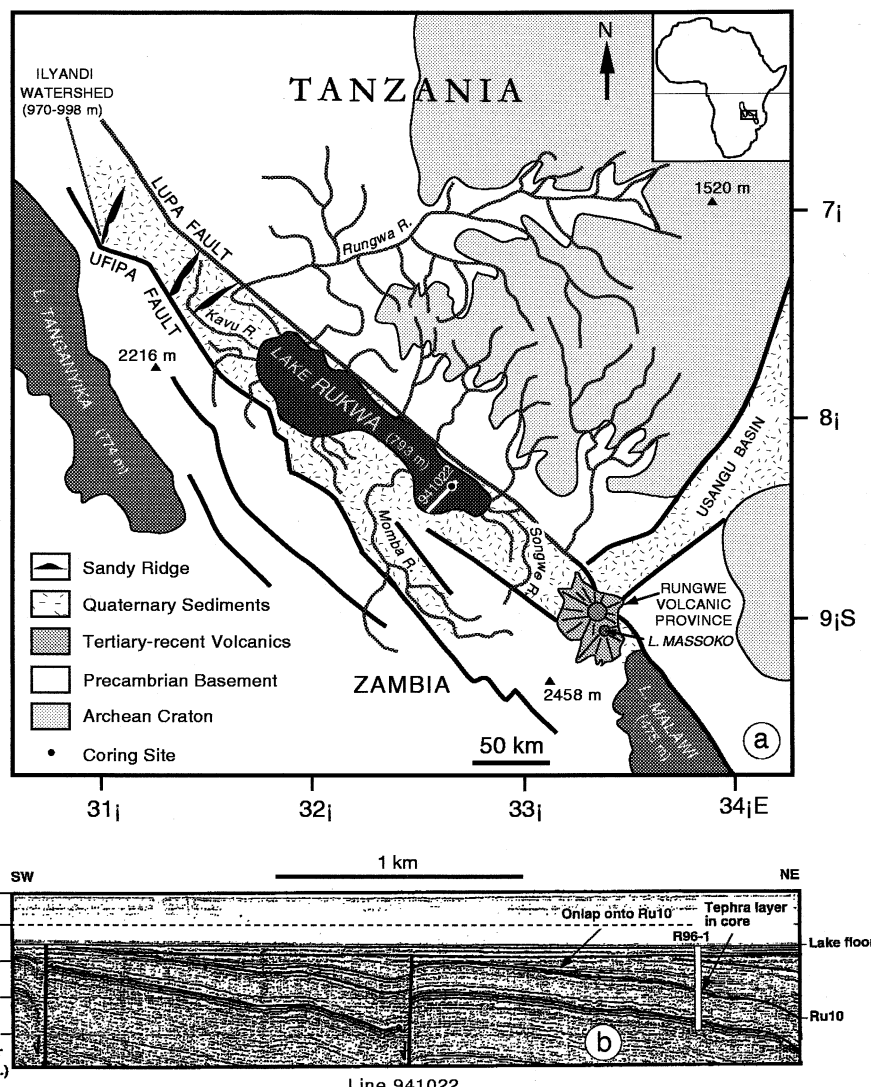


Fig. 1. Geological and structural setting of Lake Rukwa. (a) Geological map and location of core R96-I. (b) Detail of line 941022 from the high resolution seismic survey (after Morley et al., 2000), showing the Ru10 seismic reflector (see comment in the text).

gen peroxide. The mass-normalized low-field magnetic susceptibility (χ) was measured on discrete 8 cm^3 cubic samples with the Bartington Instruments MS-2 susceptibility meter (sensitivity $\sim 10^{-8} \text{ m}^3 \text{ kg}^{-1}$). To estimate the carbonate content, the Mg/Ca ratio of the carbonate fraction, and the concentration of biogenic silica, 1 g of freeze-dried samples was treated with hydrochloric acid (HCl) and sodium carbonate (Na_2CO_3).

This allowed to remove the carbonate and the biogenic silica contents. Ca, Mg and Si concentrations were measured on the corresponding leach solutions using induced coupled plasma-optical emission spectroscopy (ICP-OES). The total organic carbon (TOC) and nitrogen (N) contents were analyzed with an elemental analyzer (Fisons NA1500). The measurement error was estimated to be lower than 0.1% of the measured value.

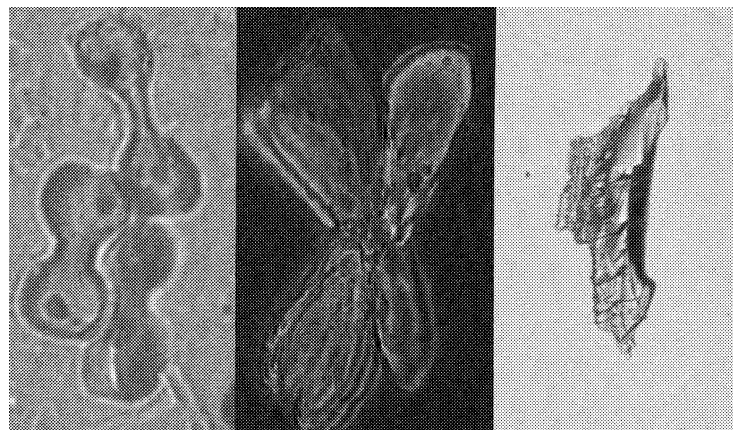


Fig. 3. Photomicrographs ($\times 2000$) of (left panel) *Gramineae* phytoliths (12 m), (middle panel) diagenetic Mg–calcite micronodule (9 m), and (right panel) volcanic ash debris (1.6 m).

1978) and Lake Tanganyika (Tiercelin et al., 1988; Williamson et al., 1991), in the vicinity of the ash layers which characterize the Pleistocene/Holocene transition in this region.

5. Lithostratigraphy

The 12.8 m cored sequence consists of nine sections separated by coring gaps of $2\text{ cm} \times 2\text{ m}$. According to the calibrated age/depth curve, apparent sedimentation rates (ASR) closely correspond to the three major lithological units of the core (Fig. 2).

Unit 3 consists of relatively slowly deposited dark silty muds ($\text{ASR} \sim 0.3\text{ mm yr}^{-1}$). Three cm thick tephra layers are located at the bottom of the core. The silty component increases from 12.8 m (22 cal kyr BP) to 10.5 m (15 cal kyr BP). The sediment contains significant contributions of iron sulfide, authigenic micrite and diagenetic Mg–calcite.

Unit 2 (9.9–5.1 m, 13.6–7 cal kyr BP; $\text{ASR} \sim 0.7\text{ mm yr}^{-1}$) is an homogeneous, organic-rich and fine-grained, brown clayed pelagic mud. In the middle of this zone, a mottled layer at 9–7.5 m (ca. 12–9.6 cal kyr BP) shows enhancements in scattered Mg–calcite micronodules (Fig. 3, middle panel), especially at 9 m (12 cal kyr BP) and between 8.5 and 8 m (12–10 cal kyr BP). Tephra debris is also abundant in this zone.

Unit 1 (5–0 m, 7–0.5 cal kyr BP, $\text{ASR} \sim 1\text{ mm yr}^{-1}$) consists of two main sedimentological units which characterize the Middle to the Upper Holocene period. The bottom part of this zone (Unit 1b, 5.1–4.5 m, 7–6.5 cal kyr BP) consists of dark silty muds with oxidized patches (Fig. 2). Abundant charcoals are observed. The upper part of this zone (Unit 1a, 4.5–0 m, 6.5–0.5 cal kyr BP) consists of green clayed silty muds, interrupted at 80–60 cm (2.0–1.4 cal kyr BP) by a very thin clay horizon, underlying a 20 cm layer of sand and ash debris (Fig. 3, right panel).

6. The sedimentological record

The vertical profiles of mean grainsize, mass-normalized magnetic susceptibility χ , the concentrations of Mg, Ca, Si, Mg/Ca, and the percentages of TOC and CaCO_3 (as calculated from the total inorganic carbon measurements) (Verardo, 1990) are presented in Fig. 4. The mean grainsize and the χ profiles show opposite trends. This is not surprising because the magnetic susceptibility of Lake Rukwa sediments mostly reflects the paramagnetic clay content, especially in two smectite-rich tephra layers at 8 and 0.8 m downcore. The geochemical records are interpreted by taking in account the smear-slide and SEM observations of diagenetic Mg–calcite, micritic calcite, and diatoms.

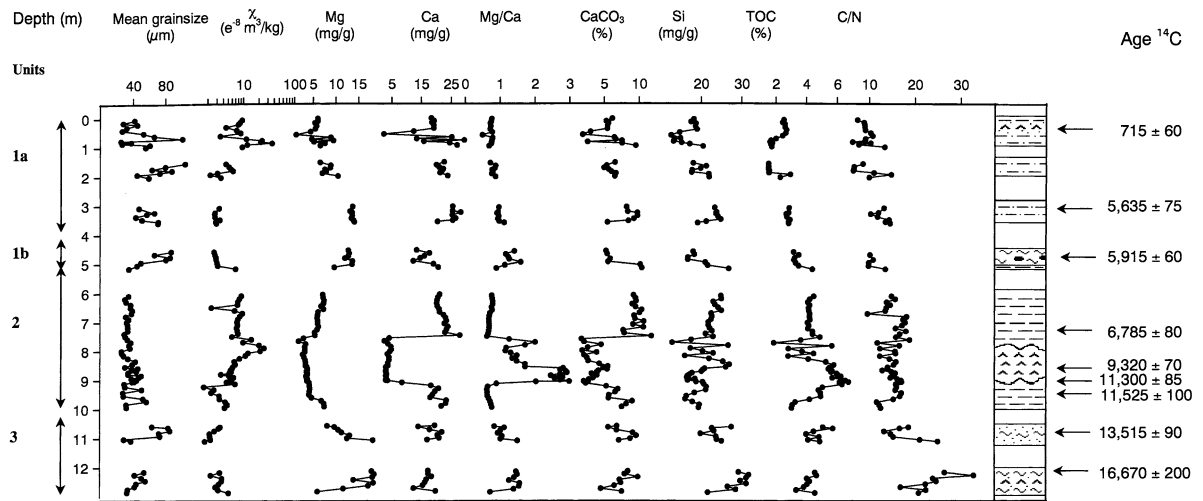


Fig. 4. The R96-I multiproxy depth record (see comments in the text).

In Unit 3, the grainsize profile shows an increase in coarse clastic deposition in the deepest part of the lake from 22 to 15 cal kyr BP (12.8–10.5 m). However, the relatively low ASR value may indicate relatively low terrigenous inputs. High carbonate contents and an increase in Mg/Ca ratio, indicative of diagenetic Mg–calcite, suggest a succession of sublittoral to saline environments. High C/N values (> 20) indicate high supply of organic matter from nearshore macrophytes or terrestrial sources rather than algae. Coarse clastic deposition revealed an increase in erosion, and abundant *Gramineae* phytoliths (Fig. 3, left panel). A. Alexandre (personal communication) suggests that open vegetation prevailed around the marsh/swamp environment of the lake. These proxies point to a period of dry climatic conditions, terminating near 15 cal kyr BP, as already observed in Lake Tanganyika from revised radiocarbon chronologies based on high-resolution magnetostratigraphy (Williamson et al., 1991). Unfortunately, due to a coring gap between 19.5 and 16.4 cal kyr BP, the R96-I core does not entirely recover the last glacial maximum (LGM) period.

The Unit 2 record is characteristic of a high lake-stand, starting after 15 cal kyr BP, and ending up near 7 cal kyr BP. During this period, the decrease in mean grainsize, together with the Mg

concentration, suggest a lower energy depositional environment and a lower water salinity. The increase in magnetic susceptibility in this zone directly reflects a relative increase in (paramagnetic) clay content. The high ASR ($\sim 0.7 \text{ mm yr}^{-1}$), the increases in TOC ($> 4\%$) and planktonic freshwater diatom species (*Stephanodiscus neoastraea* and *Cyclostephanos damasii* (Barker et al., 2002) suggest a relatively strong planktonic production. Lower C/N ratio (< 15) is consistent with the bacterial degradation of the algae organic matter (Fig. 4). Between 12 and 9.6 cal kyr BP (9–7.5 m), carbonate content is very low. This likely reflects a post-depositional dissolution of carbonate in anoxic, organic-rich environments. On one hand, high planktonic diatom productivity, combined with warm and anoxic pore waters, may provide good conditions for bacterial methanogenesis, this allowing Mg–calcite to precipitate (e.g. Cerling, 1986; Talbot and Kelts, 1986). On the other hand, in Lake Rukwa, anoxia in surficial sediments may also have been sustained by increased subsidence (Morley et al., 2000) and the concomitant input of volcanic ash, especially between 12 and 10 cal kyr BP. The tephra debris likely corresponds to a well-known period of volcanic activity in the Rungwe area (Ebinger et al., 1989). Indeed, ash layers of similar age were already identified in Lake Rukwa at ca. 12 cal kyr BP

(Haberyan, 1987), and in the Rungwe volcanic province at ca. 12.8 cal kyr BP (Crossley, 1982). This eruption was also recorded in southern Lake Tanganyika and dated between 14.4 and 12.8 cal kyr BP, according to different depth–age models taking in account variable residence time of carbon in the lake (Livingstone, 1965; Tiercelin et al., 1988; Williamson et al., 1991). Moreover, the compacted, tephra-rich mottled sediments from core R96-I likely correspond to the R10 marker horizon as defined from the seismic data set (Ceramicola et al., 1997a). According to Morey et al. (2000), an increase in the Lupa fault activity lead to increased subsidence in the Rukwa basin above this horizon. This indicates that the Unit 2 high-stand period, which started ca. 2 kyr before deposition of the tephra-rich mottled sediments, is not the result of tectonic activity and subsidence.

Unit 1 (7–0.5 cal kyr BP) shows an abrupt return to clastic deposition (increase in mean grain-size, drop in magnetic susceptibility) in relatively saline (higher Mg content and Mg/Ca ratio) and oxic environments (TOC < 3%) in the Middle and Late Holocene. Abundance of charcoal debris and *Gramineae* phytoliths indicate the occurrence of open vegetation around the lake. A high variability in mean grainsize, Mg concentration, % CaCO₃ and C/N suggests relatively shallow and unstable depositional environments, which likely dominate in the lower part of this unit, between 7 and 3 cal kyr BP (5.1–2 m). This is especially the case before 6.5 cal kyr BP (4.5 m), and at 3.6–3.1 cal kyr BP (1.8–1.5 m). The latter event, which presents the coarser grainsize and the minimum TOC values (< 2%), can be correlated with the desiccation surface as previously described in a shallower part of the lake, and dated as older than 3.1 cal kyr BP (Talbot and Livingstone, 1989). Although shallow depositional environments seem to persist in the Upper Holocene, the significant decrease in Mg concentration down to the levels of Unit 2 (< 8 mg/g) suggests a return to relatively more dilute waters after 3 cal kyr BP. Between 80 and 60 cm, the occurrence of a cm thick, smectite-rich layer, with high magnetic susceptibility, immediately overlaid by a 20 cm thick pumice layer, is interpreted as a period of

tephra deposition. This period, which occurs between 2 and 1.4 cal kyr BP, can be correlated with the tephra layers of Lake Massoko which were precisely dated at 1.2 cal kyr BP (Barker et al., 2000). Possibly, this event also corresponds to one of the last explosions of the Rungwe volcano, dated from outcrops 800 years ago (Ebinger et al., 1989).

7. Paleoenvironmental reconstruction

The sedimentary record of core R96-I reflects the main lake-level fluctuations of Lake Rukwa, for the last 22 cal kyr BP. From 22 to 15 cal kyr BP, a regression sequence indicates that the south part of the lake has been occupied progressively by shallow water to nearshore and swamp/marsh environments. This arid period corresponds to the ‘LGM’ arid period as defined in the nearby southern Lake Tanganyika (Gasse et al., 1989; Vincens, 1991).

As in many other sites from equatorial Africa (Johnson et al., 1996; Street-Perrott and Perrott, 1993), a transgression leading to the Early Holocene high-stand starts around 15 cal kyr BP (12.8 ¹⁴C kyr BP). The corresponding change in sedimentation rate and lithology likely corresponds to the seismic onlap sequence as defined by Ceramicola et al. (1997b) for Lake Rukwa. This important landward shift of base level leads to a deep lake which persisted from 13.6 to 7 cal kyr BP. From 12 to 10 cal kyr BP, anoxic lake bottom environments occurred due to the concomitant effects of high primary productivity and inputs of ash in the lake, and possibly, increased subsidence of the lake bottom. Such processes resulted in the dissolution of authigenic carbonates and allowed the precipitation of diagenetic Mg carbonates. Several paleoshoreline deposits recently dated at ~10.6 cal kyr BP by Delvaux et al. (1998) suggest that during this lacustrine optimum, the lake-level reached an elevation of ~1000 m above sea-level (i.e. ~200 m above the present-day lake-level), and probably overflowed into Lake Tanganyika.

This optimum climatic period ended up near 7 cal kyr BP. The Middle and Late Holocene

are characterized by relatively shallow depositional environments especially at 7–6.5 cal kyr BP and 3.6–3.1 cal kyr BP. These low-stands can be identified on seismic profiles as a downlapping unit (Ceramicola et al., 1997a; Morley et al., 2000). Although grainsize and TOC profiles suggest that shallow environments persisted in the Upper Holocene, relatively low Mg concentration values for the last 3 kyr may indicate a trend toward relatively more dilute environments than during the period 7–3 cal kyr BP.

According to Morley et al. (2000), fault activity in the lake, which resulted in increased accommodation space, may be associated with relatively strong deposition rates as observed after 10 kyr BP at the R96-I coring site. Although such a period roughly corresponds to a trend toward relatively shallow environments in the sedimentological record, our results suggest that hydrological changes, as superimposed on this trend, clearly dominate the sedimentological variability of core R96-I.

8. Discussion and conclusion

As in other equatorial sites located north of Lake Rukwa, our 8°S record clearly evidences (i) an arid period before 15 cal kyr BP, and (ii) a humid lacustrine optimum between 15 and 7 cal kyr BP (Johnson et al., 1996; Street-Perrott and Perrott, 1993; Williamson et al., 1991). Opposite climatic trends are observed in the southern tropics: indeed, paleohydrological records from Saltpan (Partridge et al., 1997), Cango Caves (Talma and Vogel, 1992) and Wonderkrater (Scott, 1982) suggested that arid conditions prevailed before 8 cal kyr BP in the summer monsoon area from south tropical Africa. In the same way, the 7–3 cal kyr BP arid phase at Lake Rukwa contrasts with humid conditions as observed in South Africa and Botswana (Scott, 1982). These observations suggest that the water budget in the Lake Rukwa region was constrained by Northern Hemisphere ice-sheet dynamics and by the Northern Hemisphere summer insolation

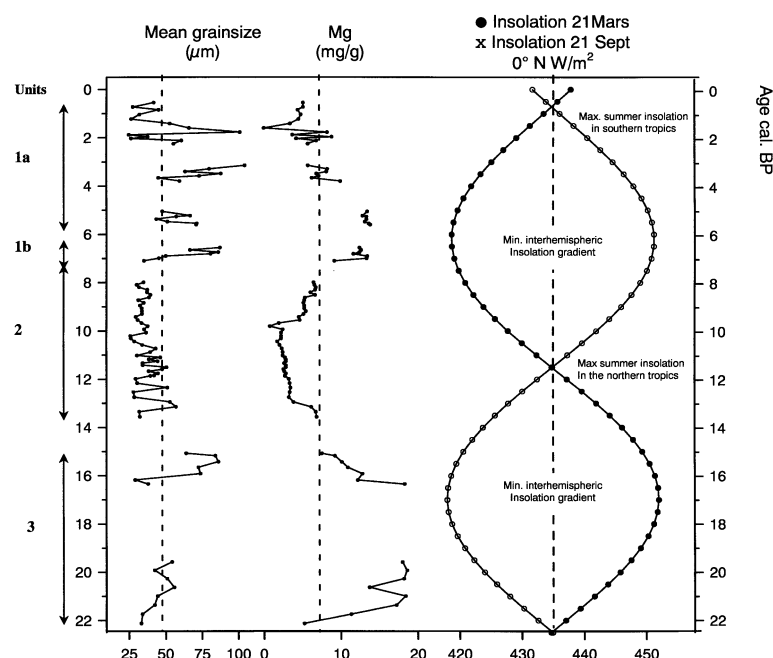


Fig. 5. The R96-I time records of mean grainsize and Mg, and the equinox insolation records at the equator (from Berger, 1978).

(high-stand at 11 cal kyr BP) (e.g. Broecker et al., 1998; Kutzbach et al., 1993; Street-Perrott and Perrott, 1990).

However, strong contrasts are observed during the Middle and Late Holocene periods. In most the northern monsoon domain of Africa, relatively humid conditions persisted until ca. 4.5–4 cal kyr BP (Gasse, 2000; Street and Grove, 1979). In contrast, arid period conditions dominated in Lake Rukwa between ca. 7 and 3 cal kyr BP.

The observed lake-level antiphasing between Lake Rukwa and other (north-) equatorial sites during the Middle and Late Holocene thus possibly reflects changes in the position of the ITCZ, which is controlled by monsoon circulation and inter-hemispheric insolation gradients. The present-day rainfall pattern at Lake Rukwa is associated to the position of the ITCZ, which locates south of the Equator from November to April (Nicholson, 1996). Summer insolation increased in the Southern Hemisphere during the last 4 kyr BP, while it decreased in the Northern Hemisphere.

In the equatorial zone, two insolation maxima occur each year during the spring and autumn solstices. As recently pointed out by Berger and Loutre (1997) and Olago et al. (2000), periods of maximum spring and autumn insolation at the Equator occurred at 17 kyr BP and 6 kyr BP, respectively (Fig. 5). They were associated with minimum inter-hemispheric insolation gradients during the year.

For the last 22 kyr BP, the two low-stands of Lake Rukwa (at 20–15 and 7–3 cal kyr BP) are precisely centered on these two last periods of maximum insolation at the Equator. Our data possibly indicate that, at these times, the meridian circulation weakened or disappeared in the current summer rainfall area of south-equatorial Africa, and the ITCZ was likely located to the north of the Lake Rukwa basin. We emphasize that Lake Rukwa hydrological changes were generally controlled by semi-precessional cycles, low-stands occurring during periods of minimum inter-hemispheric insolation gradients.

In addition, as suggested by the occurrence of the Ru10 volcano-tectonic event during a period of high lake-level, further work is needed to better

understand potential relationships between orbital and tectonic forcings on the hydrology of large rift lakes.

Acknowledgements

Many thanks to S. Massola (Ministry of Energy, Water and Minerals of Tanzania) and E.J. Kilembe (Tanzania Petroleum Development Corporation) for their help in preparing field operations. F. Chalié and F. Gasse kindly identified the main diatom species and provided help for paleoenvironmental reconstruction. A. Vincens, P. Barker and M. De Batist provided a fruitful scientific exchange. This study was funded by the RUKWA project of the EC-DGXII Environment program, and by the French CNRS-INSU Variante program.

References

- Barker, P., Telford, M., Gibert, E., Merdaci, E., Williamson, D., Taieb, M., Vincens, A., 2000. The sensitivity of a Tanzanian crater lake to catastrophic tephra input and four millenia of climate change. *Holocene* 10, 303–310.
- Barker, P., Telford, R., Gasse, F., Thevenon, F., 2002. Late Pleistocene and Holocene palaeohydrology of Lake Rukwa, Tanzania, inferred from diatom analysis. *Palaeogeogr. Palaeoclimatol. Palaeoecol.* S0031-0182(02)00482-0.
- Berger, A.L., 1978. Long-term variations of the caloric insolation resulting from the Earth's orbital elements. *Quat. Res.* 9, 139–167.
- Berger, A., Loutre, M.F., 1997. Intertropical latitudes and precessional and half-precessional cycles. *Science* 278, 1476–1478.
- Bergonzini, L., 1997. Bilan hydrique de lacs du rift est-africain (Kivu, Tanganyika, Rukwa et Nyasa). Approches mensuelle et annuelle, essai d'interprétation de la variabilité interannuelle et des fluctuations passées. Paris XI, Orsay, 204 pp.
- Broecker, W.S., Peteet, D., Hajdas, I., Lin, J., Clark, E., 1998. Antiphasing between rainfall in Africa's Rift Valley and North America's Great Basin. *Quat. Res.* 50, 12–20.
- Ceramicola, S., Vanhauwaert, P., Kilembe, E., De Batist, M., 1997a. High-resolution reflection seismic investigation of the sediments of lake Rukwa (Tanzania). *IPPCCE Newslett.* 10, 113–122.
- Ceramicola, S., Vanhauwaert, P., De Batist, M., Kilembe, E., 1997. Structure, seismic stratigraphy and a tentative level change reconstruction of Southern Lake Rukwa (Tanzania).

- In: European Union of Geosciences vol. 9. Terra Nova, Strasbourg, p. 360.
- Cerling, T.E., 1986. A mass-balance approach to basin sedimentation: constraints on the recent history of the Turkana basin. *Palaeogeogr. Palaeoclimatol. Palaeoecol.* 54, 63–86.
- COHMAP members, 1988. Climatic changes of the last 18,000 years: observations and model simulations. *Science* 241, 1043–1052.
- Crossley, R., 1982. Late Cenozoic stratigraphy of the Karonga area in the Malawi rift. *Palaeoecol. Africa* 15, 139–144.
- Delvaux, D., Kervyn, F., Vittori, E., Kajara, R.S.A., Kilembe, E., 1998. Late quaternary tectonic activity and lake level change in the Rukwa rift basin. *J. Afr. Earth Sci.* 26, 397–421.
- Ebinger, C., Deino, A.L., Drake, R.E., Tesha, A.L., 1989. Chronology of volcanism and rift basin propagation: Run-gwe volcanic province, East Africa. *J. Geophys. Res.* 94 (B11), 15785–15803.
- Gasse, F., 2000. Hydrological changes in the African tropics since the Last Glacial Maximum. *Quat. Sci. Rev.* 19, 189–211.
- Gasse, F., Lédee, V., Massault, M., Fontes, J.C., 1989. Water-level fluctuations of Lake Tanganyika in phase with oceanic changes during the last glaciation and deglaciation. *Nature* 342, 57–59.
- Haberyan, K.A., 1987. Fossil diatoms and the paleolimnology of Lake Rukwa, Tanzania. *Freshw. Biol.* 17, 429–436.
- Hecky, R.E., 1978. The Kivu-Tanganyika basin: the last 14,000 years. *Plosk. Arch. Hydrobiol.* 25, 159–165.
- Johnson, T.C., Scholz, C.A., Talbot, M.R., Kelts, K., Ricketts, R.D., Ngobi, G., Beuning, K., Ssemmanda, I., McGill, J.W., 1996. Late Pleistocene dessication of Lake Victoria and rapid evolution of Cichlid fishes. *Science* 273, 1091–1093.
- Kutzbach, J.E., Guetter, P.J., Behling, P.J., Selin, R., 1993. Simulated climatic changes: results of the COHMAP climate-model experiments. In: Wright, H.E. et al. (Eds.), *Global Climates since the Last Glacial Maximum*. University of Minnesota Press, Minneapolis, MN, pp. 24–93, 569.
- Kutzbach, J.E., Street-Perrott, F.A., 1985. Milankovitch forcing of fluctuations in the level of tropical lakes from 18 to 0 kyr B.P. *Nature* 317, 130–134.
- Livingstone, D.A., 1965. Sedimentation and the history of water level change in Lake Tanganyika. *Limnol. Oceanogr.* 10, 607–610.
- Morley, C.K., Vanhauwaert, P., De Batist, M., 2000. Evidence for high frequency cyclic fault activity from high resolution seismic reflection survey, Rukwa rift, Tanzania. *J. Geol. Soc. London* 157, 983–994.
- Nicholson, S.E., 1996. A review of climate dynamics and climate variability in Eastern Africa. In: Johnson, T.C., Odada, E.O. (Eds.), *The Limnology, Climatology and Paleoclimatology of the East African Lakes*. Gordon and Breach, Amsterdam, pp. 25–56.
- Nicholson, S.E., 1999. Historical and modern fluctuations of lakes Tanganyika and Rukwa and their relationship to rainfall variability. *Clim. Change* 41, 53–71.
- Olago, D.O., Street-Perrott, F.A., Perrot, R.A., Ivanovich, M., Harkness, D.D., Odada, E.O., 2000. Long-term temporal characteristics of palaeomonsoon dynamics in equatorial Africa. *Glob. Planet. Change* 26, 159–171.
- Partridge, T.C., DeMenocal, P.B., Lorentz, S.A., Paiker, M.J., Vogel, J.C., 1997. Orbital forcing of climate over South Africa: a 200,000 year rainfall record from the Pretoria Salt pan. *Quat. Sci. Rev.* 16, 1125–1133.
- Rogers, W.A., 1982. The decline of large mammal populations on the Lake Rukwa grasslands. *Afr. J. Ecol.* 20, 12–22.
- Scott, L., 1982. A Late Quaternary pollen record from the Transvaal bushveld, South Africa. *Quat. Res.* 17, 339–370.
- Street, F.A., Grove, A.T., 1979. Global maps of lake-level fluctuations since 30,000 yr B.P. *Quat. Res.* 12, 83–118.
- Street-Perrott, F.A., Perrott, R.A., 1990. Abrupt climatic fluctuations in the tropics: the influence of Atlantic Ocean circulation. *Nature* 343, 607–612.
- Street-Perrott, F.A., Perrott, R.A., 1993. Holocene vegetation, lake-levels and climate of Africa. In: Wright, H.E. et al. (Eds.), *Global Climates since the Last Glacial Maximum*. University of Minnesota Press, Minneapolis, MN, pp. 318–356.
- Suiver, M., Reimer, P.J., 1993. Radiocarbon calibration program 1999, rev. 4.1.2. *Radiocarbon* 35, 215–230.
- Talbot, M.R., Kelts, K., 1986. Primary and diagenetic carbonates in the anoxic sediments of Lake Bosumtwi, Ghana. *Geology* 14, 912–916.
- Talbot, M.R., Livingstone, D.A., 1989. Hydrogen index and carbon isotopes of lacustrine organic matter as lake level indicators. *Palaeogeogr. Palaeoclimatol. Palaeoecol.* 70, 121–137.
- Talma, A.S., Vogel, J.C., 1992. Late Quaternary paleotemperatures derived from a speleothem from Cango Caves, Cape Province, South Africa. *Quat. Res.* 37, 203–213.
- Tiercelin, J.J., Mondeguer, A., Gasse, F., Hillaire-Marcel, C., Hoffert, M., Larque, P., Ledee, V., Marestang, P., Ravenne, C., Raynaud, J.F., Thouveny, N., Vincens, A., Williamson, D., 1988. 25 000 ans d'histoire hydrologique et sédimentaire du lac Tanganyika, Rift Est-africain. *Comptes Rendus Acad. Sci. 307-II*, 1375–1382.
- Verardo, J., 1990. Determination of organic carbon and nitrogen in marine sediments using the Carlo Erba NA-1500 Analyzer. *Deep-Sea Res.* 37, 157–165.
- Vincens, A., 1991. Late Quaternary vegetation history of the South Tanganyika basin. Climatic implications in South Central Africa. *Palaeogeogr. Palaeoclimatol. Palaeoecol.* 86, 207–226.
- Williamson, D., Thouveny, N., Hillaire-Marcel, C., Mondeguer, A., Taieb, M., Tiercelin, J.J., Vincens, A., 1991. Chronological potential of geomagnetic oscillations recorded in Late Quaternary sediments from Lake Tanganyika. *Quat. Sci. Rev.* 10, 1–12.